MATERIAL CHARACTERISTICS AFFECTING FORMCOKE

by

WAYNE WILLIAM GILL
B.A.Sc. University of British Columbia, 1976

A THESIS SUBMITTED IN PARTIAL FULFILLMENT OF

THE REQUIREMENTS FOR THE DEGREE OF

MASTER OF APPLIED SCIENCE

in

THE FACULTY OF GRADUATE STUDIES
(Department of Metallurgical Engineering)

We accept this thesis as conforming
to the required standard

THE UNIVERSITY OF BRITISH COLUMBIA

June, 1979

© Wayne William Gill, 1979

In presenting this thesis in partial fulfilment of the requirements for an advanced degree at the University of British Columbia, I agree that the Library shall make it freely available for reference and study. I further agree that permission for extensive copying of this thesis for scholarly purposes may be granted by the Head of my Department or by his representatives. It is understood that copying or publication of this thesis for financial gain shall not be allowed without my written permission.

Department of METALLURGICAL ENGINEERING

The University of British Columbia
Vancouver 8, Canada

Date JUNE 29, 1979

ABSTRACT

The influence of aggregate and binder phase characteristics on formcoke products has been studied. This involved investigating the compaction kinetics of the system and determining the mechanical strength of the briquettes produced.

The char phase was characterized in terms of density, hardness, porosity and residual volatile matter content and the rheological properties of the binder phases used were established elsewhere. The strength and wetting behaviour of the aggregate-binder interface were studied using model materials (an SRC pitch binder and a graphite rod aggregate) as well as those produced in this work. Analysis of compaction curves was carried out using the CCWL Hot Compaction Model for Char-Binder Coal systems which was found to adequately describe the observed compaction behaviour. Briquette strength was characterized by ultimate compressive strength and comparisons were made for a constant briquette bulk porosity of 35% (by volume).

Results indicate that binder phase fluidity affects compaction viscosity during the particle flow stage of compaction and that char porosity influences final briquette bulk density by affecting the amount of total compaction required to obtain a given bulk density. In general, increased total compaction was shown to result in higher product bulk density and high bulk density was found to yield higher gross composite strength. The latter relationship was seen to be approximately linear

over the range of bulk porosity encountered in this study.

A higher briquette strength was found for systems with aggregates carbonized at lower temperatures. This was attributed to a combination of higher porosity and stronger char-binder interfacial strength, although the former effect was considered to predominate in the systems considered here. Binder phase fluidity was also seen to affect briquette strength, higher fluidity resulting in higher strength. It was concluded that this was due to increased binder penetration of the aggregate phase. With no significant pore structure in the aggregate, as found with high temperature char, briquette strength was seen to become approximately constant for the three binder coals used.

It was concluded that a good formcoke product was aided by a highly fluid binder and a char pore structure accessible to the binder phase.

ACKNOWLEDGEMENTS

The author wishes to express his gratitude for the advice and encouragement of his research supervisor, Dr. A.C.D. Chaklader. Thanks are also extended to faculty members, fellow graduate students and technical staff. The assistance of Messrs. P. Gorog, I. Franklin, P. Wenman and P. Musil is especially appreciated. Financial assistance, in the form of a fellowship from The Aluminum Company of Canada, is gratefully acknowledged.

TABLE OF CONTENTS

LIST OF TABLES

LIST OF FIGURES

LIST OF ABBREVIATIONS AND SYMBOLS

A	Fraction of total compaction attributed to the first stage of compaction (instantaneous system compaction) in CCWL model; also, aggregate-binder interfacial area.
A1	Aggregate material made from coal carbonized at 750°C.
A2	Aggregate material made from coal carbonized at 625°C.
A3	Aggregate material made from coal carbonized at 500°C.
ANCIT	Formcoke Process of Eschweiler Bergwerks Verein, an affiliate company of ARBED, S.A., Luxemburg.
B	Fraction of total compaction attributed to the second stage of compaction (particle flow) in CCWL model.
B1, B2, B3	Binder materials; properties given in Tables III and IV.
BBF	Bergbauforschung (formcoke process).
C	Fraction of total compaction attributed to the third stage of compaction (plastic deformation) in CCWL model.
CCWL	Chow-Chaklader-Warren-Leeder (hot compaction model for char/binder coal systems used to analyse compaction curves).
DKS	Didier-Kellogg-Sumitomo (formcoke process).
DPH	Diamond Pyramid Hardness.
FMC	Food Machinery and Chemicals Corporation (formcoke process).
HBN	Houilleries du Basin du Nord et du Pas-de-Calais (formcoke process).
k	Total compaction in CCWL model; for computations, taken to be compaction at three minutes after application of pressure.
M_i	Rigidity of i-th element in CCWL model.
M_T	Total System Rigidity in CCWL model.
P_b	Briquette Bulk Porosity.
RVM	Residual Volatile Matter.
SRC	Solvent Refined Coal.

t	Time.
T	Temperature.
UCS	Ultimate Compressive Strength.
α, β, γ	Exponential coefficients in 1st, 2nd and 3rd terms of experimental equation in CCWL model respectively ($\alpha = M_1/\eta_1$; $\beta = M_2/\eta_2$; $\gamma = M_3/\eta_3$).
γ_{LV}	Liquid-vapour interfacial energy.
γ_{SL}	Solid-liquid interfacial energy.
γ_{SV}	Solid-vapour interfacial energy.
ε_t	Normalized compaction strain at time, t.
η_i	Viscosity of i-th element in CCWL mdoel.
ρ	Density.
Θ	Contact angle.
σ	Applied stress.

1. INTRODUCTION

Formcoke is a manufactured carbonaceous product intended to replace conventional coke in the ironmaking blast furnace. The impetus for formcoke development comes from several sources. Among the major attractions is the ability to utilize a wider range of coals, this being especially important in iron and steel producing areas with little or no indigenous reserves of classical coking coal. Further advantages are seen in a more closely controlled and reproducible product, a choice of continuous or intermittent operation and greatly improved pollution control.

To better understand the nature and requirements of formcoke, it is necessary to appreciate the nature and requirements of conventional coke, which formcoke is intended to replace. It is therefore useful to first consider the process of conversion of coal to coke, both at the fundamental level and as it is conventionally practiced. The advantages of and problems associated with formcoke will then be apparent.

1.1 The Pyrolytic Behaviour of Coal

Blast furnace coke is the major product of high temperature carbonization of certain types of coal. Conventionally, these coking coals are of the bituminous caking type. The role of coke in the blast furnace is threefold: providing fuel for combustion; supply reductant for smelting; and physically supporting the burden. To perform these functions properly, coke must meet a number of physical and chemical specifications including

strength, abrasion resistance, reactivity and maximum limits on sulphur, ash and residual volatile matter contents. These parameters are in turn determined by the type of coal used and the carbonization conditions employed.

As coal is heated, it undergoes a number of reactions. The first of these is removal of moisture which occurs between 100°C and 200°C. The major volatile components are evolved between 400°C and 500°C, depending on the rank of the coal. Between 500°C and 1000°C the remaining volatiles are evolved, the structure undergoes densification and a slow residual outgassing takes place. At 1000°C, the carbonization process is essentially complete, the solid product being carbon and the originally contained mineral matter which is converted to ash.

The stage of most interest in cokemaking is devolatilization. The coal's behaviour during this stage determines the physical properties of the resulting coke. The devolatilization process consists of two consecutive reactions. The first of these is a depolymerization reaction in which weaker oxygen linkages between aromatic lamellae are ruptured. The result of this reaction is the formation of a fluid or plastic mass termed mesophase or metaplast, the amount of plasticity being related to the degree of depolymerization. The second is a cracking process involving the evolution from the mesophase of gaseous products, such as hydrogen, carbon monoxide, methane and higher order hydrocarbons, and solidification of the remainder into a residue, semicoke. The two reactions can be written schematically as

$$\text{Coal} \xrightarrow{k_1} \text{Mesophase} + \text{Minor Gaseous Products} \qquad (1)$$

$$\text{Mesophase} \xrightarrow{k_2} \text{Evolved Gases} + \text{Semicoke} \qquad (2)$$

where k_1 and k_2 represent the rate constants for the two reactions.

At higher temperatures, the semicoke undergoes a series of decomposition and condensation reactions. These result in further weight loss, densification and a completely carbonized solid product—coke. Temperatures of the order of 1000°C are necessary to obtain this final product. Although material properties are continually altered during this high temperature carbonization stage, the coal's behaviour in the low temperature stages influences the final product to a large extent.

The relative magnitudes of the rate constants of reactions (1) and (2) determine whether a given coal will be physically acceptable for the production of metallurgical coke. If k_1 is much larger than k_2, there will be an accumulation of the mesophase, resulting in the development of a plastic character. A coal of this type is known as caking since it will fuse into a solid mass upon completion of reaction (2). A certain amount of caking behaviour is required in the conventional cokemaking process. If k_2 is much larger than k_1, any mesophase that forms will immediately transform to volatile gases and semicoke. This is the case of a non-caking coal where no plastic behaviour is observed and the coal appears to be converted directly to semicoke or char. No agglomeration is noticed with this type of coal.

1.2 The Conventional Cokemaking Process

Conventional cokemaking is carried out in externally heated refractory lined slot-type ovens operated in batch mode. The modern version of the slot oven is approximately 15 m long, 6 m high and 0.5 m wide. Gaseous carbonization products are collected and processed into useful fractions, giving the assembly its common name: the by-product coke oven. These

are usually arranged in batteries with heating flues alternating with oven chambers to conserve fuel and maximize heating efficiency.

A schematic representation of a standard coke oven is shown in figure 1. Heat from the long walls of the oven passes through the coal charge toward its centre. As the charge temperature adjacent to the wall reaches the softening point of the coal, a plastic zone develops and moves inward. The width of this zone depends on the plastic range of the coal while the speed at which it moves depends on the heat transfer conditions. In the plastic region, the coal swells causing compaction of the untransformed charge ahead of it and pressure on the oven wall behind. As the zone moves toward the centre of the oven, the semicoke left behind continues to transmit this pressure. The agglomerated mass curves away from the wall, fissures appear and the charge may break into a number of pieces. Resultant coke properties vary considerably across the width of the oven due to a significant temperature gradient from wall to centre. Final porosity in the coke is the result of evolution of volatile matter into the plastic phase.

In conventional practice, the balance required between volatile matter content, plastic character and mechanical strength has restricted suitable coal supplies to the low volatile (14%-22%) bituminous caking type. Modern improvements to the conventional process such as charge blending and preheating now allow medium volatile (22%-30%) bituminous coals to be used as well. A stamp charging technique, involving formation of the charge into a compact before placing it in the oven, has proved successful in utilizing a proportion of high volatile coal. However, only low and low-medium volatile bituminous caking coals are referred to as prime coking coals.

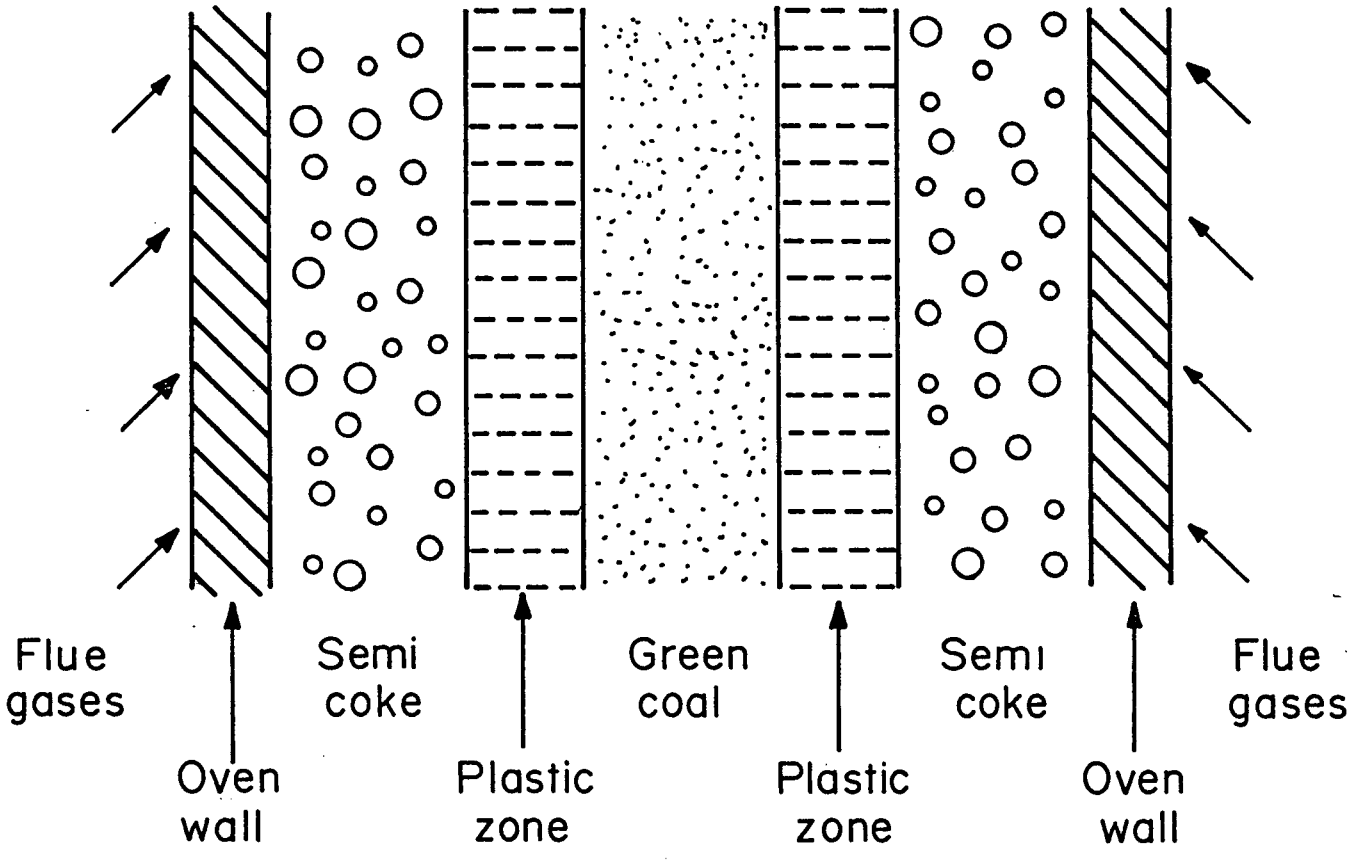

Figure 1: Schematic Cross-Section of a Conventional Coke Oven

Numerous surveys and estimates [1-6] have been made of the size of coal resources through the world and demand for coking grade types. These indicate that small fractions of total supply can be considered of coking quality and that three quarters of these are located in North America, the U.S.S.R. and China. To meet projected future demands it will be necessary to further broaden the metallurgical coal base. This is especially true for areas with little or no indigenous coking coal supplies, such as Japan, but is also significant on a more local scale within North America.

1.3 The Formcoke Alternative

A number of alternative processes to the conventional by-product coke oven are now being developed. These are collectively termed formcoke processes. Although many different processes have been developed, they all follow a common approach. Conventionally unsuitable coal is briquetted with a carbonaceous binder and the product is carbonized to yield a coherent blast furnace feedstock. The coal may be mixed and briquetted directly with a binder followed by carbonization steps. This is the approach of the HBN [7], Ancit [8], DKS [9], Iniex and Auscoke [10] processes. Alternatively, the coal may be charred at a low temperature (400°C-600°C) and subsequently mixed with a binder and briquetted. A high temperature carbonization stage follows to complete the coking operation. This is the route followed by such processes as FMC [11] and BBF [12].

The type of binder used also varies from system to system. This may be: tar or pitch, as in Auscoke, Iniex or DKS; a caking coal, as in BBF or Ancit; or the condensate tar by-products recovered in a previous charring stage, as is practiced in one version of the FMC operation. Further differences may be discerned in the heating methods employed.

These include fluidized sand or air beds for the charring operation and shaft furnaces, rotary kilns and fluidized beds in the final high temperature stage. Extensive lists of formcoke processes can be found in references 3 and 13. A number of these are now in the pilot plant stage and construction of commercial operations is reported [5].

Formcoke must equal or exceed the performance of conventional coke in the blast furnace if it is to be used as a substitute and is, therefore, subject to the same physical and chemical requirements as the conventional product. Table I shows blast furnace coke specifications for various countries [2] and formcoke briquette properties for different processes [14]. With adoption of formcoking techniques, the caking characteristics of the char-producing coal become unimportant. Selection of coal for metallurgical coke production can then be based on chemical composition alone. This will expand the suitable coal base to include almost all anthracitic, bituminous and sub-bituminous types.

The suitability of more widely available, less expensive coals, holds the greatest attraction for introduction of formcoke technology. The cost of coal has been estimated [3] as 70% of total coke cost. At the same time, there appears to be agreement [2-4,15] that formcoke operating and capital costs will equal or better those of the conventional route. Consistent with this attitude is the fact that improvements to the conventional oven battery, such as preheating, pipeline charging and dry quenching, are expensive and difficult to implement. Existing coking facilities will likely be operated without major improvement for their projected life. In a greenfield site situation, formcoking provides attractive alternatives in many regions.

TABLE I

SPECIFICATIONS FOR BLAST FURNACE COKE
REQUIREMENTS FOR VARIOUS COUNTRIES

PROPERTIES OF METALLURGICAL COKE

PROPERTY	UNITED KINGDOM	CANADA	JAPAN
Moisture (%)	⩽3	-	≃4
Shatter Index	0.5 in.>90%	0.5 in.>90%	-
M_{40} Index	>75%	ASTM Stab.⩽55	DI(30/15)>93.5
M_{10} Index	<7%	ASTM Hard. 70	DI(150/15)>81.5
Ash (%)	⩽8	⩽8	11-12
Sulphur (%)	⩽0.6	⩽0.7	0.55-0.65
V.M. (%)	≃0.8	≃0.7	≃0.7
Size Range (mm)	20-65	13-65	30-75

BRIQUETTE PROPERTIES

PROPERTY	BBF (GERMAN)	BBF (BRITISH)	FMC (USA)	DKS (JAPAN)
Moisture (%)	3.0	4.9	4.7	3.1
Fixed Carbon (mf)*	81.5	81.2	89.9	80.3
Ash (mf)	5.5	12.1	5.5	12.6
Volatile Matter (mf)	9.1	6.0	3.9	6.5
Sulphur (mf)	0.9	1.0	0.7	0.5
Bulk Density (kgm^{-3})	578	622	554	779
M_{40} Index	84	86	-	-
M_{10} Index	9.3	10.9	5.1	5.6

*(mf) - moisture free basis

As a fuel and reductant formcoke relies on the chemical nature of the parent coal, while as a burden support it depends on the physical nature of the briquette composite. Mechanical parameters characterizing formcoke may be divided into three groups: those of the aggregate phase, strength (hardness and density), texture (porosity) and surface chemical nature; those of the binder phase, strength and fluidity; and those of aggregate binder interaction, interfacial strength, wetting and spreading behaviour and gross composite strength.

Little fundamental work on formcoking has appeared to date. A survey of the available literature shows that some relationships between process parameters and material properties have been established. More recent work has involved studying the compaction behaviour during briquetting to identify the mechanisms of the composite forming process.

1.4 Previous Studies

Comprehensive reviews of briquetting theory and practice have been published, including that by Rhys Jones [16] on binderless briquetting practice and the general overview of coal briquetting by Berkowitz [17]. The supplementary volume of Chemistry of Coal Utilization [18] is an excellent general reference source. Aside from the state of the art summaries noted earlier [1-15], studies concerning the individual aspects of characterization and interaction of the char-binder system have been reported. These may be grouped according to the material property considered.

1.4.1 Material Characteristics

1.4.1.1 Char Strength and Hardness

Smith and Reynolds [19] found that coke strength, measured as a

relative 1/4" tumbler index, increased with carbonization temperature. Dainton [20] used a simple beam-bending apparatus to measure the Young's modulus of semi-coke and found it increased from 400 MPa at 500°C to 1700 MPa at 800°C. Gryaznov et al. [21] found similar increases from 290 MPa at 500°C to 1400 MPa at 1000°C, suggesting this was due to polycondensation brought about by continuing pyrolysis.

Toda and Toyoda [22] calculated values of Young's modulus from compressibility plots and compared them with measured Knoop hardness values. They stated the direct proportionality observed was reasonable because both Knoop hardness and Young's modulus are reflections of the binding energy between molecules. Chaklader et al. [23] showed the 136° diamond pyramid hardness of char to increase from DPH 20 at 500°C to DPH 200 at 750°C for a sub-bituminous coal char. A summary of these results is shown in figure 2.

1.4.1.2 Char Density

Studies of true char density have shown it to increase with carbonization temperature. Evans and Hermann [24] found values of 1.4 gcm^{-3} at 400°C increasing to 1.9 gcm^{-3} at 1000°C. White and Zimmer [25] measured a higher value of 2.2 gcm^{-3} at the higher temperature, while Jasienko [6] found the 1000°C density to be between 2.0 and 2.1 gcm^{-3}.

1.4.1.3 Char Porosity

Toda et al. [26] followed the fine structure of both caking and non-caking coals as a function of heat treatment temperature using adsorption isotherms, differences in volume in mercury and methanol, and mercury penetration porosimetry. They concluded that the micropore structure is closed off up to 400°C due to oozing out of tarry material from the char. This caused a decrease in pore volume with increasing temperature. From

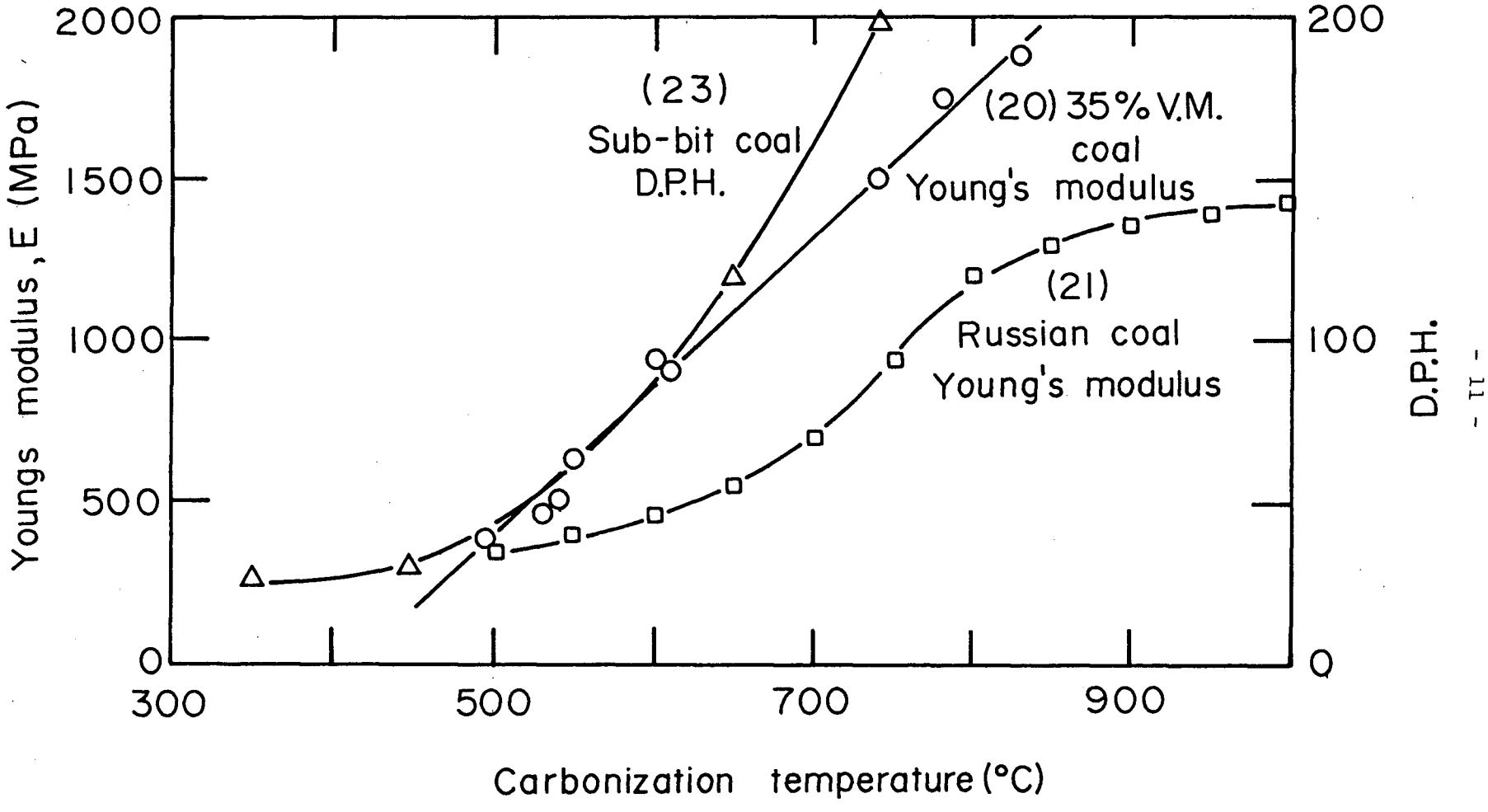

Figure 2: Selected Relationships Between Char Strength and Carbonization Temperature

400°C to 600°C, an increase in pore volume was noted, attributed to removal of the tarry material and such reactions as demethanation and dehydrogenation. Pore volume decreased again above 600°C due to thermal shrinkage of the pore structure. The authors also showed mercury penetration volume decreased in a caking coal from 75 mm^3g^{-1} at 400°C to 25 mm^3g^{-1} at 800°C.

March and Rand [27] considered that microporosity in char arose from non-parallel joining of sheets of the coal molecular structure and from evolution of low molecular weight materials such as water, methane and hydrogen. They found experimentally that micropore volume in the carbons studied increased with carbonization temperature from 400°C to 700°C and then decreased upon further heating. Gregg et al. [28] measured adsorption isotherms of butane and found results that indicated constrictions in micropores obstructed passage of the measuring fluid into larger cavities.

McCartney [29] employed a scanning electron microscope to investigate bubbles sizes in conventional coke. Patrick et al. [30] developed an automated procedure for textural characterization of coke using a Quantimet 720 Image Analyser. They measured total pore volume, number of pores, pore wall thickness, pore perimeter and pore diameter. Good agreement between this procedure and the density difference method of pore volume determination was demonstrated. They correlated increasing char strength with increasing pore wall thickness and decreasing perimeter per pore and total pore volume.

Toda and Toyoda [22] studied the porosity of 17 different coals comparing results of mercury penetration and density difference calculations.

Good agreement was found and the suggestion made that increases in pore volume measured in the penetration program above 100 atm, corresponding to a pore diameter of 0.1 μm, were due to compressibility of the specimens. In a later study, Toda [31] found an increase in pore volume up to 400°C followed by a decrease up to 800°C. This was the case for both caking (a drop from 80$mm^3 g^{-1}$ at 400°C to 20 $mm^3 g^{-1}$ at 800°C) and non-caking coals (a drop from 90 $mm^3 g^{-1}$ at 400°C to 60 $mm^3 g^{-1}$ at 800°C). Figure 3 shows the porosity-temperature relationships established in various studies.

In more recent work, Spitzer et al. [32] compared various methods of pore structure analysis and reconfirmed their close agreement. Chaklader et al. [33] used the mercury penetration technique and concluded that pore volume in non-caking coal char does not vary widely, but does decrease with heat treatment temperature so that only micropores (<0.003μm) remain above 900°C.

1.4.1.4 Coal Extracts

The organic solvent soluble fractions produced at carbonization temperatures have been associated with the intermediate plastic phase which is seen to accumulate in caking coals at these elevated temperatures. Loison et al. [34], in their review of the plastic properties of coal, pointed out that a number of facts support this association. The concentration of chloroform-soluble extract increased with temperature, passed through a maximum, and decreased—in a manner parallel with measured plasticity. The yield of extract was increased by pressure, as was plasticity and the extract was decomposed to gas and an insoluble residue under heat. However, the fluidity maximum was reached after that of extract concentration. The authors concluded that this did not disprove the

Figure 3: Selected Relationships Between Char Porosity and Carbonization Temperature

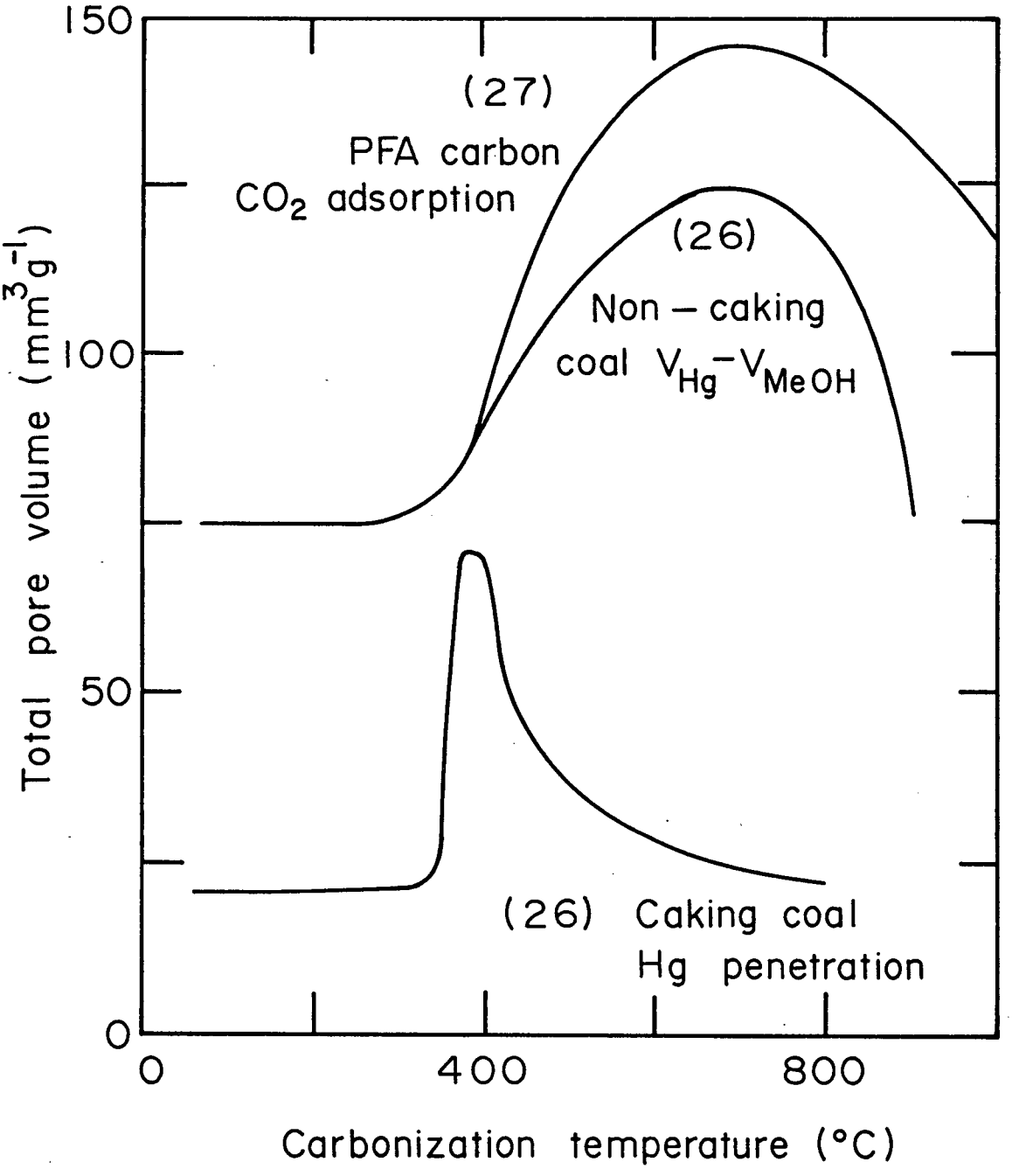

association because fluidity may be somewhat dependent on pore structure which developed with time. They also noted that chloroform-soluble extracts were only a fraction of the metaplast.

In another review, Howard [35] compared Gieseler Plasticity curves at a constant temperature with the rate of formation of chloroform-soluble extract. It was found that the extract was formed much faster than fluidity and concluded that the chloroform extract per se was not responsible for fluidity.

1.4.2 Char-Binder Interaction

As formcoke is a two-phase composite material, final properties are dependent on aggregate-binder interaction. The extent to which the binder phase wets the aggregate controls the spreading and distribution of the binder matrix around the aggregate particles. Char porosity and roughness also influence this binder distribution.

In considering wetting phenomena in the textile industry, Wenzel [36] began with the Young-Dupré equation for equilibrium contact angles:

$$\gamma_{SL} = \gamma_{SV} - \gamma_{LV} \cos \theta$$

where γ is the interfacial energy of the boundaries corresponding to the subscripts: S-solid L-liquid, V-vapour; and θ is the angle between solid and liquid at their point of contact. The physical situation is shown in figure 4.

Figure 4: Schematic Equilibrium Contact Angle Force Balance

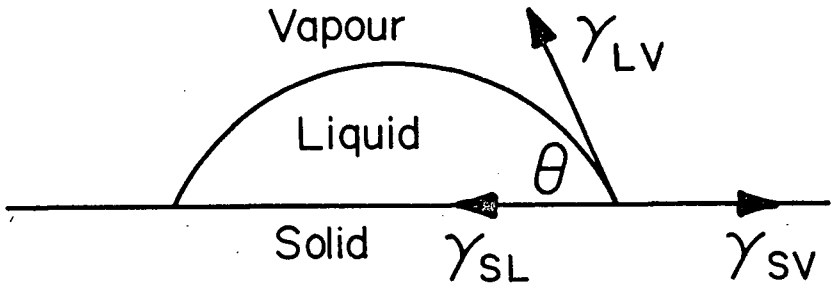

He modified the equation to account for the effect of surface roughness by introducing a roughness coefficient, r, being the ratio of apparent to true contact area

$$\gamma_{SL} = \gamma_{SV} - \frac{\gamma_{LV}}{r} \cos \theta$$

A thermodynamical derivation of this modified form has been given by Good [37]. Adam [38] summarized its importance by stating that the effect of surface roughness was to increase the difference between the contact angle and 90°. That is, if the real angle was less than 90°, the apparent angle would be less than the real value and if the real angle was greater than 90°, the apparent value would be greater than the real value.

Sukhorukov et al. [39] studied the wettability of carbonaceous materials by pitch and found the contact angle decreased sharply with temperature to below 20° in all cases. They considered the effect of capillary penetration, finding a negative capillary pressure up to about 150°C which prevented penetration. However, the pressure was seen to become positive above 150°C and therefore assist the penetration process. The authors also found that a more ordered carbonaceous surface (ranging from crude to calcined petroleum coke to roasted material to artificial graphite) led to a weaker bond, the adhesion forces being van der Waals and chemisorption.

Agrawal and Berkowitz [40] measured equilibrium contact angles between binders made from asphaltic materials and various coal and char substrates. They found that all the binders studied stopped just short of complete wetting and calculated energies of adhesion of around 90 mJm^{-2}.

This was shown to be insensitive to the identity of the substrate. Dmitrieva et al. [41] showed that adhesion energy could be increased by addition of a surface active agent (oleic acid) and Vetyukov et al. [42] have agreed that the nature of the carbon material is relatively unimportant. They concluded that the extent of surface roughness was more important.

Dell and Peterson [43], in studying Soderberg anodes, found that at low temperatures, high viscosity of the binder pitch prevented substantial penetration into remote pores. From the accompanying strength measurements they concluded composite strength was the result of mechanical interlocking of the binder and aggregate. Therefore, a pore structure accessible to the binder was deemed essential for a good bond.

Lahaye and Aubert [44] carried out two investigations into the interaction between a coke and a tar. In the first they studied the effect of the surface chemical state, concluding that as the oxygen surface functions increased, the contact angle decreased. When a critical value of oxygen function was exceeded, the contact angle would remain constant at a low value. This critical value corresponded to that producing complete satisfaction of all possible hydrogen bonds. In the second paper they found the limiting pore diameter into which the tar would penetrate to be 5-6 μm for non-outgassed and 1-2 μm for outgassed char.

Greenhalgh and Moyse [45] showed that penetration of the porous structure would occur for a contact angle less than 90° if given sufficient time. In addition, they found that once the pitch had spread mechanically, it would not recede to its equilibrium contact angle. Chaklader et al. [23] measured contact angles of pitch on various chars and found that the

angle did not drop to zero in all cases. Some systems were seen not to fall below 40°.

1.4.3 Compaction Kinetics

Fitzgerald [46] has modelled the viscoelastic response of a caking coal in the plastic state to an applied stress using a series coupling of a Maxwell and a Kelvin element. He suggested the retarded elasticity observed in the coal was associated with the many possible configurations of the cross links between molecular lamellae. Habberjam [47] studied compaction of binderless char mixtures at the carbonization temperature. A model was developed employing two Kelvin elements and an additional spring in series.

In an attempt to determine if compaction behaviour observed in char systems was due to the presence of a viscoelastic component, Jayasinghe and Pilpel [48] coated char particles with a viscoelastic polymer, polyisobutane. They found close correlation between the model system and char behaviour, concluding a thin film of viscoelastic material is formed on the char surface during compaction. Bradford et al. [49] measured electrical resistance and change in volume with pressure to investigate particle behaviour during compaction. They found that without a binder, deformation of the particles was elastic (shape altering), but with sufficient binder present, compaction was isostatic and relatively small. A critical binder content of 27% was found necessary to obtain the latter condition.

Recently, Collett and Rand [50] have indicated that coal-tar pitch can be considered a Newtonian liquid at low temperatures, but non-Newtonian above 380°C. They suggested pitch be thought of as an emulsion: initially

as one of mesophase in an isotropic liquid and then as one of isotropic liquid in mesophase as temperature rises.

The above models were concerned with binderless systems or idealized aggregate-binder materials. Chow et al. [51] developed a hot compaction model for char-binder coal systems (the CCWL model). They found that experimental compaction curves could be fitted satisfactorily with an equation expressing compaction strain, ε_t, as the sum of three exponential time terms:

$$\varepsilon_t = k\ (1 - Ae^{-\alpha t} - Be^{-\beta t} - Ce^{-\gamma t})$$

where k, A, B, C, α, β and γ are experimentally determined constants.

A third order differential equation, shown below, was generated from the experimental equation following the procedure described by Bradbeer and Chaklader [52].

$$\dddot{\varepsilon} + M\ddot{\varepsilon} + N\dot{\varepsilon} + T\varepsilon = P\ddot{\sigma} + Q\dot{\sigma} + R\sigma$$

Various mechanical analogs consisting of spring and dashpot combinations were considered and it was found that the response of a series coupling of three Kelvin viscoelastic elements (each being a spring and dashpot in parallel) to an applied stress was given by an equivalent expression. This model is shown schematically in figure 5. In employing this mechanical analog, it was recognized that for the case of successive element half-lives, the three model elements could be considered non-interacting. The values of the model parameters, η_1, η_2, η_3, M_1, M_2 and M_3, were determined from the experimental constants, k, A, B, C, α, β, and γ, which were determined from the isothermal compaction curves.

Based on the observation that only two of the Kelvin elements were

Figure 5: Schematic Representation of the Mechanical Analog of the CCWL Hot Compaction Model

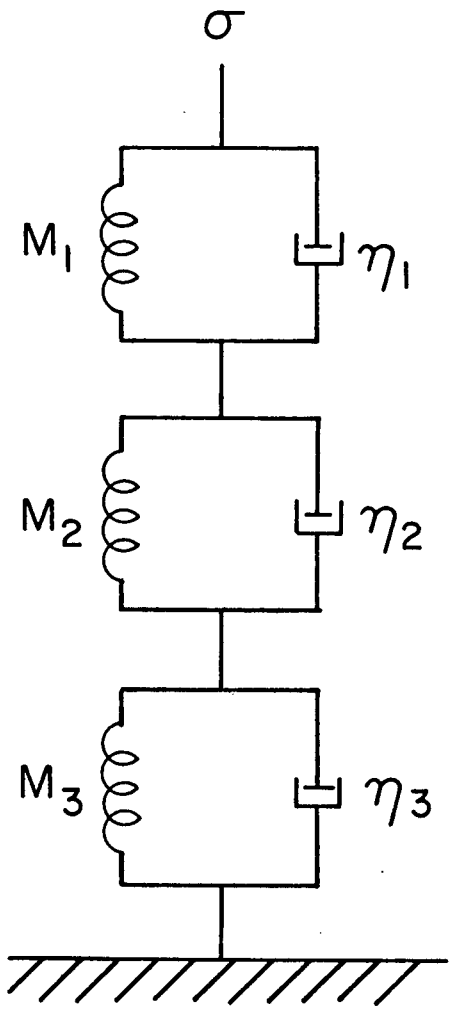

temperature sensitive, it was concluded that the model elements could be associated with one of three compaction mechanisms: instantaneous system compaction, particle flow and plastic deformation. The half-lives of these elements were suggested to be 0; 0.5; and 3-10 minutes, respectively. A more thorough derivation of this model is presented in Appendix A.

1.5 Objectives of Present Study

Despite the importance of the mechanical stability of formcoke in the blast furnace, no comprehensive study of the influence of ingredient mechanical parameters on formcoke composite strength has been reported. The effects of carbonization conditions on char properties have been studied; experimental techniques have been developed to quantify binder characteristics; and char binder interactions have been investigated. However, these have generally been individual studies of different parameters in varying systems.

The object of this work is to study the fundamental relationships between the aggregate and binder material characteristics and the formcoking process and its final product. This is carried out by investigating two ways in which material properties can affect the final briquette product:

1) by influencing the compaction kinetics of the briquetting process; and

2) by directly influencing the physical nature of the final briquette product.

2. EXPERIMENTAL

A non-caking coal char aggregate-caking coal binder system was chosen for study. Commercial process of this type have shown promise [8,12] and this type of system is suited to the Canadian coal resource situation. The experimental variables involved were identified as:

Aggregate Phase

Independent Variables (controlled)

(i) rank of parent coal
(ii) carbonization atmosphere
(iii) carbonization heating rate
(iv) maximum carbonization temperature
(v) soaking time at maximum temperature

Dependent Variables (measured)

(vi) char strength (hardness and density)
(vii) char porosity
(viii) equivalent char rank (residual volatile matter content)

Binder Phase

Independent Variable (controlled)

(ix) rank of binder coal

Dependent Variables (measured)

(x) caking properties
(xi) strength after briquetting

Briquettes

Independent Variables (controlled)

(xii) aggregate-binder ratio
(xiii) particle size distribution

(xiv) charge size
(xv) briquetting heating rate
(xvi) briquetting maximum temperature
(xvii) briquetting pressure
(xviii) duration of briquetting at temperature and pressure

Dependent Variables (measured)

(xix) aggregate-binder wetting conditions
(xx) mixture viscosity under compaction conditions
(xxi) briquette bulk porosity
(xxii) briquette strength

All independent variables except aggregate carbonization temperature and binder coal rank (variables (iv) and (ix)) were held constant at the values given in Table II. In the case of briquetting temperature, the temperature at which the mixture exhibited the greatest fluidity was used. This was found to be constant for a given binder. The higher briquetting pressure for mixtures containing binder B2 was necessary to produce coherent briquettes of comparable bulk porosity.

Varying the aggregate charring temperature and the coal used as binder, produced variations in the mechanical properties of the system which were characterized and compared to identify those properties influencing briquette strength. Characterization was performed as follows.

TABLE II

VALUES OF FIXED EXPERIMENTAL PARAMETERS

PARAMETER	VALUE
CARBONIZATION:	
HEATING RATE	6°C min^{-1}
TIME AT TEMP.	120 min
ATMOSPHERE	Argon
BATCH SIZE	ca. 40 g
BRIQUETTING:	
HEATING RATE	80°C min^{-1}
TEMPERATURE	B1 - 430°C B2 - 500°C B3 - 480°C
PRESSURE	10 MPa (13.8 MPa for B2)
TIME AT TEMP. AND PRESSURE	3 min
CHARGE SIZE	0.75 g

2.1 Aggregate Char Characterization

The aggregate phase of the briquetting mixtures was produced by carbonization of a high volatile sub-bituminous coal which had a low inherent moisture content and a lustrous non-banded appearance. The proximate analysis of this coal is given in Table III.

TABLE III

PROXIMATE ANALYSES OF COALS USED

	COAL FOR CHAR	COAL FOR B1	COAL FOR B2	COAL FOR B3
Moisture (%)	20.3	1.2	0.8	0.9
Ash (dry basis %)	6.0	3.2	9.0	3.8
Volatile Matter (db %)	42	34.3	21.1	22.0
Fixed Carbon (db %)	52	62.5	69.9	74.2

The coal was initially broken to -10 + 4 mm. This material was weighed into a standard No. 13 porcelain boat, batch sizes being approximately 40 grams, and placed in the 50 mm diameter tube furnace. With the sample thermocouple buried in the coal and the furnace ends sealed, the tube was flushed with argon for 30 minutes. The programmed controller was then engaged to bring the charge up to the selected charring temperature at the constant rate of 6 ($\pm$0.2)°C min^{-1}. A slow argon flow was maintained throughout the carbonizing/cooling cycle to prevent oxidation and to remove the volatile matter evolved.

The charring temperatures selected were 500°C, 625°C and 750°C, while soaking time at temperature was kept constant at the specified two

hours. With the apparatus employed, it was not possible to accurately attain the programmed temperature, but it was possible to accurately measure the temperature reached. Hence, charring temperatures varied up to 13°C from the selected value. The temperature at the ends of the boat was approximately 20°C lower than at the centre. The sample thermocouple was located at the boat centre.

After a two hour soaking at temperature, the furnace was shut off and the sample was allowed to cool under a slow argon flow with the furnace sealed. This cooling time was of the order of 15-18 hours. The char product was weighed after removal from the furnace to determine the weight loss due to devolatilization. Nine char batches were produced at 750°C and five were produced at each of 625°C and 500°C.

2.1.1 Hardness

From each char batch, six specimens of approximately 5 mm size were selected and mounted in a quick-set mounting block. These were then polished to a 5 μm - alumina finish. A thin film of carbon soot was deposited on the surface by passing the block through a candle flame. This allowed the diamond pyramid indentation made by a Tukon Microhardness Tester to be seen. An indentor weight of 300 g and a magnification of 20X were used. With this technique it was also possible to discern an elastic component in the char's response to the indentation.

Three separate hardness measurements were taken on each of the six pieces of char in the samples, although some pieces were of too high a porosity to provide a suitable surface for hardness measurement. Only the permanently deformed portion of the indentation was used in determining the DPH value. However, the amount of the indentation which appeared to

be elastic in nature was also recorded. This was done by recording the diagonals of the permanent indentation as a percentage of the diagonals of the area of the soot film disturbance.

2.1.2 Density

Approximately 2 grams of each char batch was used in the determination of true density. This was the density as measured when the entire pore structure was open to the measuring fluid. To eliminate any closed porosity in the sample, the char was ground to less than 75 μm and weighed into a 25 ml pycnometric flask. The sample was covered with the measuring fluid, methanol, and evacuated to remove any trapped air and promote complete penetration of the sample by fluid. The true density of the char was calculated in the following manner:

$$\text{Density} = \frac{W_2 - W_1}{\frac{(W_4 - W_1)}{\rho_{CH_3OH}} - \frac{(W_3 - W_2)}{\rho_{CH_3OH}}}$$

where: W_1 = Weight of Pycnometer
W_2 = Weight of Pycnometer + Sample
W_3 = Weight of Pycnometer + Sample + Fluid
W_4 = Weight of Pycnometer filled with Fluid alone
$\rho_{CH_3OH} = 0.792 \text{ g cm}^{-3}$

2.1.3 Porosity

Other char pieces were also used as specimens in the determination of char porosity. For these experiments a Micromeritics Model 910 Mercury Penetration Porosimeter was used. This technique involved measuring the volume of mercury forced into the pore structure of the sample as a function of the isostatic pressure applied to the system. Total pore volumes were equated to the penetrated mercury volume up to the maximum pressure of 345 MPa (50,000 psi). Quantitative values of pore sizes and

pore size distributions could be made based on assumptions of a constant mercury-sample contact angle (130°) and the geometry of pore cross-section (circular). Five runs were carried out on each char type.

The remaining material was mixed according to charring temperature producing, from nineteen individual char batches, three char types: 500°C, 625°C and 750°C. Each of these was ground and separated into three size fractions: -300 + 150 μm; -150 + 75 μm and -75 + 37 μm. The fractions were then remixed in selected proportion to produce the three Aggregate Batches used in the briquetting program:

Aggregate Batch, A1:	50% - 300 + 150 μm 750°C char
	35% - 150 + 75 μm 750°C char
	15% - 75 + 37 μm 750°C char
Aggregate Batch, A2:	50% - 300 + 150 μm 625°C char
	35% - 150 + 75 μm 625°C char
	15% - 75 + 37 μm 625°C char
Aggregate Batch, A3:	50% - 300 + 150 μm 500°C char
	35% - 150 + 75 μm 500°C char
	15% - 75 + 37 μm 500°C char

2.2 Binder Coal Characterization

The binder phase of the briquetting mixtures was composed of one of three caking coals which when heated was expected to fluidize and flow around the char aggregate. These were: (i) a high volatile bituminous; (ii) a low volatile bituminous with relatively high ash and poor caking quality; and (iii) a low volatile bituminous with lower ash and better caking properties. These were designated as binders B1, B2 and B3, respectively. Their proximate analyses are given in Table III while their plastic properties (in terms of Gieseler Plasticity and Ruhr Dilatometer data) as determined by the Energy Research Laboratory, Ottawa, are presented in Table IV.

TABLE IV

GIESELER PLASTICITY AND RUHR DILATOMETER DATA

GIESELER PLASTICITY

	B1	B2	B3
Start of plastic range (°C)	402	444	423
Fusion temperature (°C)	417	-	437
Temp. of maximum fluidity (°C)	442	465	462
Final fluid temperature (°C)	472	483	492
Solidification temperature (°C)	476	492	494
Melting range (°C)	70	39	69
Maximum fluidity (dd m^{-1})	994	4.6	127
Torque (g in.)	40	40	40

RUHR DILATOMETER

	B1	B2	B3
Softening temperature, T_i (°C)	355	409	390
Maximum contraction temp., T_{ii} (°C)	419	474	441
Maximum dilatation temp., T_{iii} (°C)	457	-	474
Maximum contraction (%)	27	22	25
Maximum dilatation (%)	109	61	39

Initially, each binder was ground and separated into the same size fractions and remixed in the same proportion as were the aggregate batches:

Binder Batch, B1: 50% - 300 + 150 μm hvb coal
35% - 150 + 75 μm hvb coal
15% - 75 + 37 μm hvb coal

Binder Batch, B2 50% - 300 + 150 μm lvb (poor caking) coal
35% - 150 + 75 μm lvb (poor caking) coal
15% - 75 + 37 μm lvb (poor caking) coal

Binder Batch, B3: 50% - 300 + 150 μm lvb (good caking) coal
35% - 150 + 75 μm lvb (good caking) coal
15% - 75 + 37 μm lvb (good caking) coal

This ensured that the briquetting mixtures would be of a constant particle size distribution and therefore of a constant packing density. In addition to these aggregate and binder characterizations, it was necessary to investigate the nature of the aggregate-binder interface.

2.3 Char-Binder Interaction

Three experiments were performed to characterize the char-binder interface:

i) The effect of physical interlocking of binder and aggregate was studied by measuring the strength of a bond between a binder and a model carbonaceous material (graphite) with varying degrees of surface roughness.

ii) The wettability of the chars was studied using a model binder material (an SRC pitch) on different char surfaces to study the effect of variation in char on the wetting characteristics of the system.

iii) Since a number of previous works had indicated a correlation between the plastic mesophase and the organic solvent soluble fractions formed at carbonization temperatures, the wetting behaviour of one of

these fractions (benzene-soluble) on a model substrate (amorphous carbon) was also studied.

2.3.1 Interfacial Strength

For this study, a set of 6.5 mm diameter graphite rods was used, the surfaces of which were prepared in one of three ways:

1) Polished with a soft cloth to yield a visually smooth surface.

2) Polished and then grooved radially with a razor blade (approximately 1 mm spacing between grooves).

3) Polished and then roughened with 100 grit sandpaper in a radial manner.

These were placed in graphite moulds as shown in figure 6. Five grams of a binder was added and the arrangement was heated to the plastic range of the binder phase and allowed to cool. The specimen was then supported by a flat disc with a 10 mm diameter hole through the center and the graphite rod was pushed out using an Instron machine with an FR tension-compression cell under the following conditions: full scale load 200 lb (900 N); cross-head speed 0.005 in. (0.127 mm) min^{-1}; chart speed 5 in (127 mm) min^{-1}.

The area of contact between binder and rod was measured as follows:

$$A = \text{surface area of rod embedded in binder}$$

$$= \pi \cdot (\text{Diameter of rod}) \cdot (\text{Depth of rod in binder})$$

$$= 20.42\ (\text{Depth}) \times 10^{-6}\ m^2$$

The strength of the bond (in shear) was calculated by:

$$S = \frac{\text{load to failure}}{A}$$

Binder B2 was used in this study. Binders B1 and B3 were found to be unsuitable because their high fluidities led to frothing during devolatilization.

Figure 6: Schematic Diagram of Binder-Graphite Rod Interfacial Strength Specimen

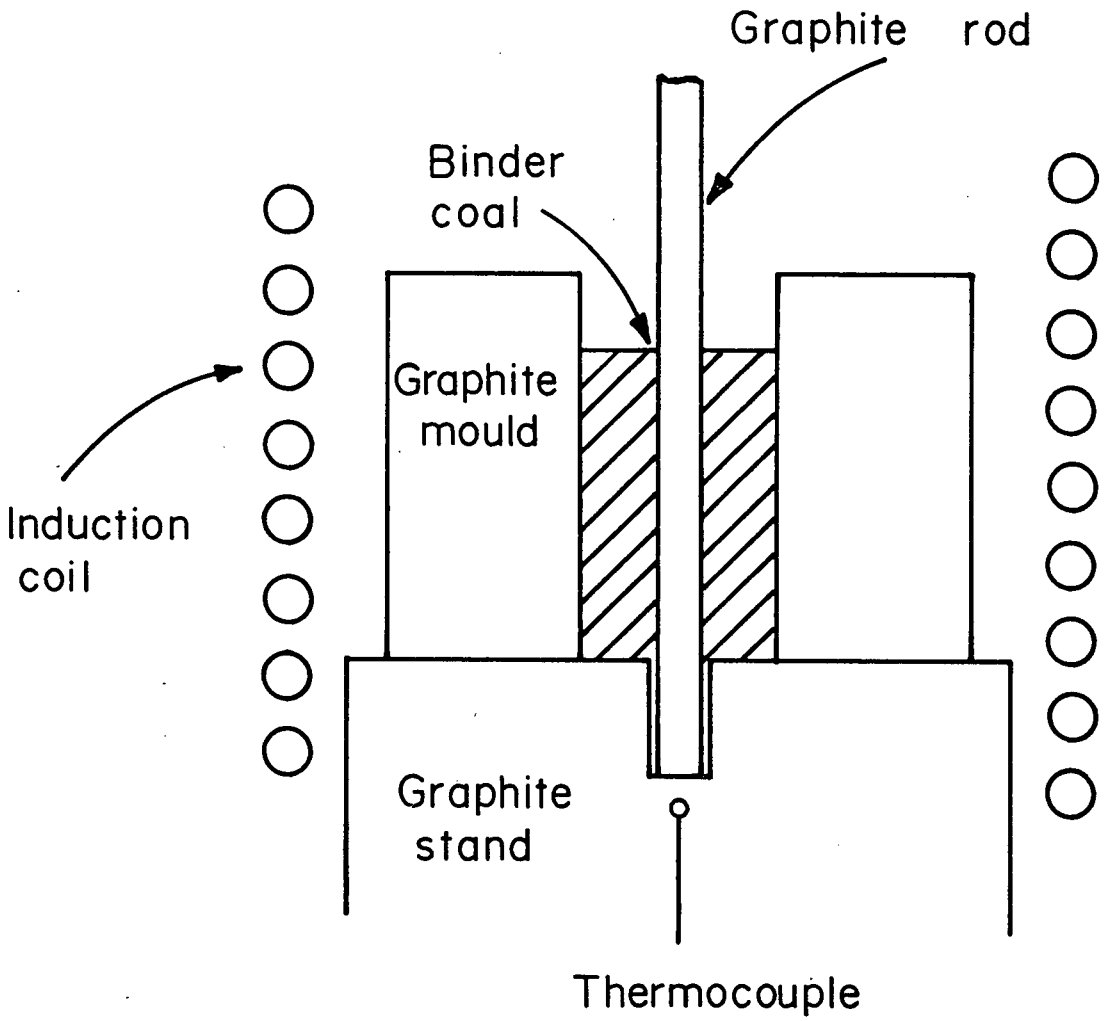

2.3.2 Wettability of Chars

In another set of experiments the wettability of the three char types by a single model binder was studied. The model binder used was an SRC pitch, the same material used in previous studies [23] on wettability of various char substrates. Samples of each char type were polished flat and used as substrates onto which the SRC pitch binder was placed. Contact angle measurement was carried out as follows.

The binder pitch was placed on a char substrate and inserted in a standard sessile drop apparatus (figure 7).

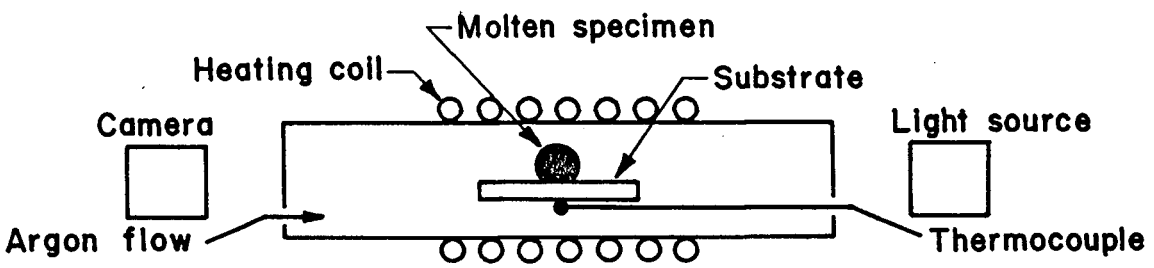

Figure 7: Schematic Diagram of Sessile Drop Apparatus

The power supplied to the resistance heating coil was adjusted to increase the temperature in a step-wise manner while the system was continually flushed with argon. By aligning the system so that the camera-furnace-light source axis fell in the plane of the substrate, an accurate photographic record of the contact angle between extract and substrate was produced.

2.3.3 Wetting Behaviour of Coal Extracts

The wetting behaviour of the benzene-soluble fraction of each binder was investigated. A five-gram sample of each binder batch was placed in a No. 5 porcelain crucible and set in the charring furnace. After flushing with argon for 30 minutes, the sample was brought to its

temperature of maximum fluidity at a heating rate of approximately 70°C min^{-1}. The sample was held at this temperature for ten minutes and then withdrawn from the furnace and cooled quickly.

The cooled material was first coarsely ground and dried at 110°C for one hour and then ground further to pass a 75 μm screen. Extraction of the benzene soluble fraction was accomplished by placing the ground material in a 25 ml soxlet thimble, inserting it in the soxlet-type apparatus and refluxing with 50 ml benzene for approximately 25 hours. With the water bath maintained at 98°C the benzene was seen to circulate freely through the reflux cycle. The extract containing solution was poured into a watchglass and the excess benzene removed by evaporation. The extract left was scraped from the watchglass, weighed and pressed into cylindrical pellets approximately 4 mm in diameter and 10 mm long.

The extract pellet was placed on a 10 mm x 15 mm substrate of vitreous carbon. This was inserted in the sessile drop apparatus shown in figure 7 and the relationship between contact angle and temperature was determined in the manner described above.

2.4 The Briquetting Program

Nine briquetting mixtures were made from combinations of the three aggregates and three binders. These are summarized in Table V. In each case the proportion was 70% aggregate char to 30% binder coal by weight.

The briquetting apparatus is shown in figure 8. Approximately 0.75 g of a mixture was poured into the die assembly which was then set in the hot pressing arrangement shown in the figure. The powder was initially compacted cold by the same pressure as was to be used during the briquetting stage. Power was supplied to the inductive heating unit so

TABLE V

CHAR-BINDER COMPOSITION
OF BRIQUETTING MIXTURES USED

		AGGREGATE		
		A1	A2	A3
BINDER	B1	MIX 1	MIX 4	MIX 7
	B2	MIX 2	MIX 5	MIX 8
	B3	MIX 3	MIX 6	MIX 9

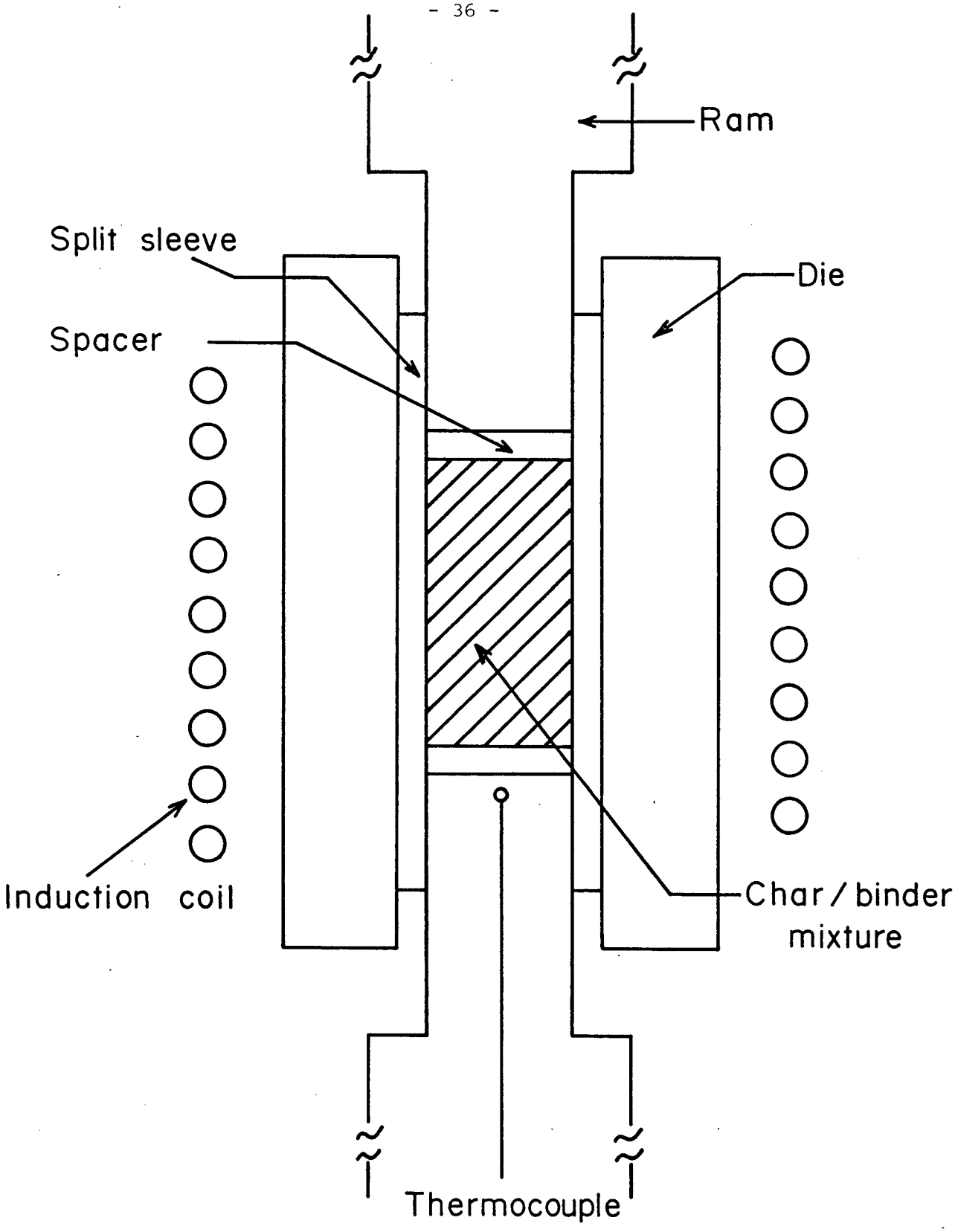

Figure 8: Schematic Diagram of Briquetting Apparatus

as to maintain a constant heating rate of approximately 80°C min^{-1} up to the maximum fluidity temperature of the binder being used. This was found to be 430°C, 500°C and 480°C for binders B1, B2 and B3, respectively. Upon reaching this temperature a compacting pressure of 10 MPa was applied and a constant temperature was maintained. In the case of binder B2 mixtures, where a 10 MPa pressure was found to be insufficient to produce briquettes of comparable bulk density, the pressure was increased to 13.8 MPa. A pressing time of three minutes was used in all cases. The cylindrical briquette product was approximately 10 mm in diameter and 8 mm in length.

Compaction was recorded as a function of time on a Sargent model SR strip chart recorder. This was calibrated to give a 10 mm pen deflection for a 0.25 mm compaction and the chart was run at 1.0 in (25.4 mm) min^{-1}. Volume and weight measurements were taken to determine bulk densities and bulk porosities based on the true densities determined in the previous section.

2.5 Briquette Strength

The Ultimate Compressive Strength (UCS) of each briquette was determined using an Instron testing machine. An FR tension-compression cell was used with a full scale load of 500 lb. (2240 N). A cross-head speed of 0.01 in min^{-1} (0.254 mm min^{-1}) and a chart speed of 5 in min^{-1} (127 mm min^{-1}) were used.

An ETEC Autoscan Scanning Electron Microscope was used to investigate the nature of the aggregate-binder interface, the aggregate particles themselves and the fracture behaviour of a number of briquettes. It was necessary to deposit a thin gold film on the surface of the specimens

due to the non-conducting nature of the ash content. A 20 kV excitation voltage was employed.

3. RESULTS AND ANALYSES

3.1 Char Characterization

The char material used was characterized by four parameters: density, hardness, porosity and residual volatile matter content. The relationships between these measured parameters and the independent variable-charring temperature, are presented in figures 9-14. A significant amount of scatter can be seen in each of these plots due to the heterogeneity of the material being studied. Coal is a complex mixture of many components and therefore the statistical significance of the results obtained must be considered. Despite this experimental difficulty, changes in characteristics from char to char are apparent.

3.1.1 Density

The results of the pycnometric density measurements are shown in figure 9. The indicated increase in true density with carbonization temperature is in agreement with previous studies [6,24,25] mentioned earlier. Char density follows a sigmoid behaviour, increasing from that of the untreated coal (1.4 g cm^{-3}) to that of amorphous carbon (1.8-2.1 g cm^{-3}) produced at temperatures in excess of 1000°C.

3.1.2 Hardness

The variation of char microhardness with charring temperature is shown in figure 10 where 136° Diamond Pyramid Hardness is plotted against temperature. Increasing hardness is seen to accompany an increase in

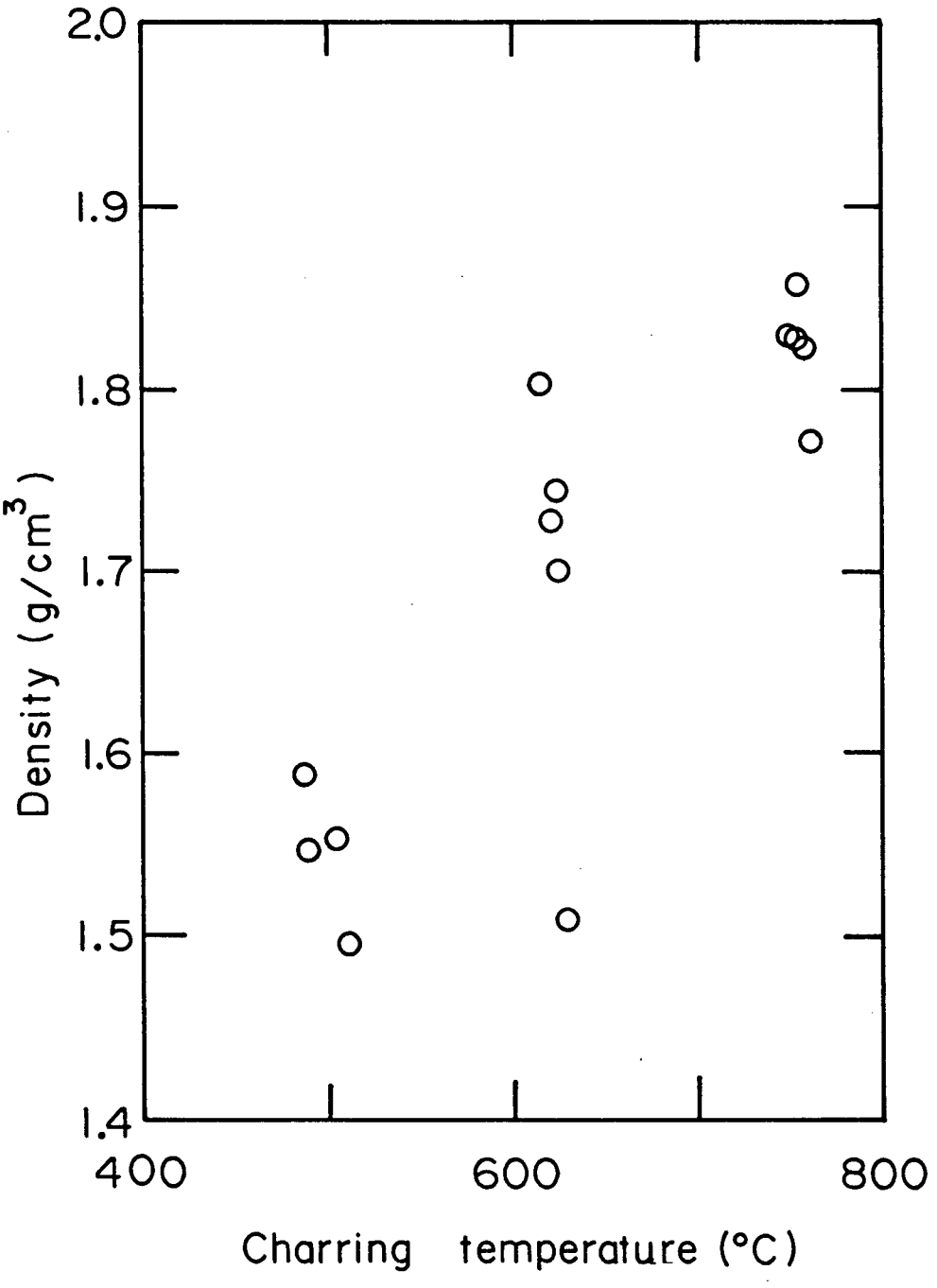

Figure 9: Relationship Between True Char Density and Charring Temperature

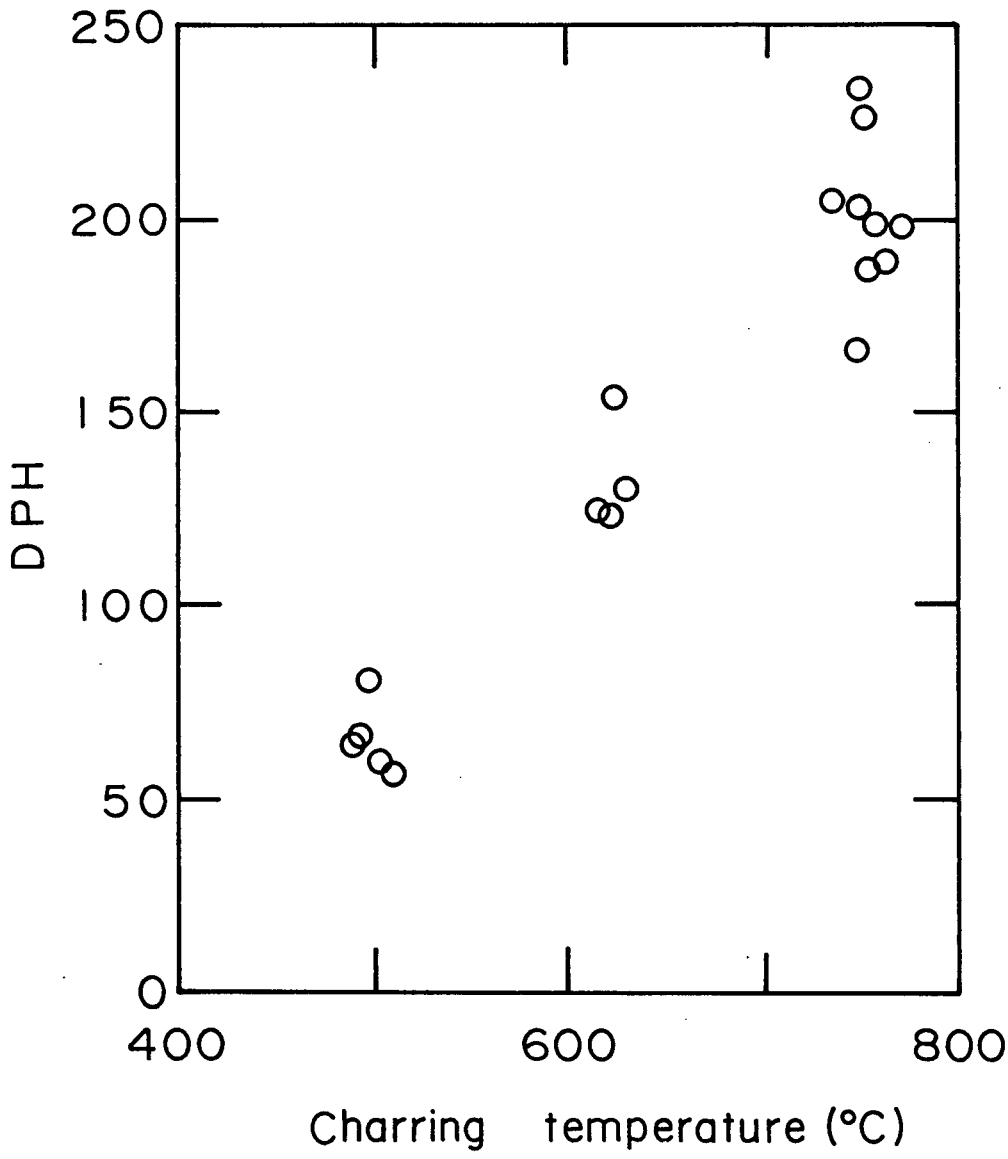

Figure 10: Relationship Between Char Microhardness and Charring Temperature

carbonization temperature, the relationship being linear over the range considered. Each point on this plot represents the mean of between 10 and 18 microhardness readings. This variation was due to excessive char porosity preventing testing on some samples.

The elastic behaviour of the char in microhardness testing is shown in figure 11 as a function of charring temperature. This was quantified as percentage of the area disturbed by the indentor which recovered elastically. Figure 12 shows a photomicrograph (1400X) of a DPH indentation. The inner rectangle is the permanent deformation from which the hardness values of figure 10 were determined. The outer rectangle marks the extent of the area disturbed by the indentor. The elastic nature of response to indentation was found to increase with charring temperature.

3.1.3 Porosity

The penetration porosimetry technique allows determination of pore size distribution in the char based on two assumptions. The contact angle of mercury on the samples must be known; it was taken in the present case to be 130°. The pore geometry must also be known. A circular cross-section was assumed and plots of cumulative pore volume against pore diameter were produced. These are presented in figures 13a, b and c, where upper and lower bounds are shown.

Both mean pore size and total pore volume were shown to decrease with increasing charring temperature. Table VI shows average pore volumes above various pore diameters. It is seen that the highest temperature char (750°) has virtually no pore structure above 1 μm diameter. Figure 14a and b show the type of pore structure found in chars A3 and A1, respectively.

Figure 11: Relationship Between Elastic Behaviour of Char in Microhardness Test and Charring Temperature

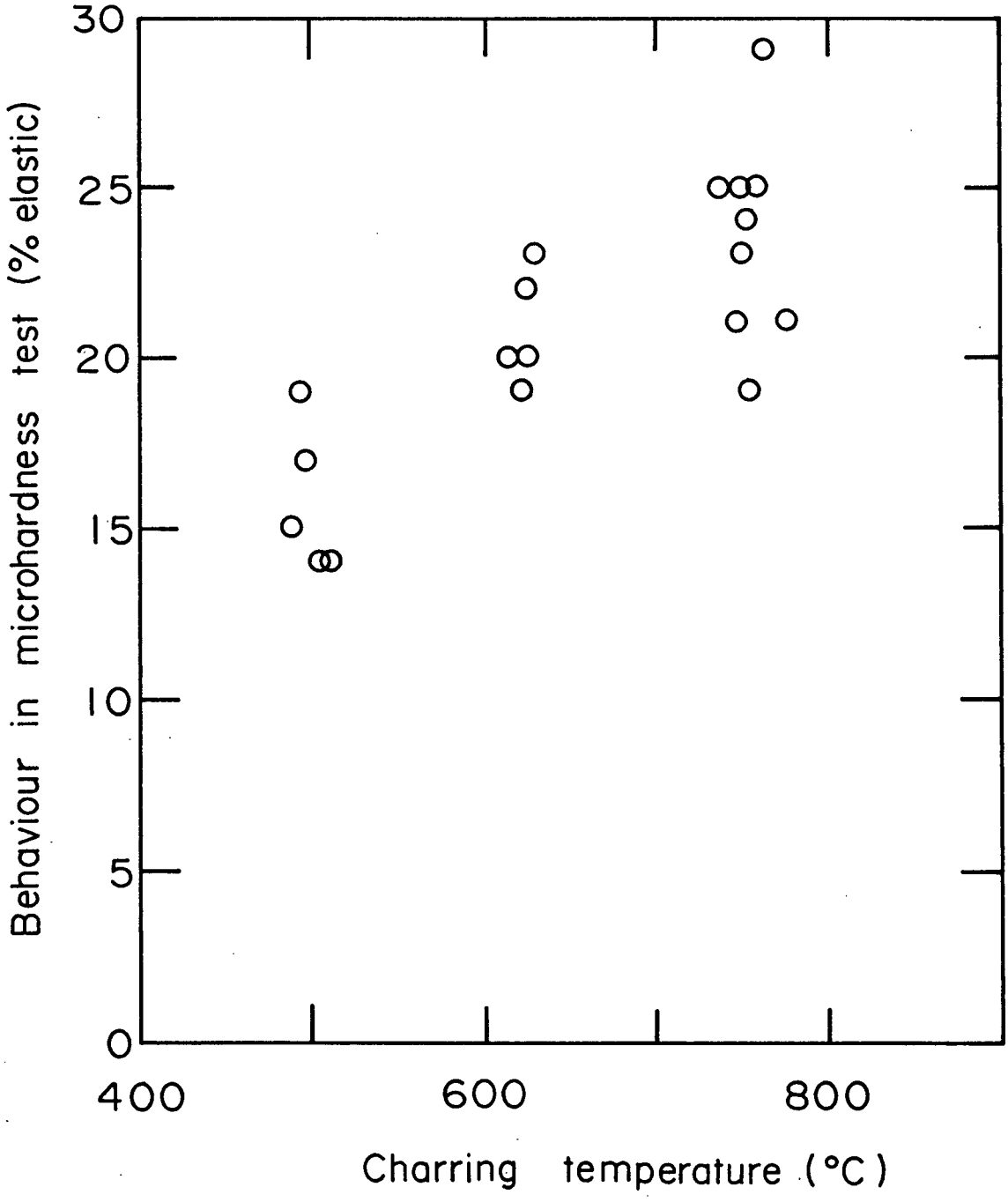

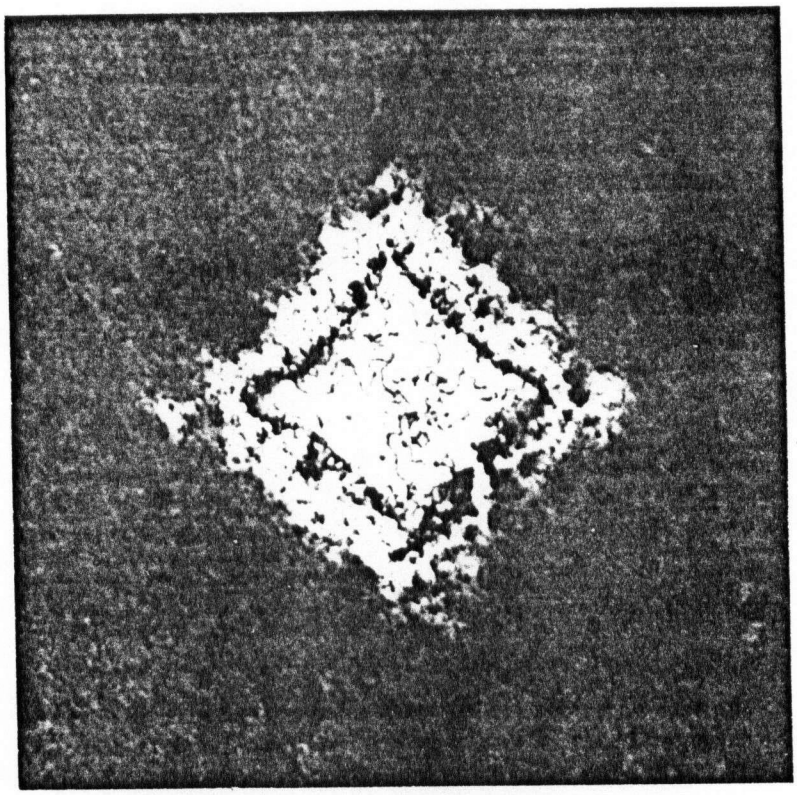

Figure 12: Photomicrograph of Microhardness Indentation (1400X)

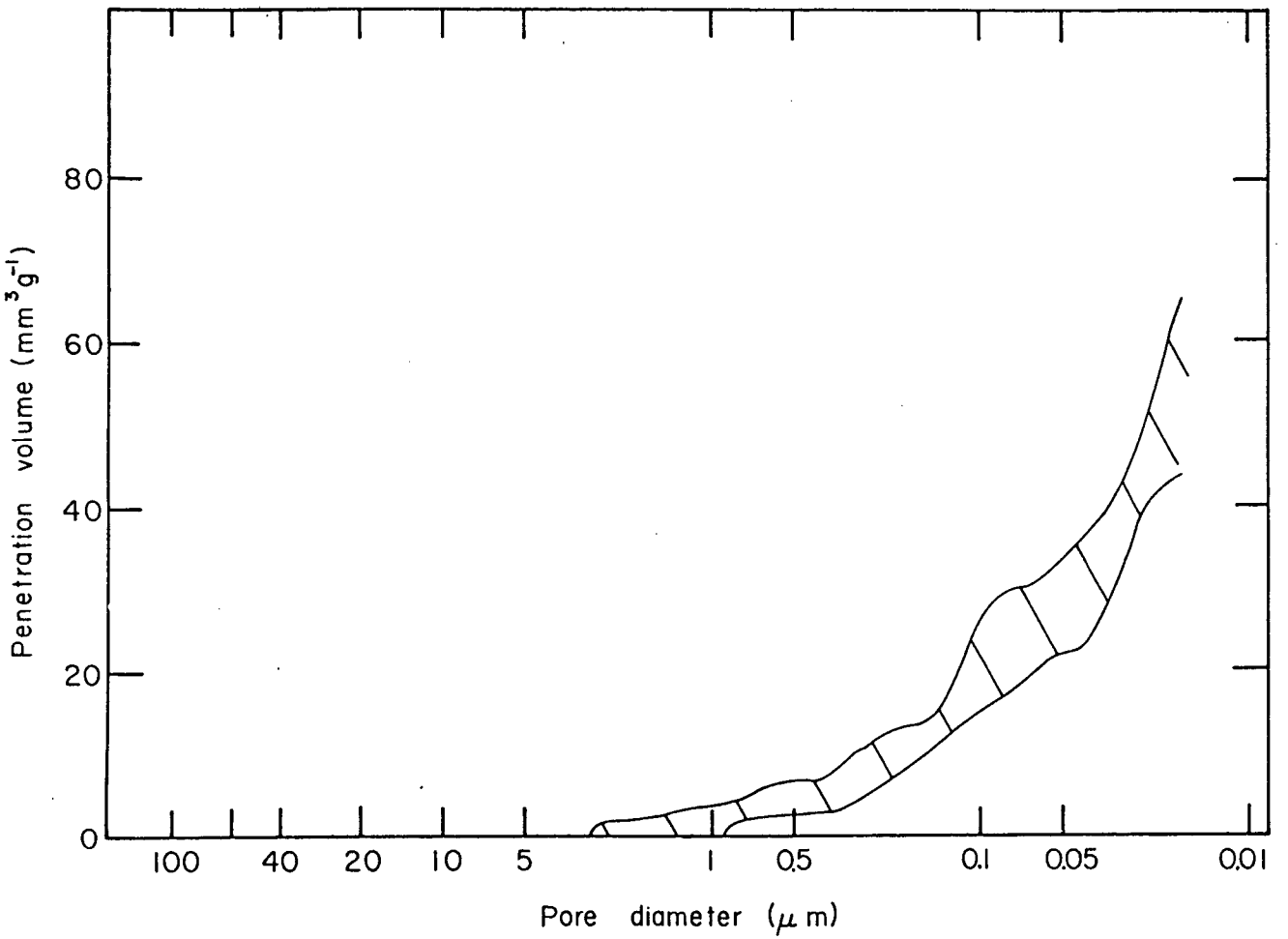

Figure 13a.: Cumulative Pore Size Distribution for Char A1 (Carbonized at 750°C)

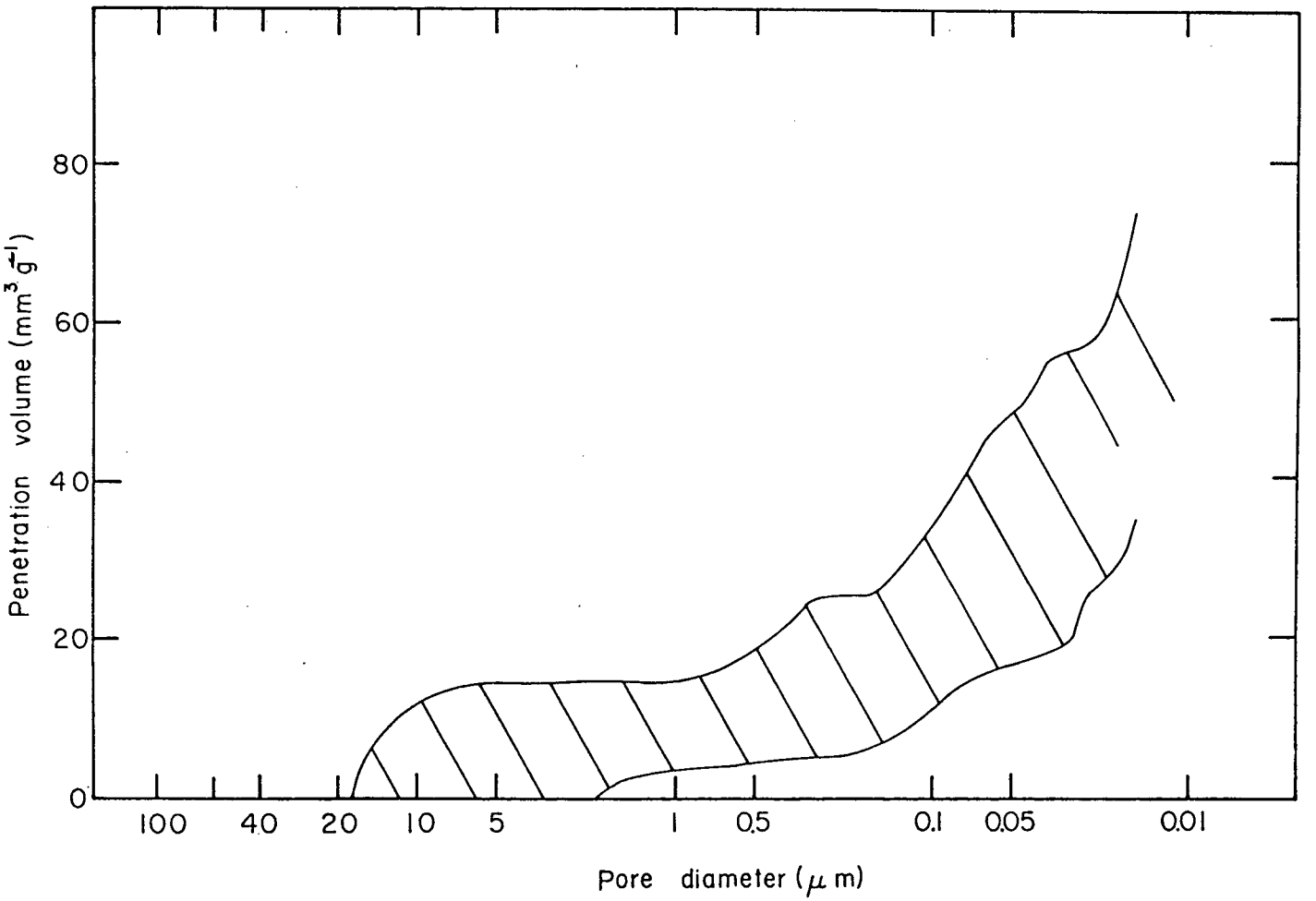

Figure 13b.: Cumulative Pore Size Distribution for Char A2 (Carbonized at 625°C)

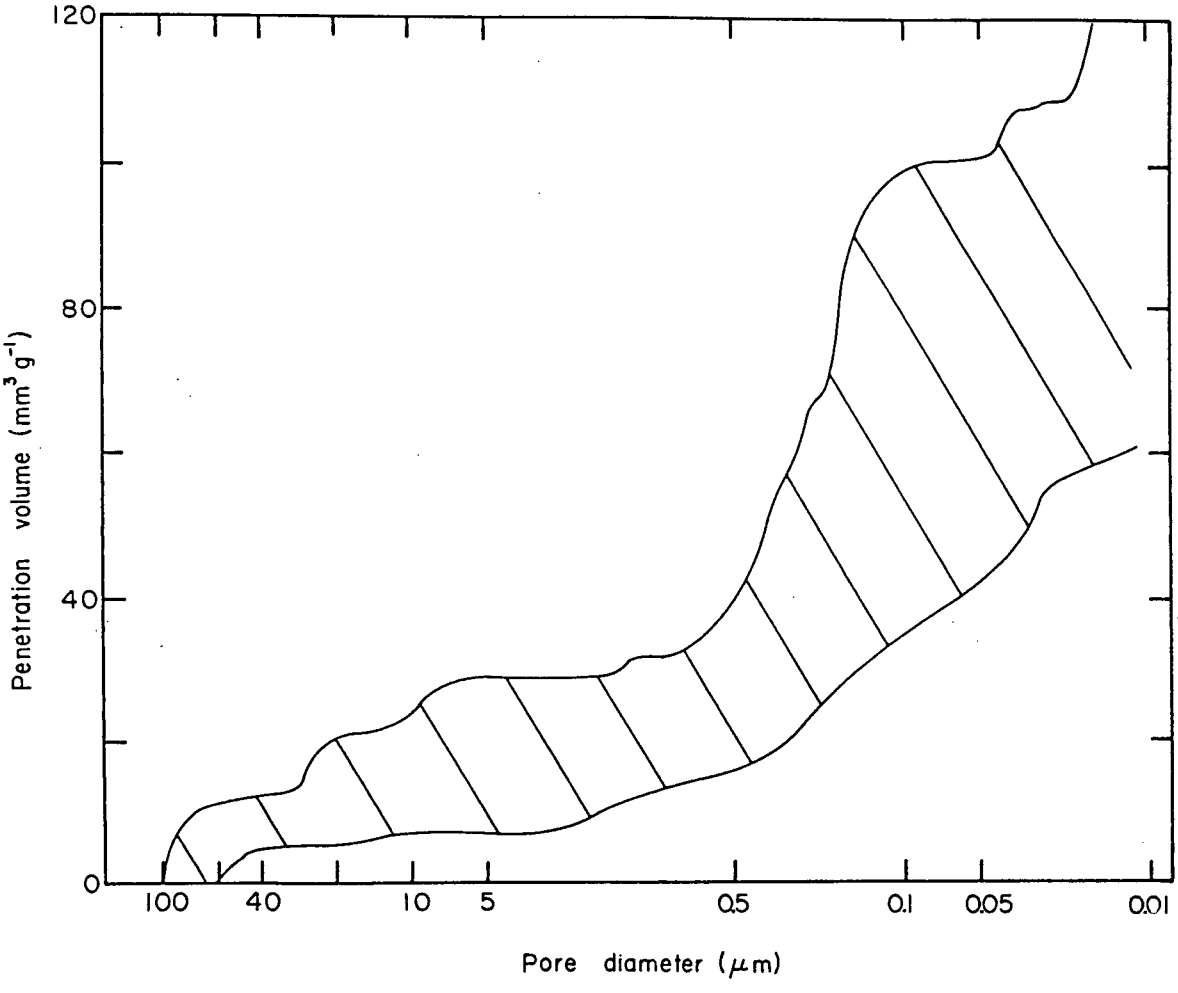

Figure 13c.: Cumulative Pore Size Distribution for Char A3 (Carbonized at 500°C)

TABLE VI

VOLUME CONTAINED IN AGGREGATE-CHAR PORES ABOVE GIVEN DIAMETERS

DIAMETER (μm)	A1 (750°C) ($mm^3\ g^{-1}$)	A2 (625°C) ($mm^3\ g^{-1}$)	A3 (500°C) ($mm^3\ g^{-1}$)
15	0	4	14
5	0	7	18
1.0	2	10	22
0.1	20	23	67
0.01	54	55	90

Figure 14a.: Photomicrograph Showing Macropore in Char A3 (Carbonized at 500°C) (160X)

Figure 14b.: Photomicrograph Showing Micropores in Char A1 (Carbonized at 750°C) (16800X)

3.1.4 Residual Volatile Matter Content

The residual volatile matter (RVM) content of the char decreased with increasing carbonization temperature. This effect can be seen in figure 15 where RVM, being the difference between volatile matter content of the char and that of the original coal (42%), is plotted against charring temperature. The RVM content appears to follow a linear relationship, falling from 42% with no heat treatment to approximately zero at carbonization temperatures above 1000°C.

3.2 Char-Binder Interaction

The interfacial strength measurements showed the binder-graphite bond to be very weak. The shear strengths measured for specimens with different surface preparations are presented in Table VII.

Graphite Rod Preparation	Maximum (Load) (N)	Calculated Area of Contact (mm^2)	Interfacial Strength (kPa)
Polished	16	525	30
Grooved	29	435	67
Roughened	49	470	104

TABLE VII: INTERFACIAL SHEAR STRENGTH OF BINDER-GRAPHITE ROD SPECIMENS

Figure 15: Relationship Between Residual Volatile Matter Content of Char and Charring Temperature

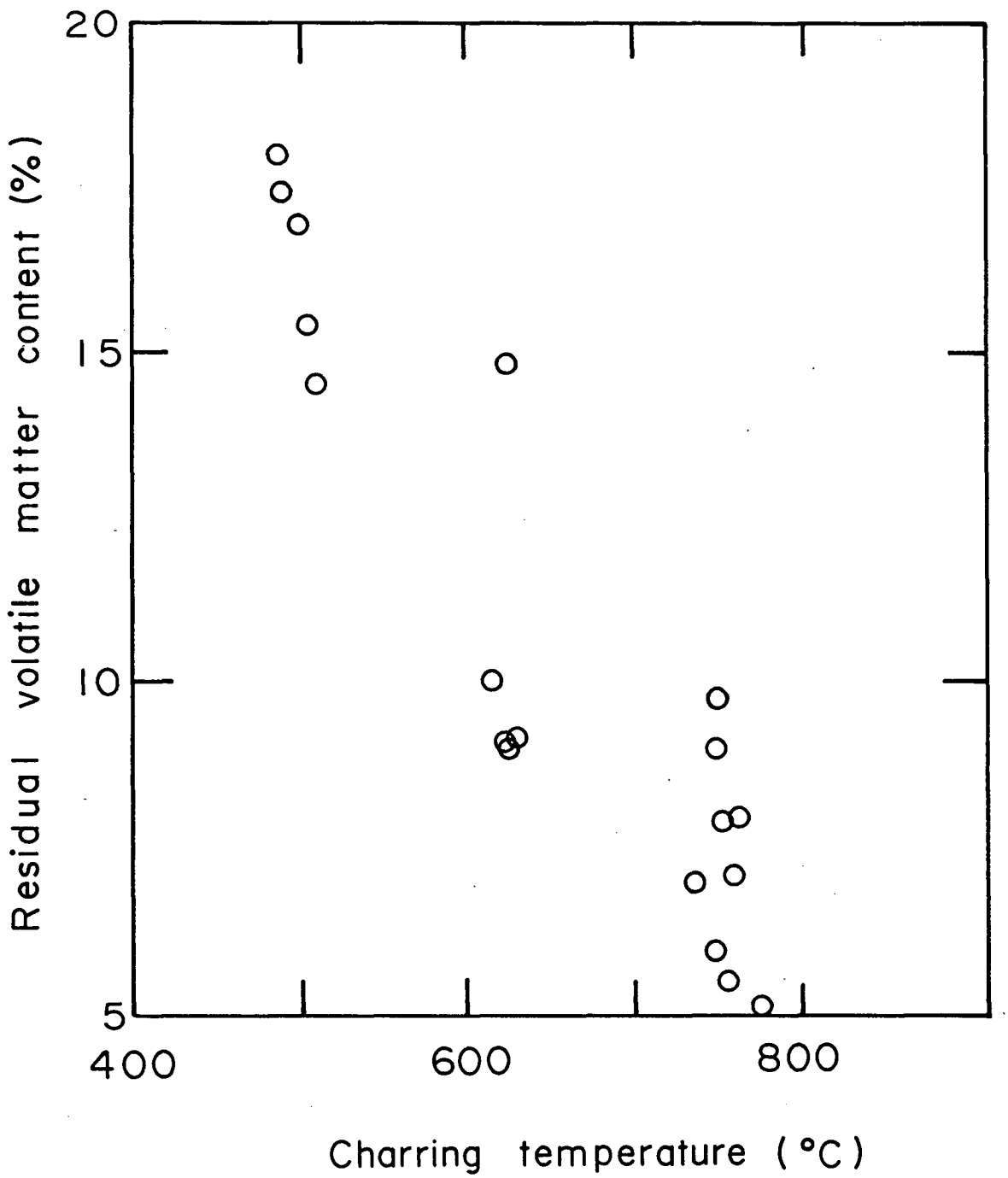

It is seen that the rod roughened with 100 grit sandpaper produced the highest shear strength, while the polished rod gave the lowest and the grooved rod gave an intermediate value. This indicates the relative effect of surface texture on the interfacial shear strength.

The contact angle-temperature relationships for the SRC pitch on each char is presented in figure 16. Initial softening of the pitch was seen to occur at approximately 200°C and the angle fell to a constant value of approximately 20° when the temperature was increased to 320°C.

The yield of benzene-soluble material after twenty-five hours extraction was found to be very small ∿1.5% (±0.5%) for each binder coal. Complete wetting of the amorphous carbon substrate was observed with each binder extract and this was seen to occur immediately after the extract became molten. The melting point of these materials was measured as 180°C ± 20°C in each case.

3.3 Compaction Analysis

The CCWL hot compaction model for char/binder coal systems is composed of three Kelvin viscoelastic elements in series, as discussed in section 1.4.3. This model was originally derived using an electrical analog with the equations formulated for the general case (i.e. with no assumptions concerning interaction of model elements). It was found that the simplest case to which this general solution could be applied was that of three non-interacting elements and the solution for a mechanical analog of this type was obtained by substituting springs for capacitors, dashpots for resistors and changing series coupling to parallel and parallel to series. From this, the values of the mechanical model parameters (η_i and M_i) were related to the experimental constants. However,

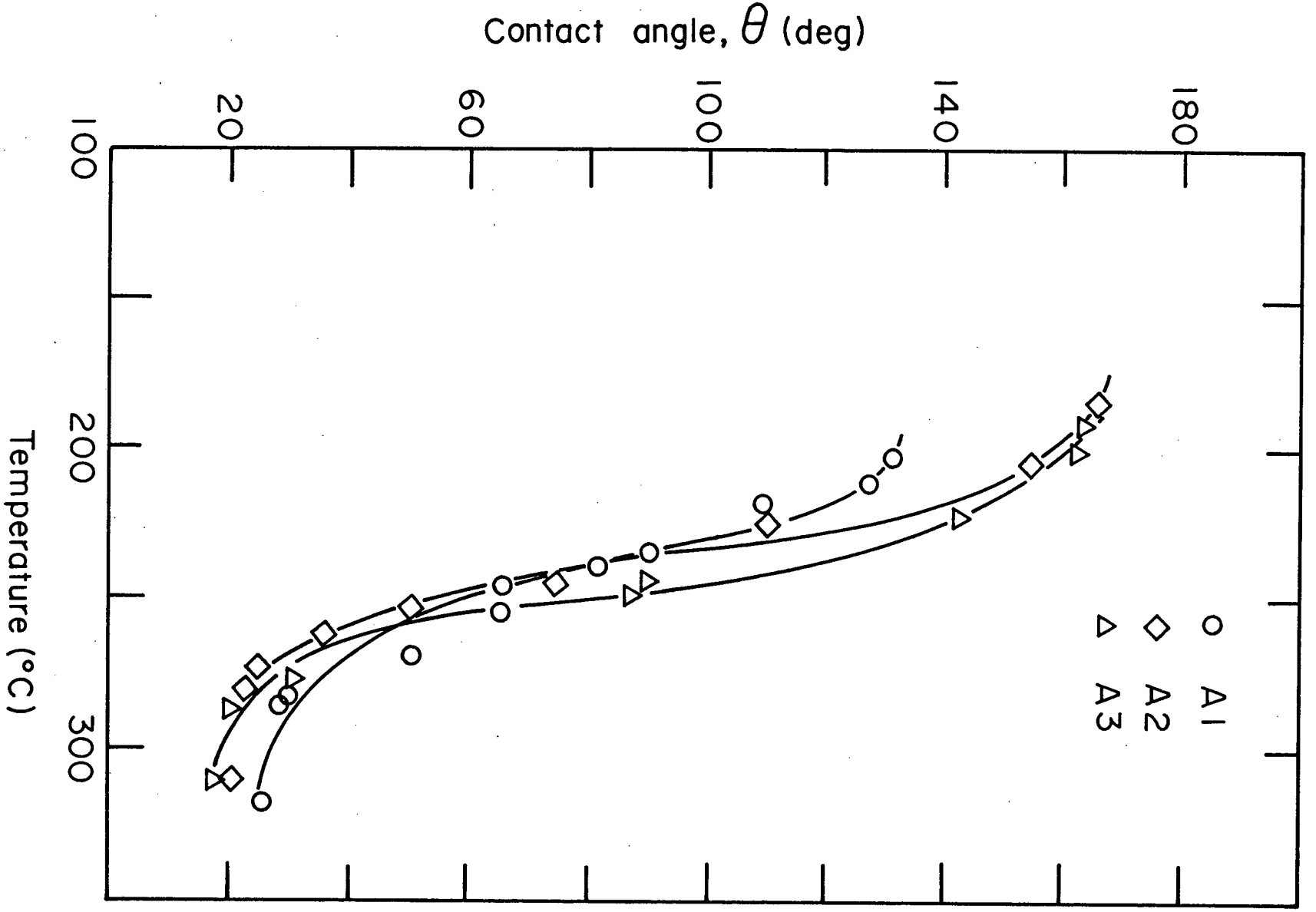

Figure 16: Relationship Between Contact Angle of an SRC Pitch on Char and Temperature

once this non-interacting mechanical analog is proposed, the relationships between model parameters and experimentally determined constants can be more directly solved as follows:

The response of a single Kelvin element to an applied stress is given by [53]:

$$\varepsilon_t = \frac{\sigma}{M_i}\left(1 - e^{-(M/\eta)t}\right) \tag{1}$$

where σ is the applied stress, M the elastic constant of the spring, η the viscosity of the dashpot, and ε_t the observed strain at any time, t. A series of n of these elements will have the response:

$$\varepsilon_t = \sum_{i=1}^{n} \frac{\sigma}{M_i}\left(1 - e^{-(M_i/\eta_i)t}\right) \tag{2}$$

and, for the case of figure 5,

$$\varepsilon_t = \frac{\sigma_o}{M_1}\left(1 - e^{-(M_1/\eta_1)t}\right) + \frac{\sigma_o}{M_2}\left(1 - e^{(M_2/\eta_2)t}\right) + \frac{\sigma_o}{M_3}\left(1 - e^{-(M_3/\eta_3)t}\right) \tag{3}$$

Expanding this expression and collecting terms yields:

$$\varepsilon_t = \sigma_o\left[\frac{1}{M_1} + \frac{1}{M_2} + \frac{1}{M_3} - \frac{e^{-(M_1/\eta_1)t}}{M_1} - \frac{e^{-(M_2/\eta_2)t}}{M_2} - \frac{e^{-(M_3/\eta_3)t}}{M_3}\right] \tag{4}$$

The total rigidity of the system, M_T, is related to the individual element rigidities by:

$$\frac{1}{M_T} = \frac{1}{M_1} + \frac{1}{M_2} + \frac{1}{M_3} \tag{5}$$

Introducing M_T and rewriting gives:

$$\varepsilon_t = \frac{\sigma_o}{M_T}\left[1 - \left(\frac{M_T}{M_1}\right)e^{-(M_1/\eta_1)t} - \left(\frac{M_T}{M_2}\right)e^{-(M_2/\eta_2)t} - \left(\frac{M_T}{M_3}\right)e^{-(M_3/\eta_3)t}\right] \tag{6}$$

and by defining:

$$k \equiv \frac{\sigma_o}{M_T} ; \quad A \equiv \frac{M_T}{M_1} ; \quad B \equiv \frac{M_T}{M_2} ; \quad C \equiv \frac{M_T}{M_3}$$
$$\alpha \equiv \frac{M_1}{\eta_1} ; \quad \beta \equiv \frac{M_2}{\eta_2} ; \quad \gamma \equiv \frac{M_3}{\eta_3} , \tag{7}$$

equation (6) can be written:

$$\varepsilon_t = k \left(1 - Ae^{-\alpha t} - Be^{\beta t} - Ce^{-\gamma t}\right) \tag{8}$$

which is the experimental equation (p. 19)

By considering the boundary condition:

$$\varepsilon_{t=\infty} = \frac{\sigma_o}{M_T} = k , \tag{9}$$

the total system rigidity is seen to be given by:

$$M_T = \frac{\sigma_o}{\varepsilon_{t=\infty}} = \frac{\sigma_o}{k} . \tag{10}$$

Substituting equation (10) into equations (7), the relationships between the viscoelastic parameters of figure 5 and the coefficients of equation (8) are given by:

$$M_1 = \frac{M_T}{A} = \frac{\sigma_o}{kA} \qquad \eta_1 = \frac{M_1}{\alpha} = \frac{\sigma_o}{kA\alpha}$$
$$M_2 = \frac{M_T}{B} = \frac{\sigma_o}{kB} \qquad \eta_2 = \frac{M_2}{\beta} = \frac{\sigma_o}{kB\beta} \tag{11}$$
$$M_3 = \frac{M_T}{C} = \frac{\sigma_o}{kC} \qquad \eta_3 = \frac{M_3}{\gamma} = \frac{\sigma_o}{kC\gamma}$$

This is a particular solution of the more general form considered in the original model development.

Equation (8) may be manipulated as follows to experimentally

determine the coefficients k, A, B, C, α, β and γ. An expanded form of equation (8),

$$\varepsilon_t = k - kAe^{-\alpha t} - kBe^{-\beta t} - kCe^{-\gamma t} \quad (12)$$

may be differentiated to yield:

$$\dot{\varepsilon} = \alpha kAe^{-\alpha t} + \beta kBe^{-\beta t} + \gamma kCe^{-\gamma t} \quad (13)$$

Taking the natural logarithm of both sides:

$$\ln(\dot{\varepsilon}) = -\alpha t + \ln(\alpha kA) - \beta t + \ln(\beta kB) - \gamma t + \ln(\gamma kC) \quad (14)$$

Since the time intervals over which the three mechanisms predominate do not overlap, a plot of $\ln(\varepsilon)$ vs. t will have three straight-line sections, the slopes of which correspond to $-\alpha$, $-\beta$ and $-\gamma$. The intercepts of the straight sections will correspond to $\ln(\alpha kA)$, $\ln(\beta kB)$ and $\ln(\gamma kC)$, respectively.

As indicated by equation (8), the constant, k, may be equated to the value of compaction strain at long times when the exponential terms go to zero.

This model was used to quantify the compaction behaviour of each mixture. The second element in the model—that associated with particle flow—was selected as being representative of char/binder interaction. Specifically, the slope of the central portion of the $\ln(\varepsilon)$ vs. t plot was equated to $-\beta$ while the intercept was set equal to $\ln(kB\beta)$, allowing determination of the pre-exponential coefficient, B. The rigidity and viscosity of the compacting mixture during the particle flow stage was then calculated, following the above derivation:

$$\text{Rigidity, } M_2 = (kB)^{-1}$$

$$\text{Viscosity, } \eta_2 = (kB\beta)^{-1}$$

The chart recorder attached to the briquetting apparatus produced a chart record of compaction vs. time. These curves were supplied to a computer program in the form of digitized x(time), y(compaction) pairs. The program then treated the data as follows:

1. Normalize compaction with respect to initial briquette length, giving compaction strain vs. time data.

2. Determine slope ($\dot{\varepsilon}$) of ε vs. t curve at various values of t and plot values of $\ln(\dot{\varepsilon})$ against t.

3. Determine best least squares linear fit for the second region, calculating values of β and B from the slope and intercept of the curve.

4. Calculate rigidity and viscosity parameters M_2 and η_2.

The strain-time curves for mixture 6, shown in figure 17, are typical of the results obtained (the remaining normalized compaction curves analysed are presented in Appendix B). Although the final compaction varies somewhat from briquette to briquette, the compaction behaviour in the region 0-1 minute appears to be similar. Variations within a mixture type can arise from a number of sources: small variations in heating rate, final temperature attained, and how closely this final temperature is maintained during the compaction procedure, dimensional variations in the die assembly, and the heterogeneous nature of the materials involved.

The derived plot of $\ln(\dot{\varepsilon})$ vs. t for one briquette of mixture 6 is shown superimposed on the compaction curve in figure 18 where the circles correspond to the calculated $\ln(\dot{\varepsilon})$ values. In figure 19, the predicted curve generated from the calculated values of β and B is plotted on the same axes as the original compaction curve. Reasonable agreement is shown

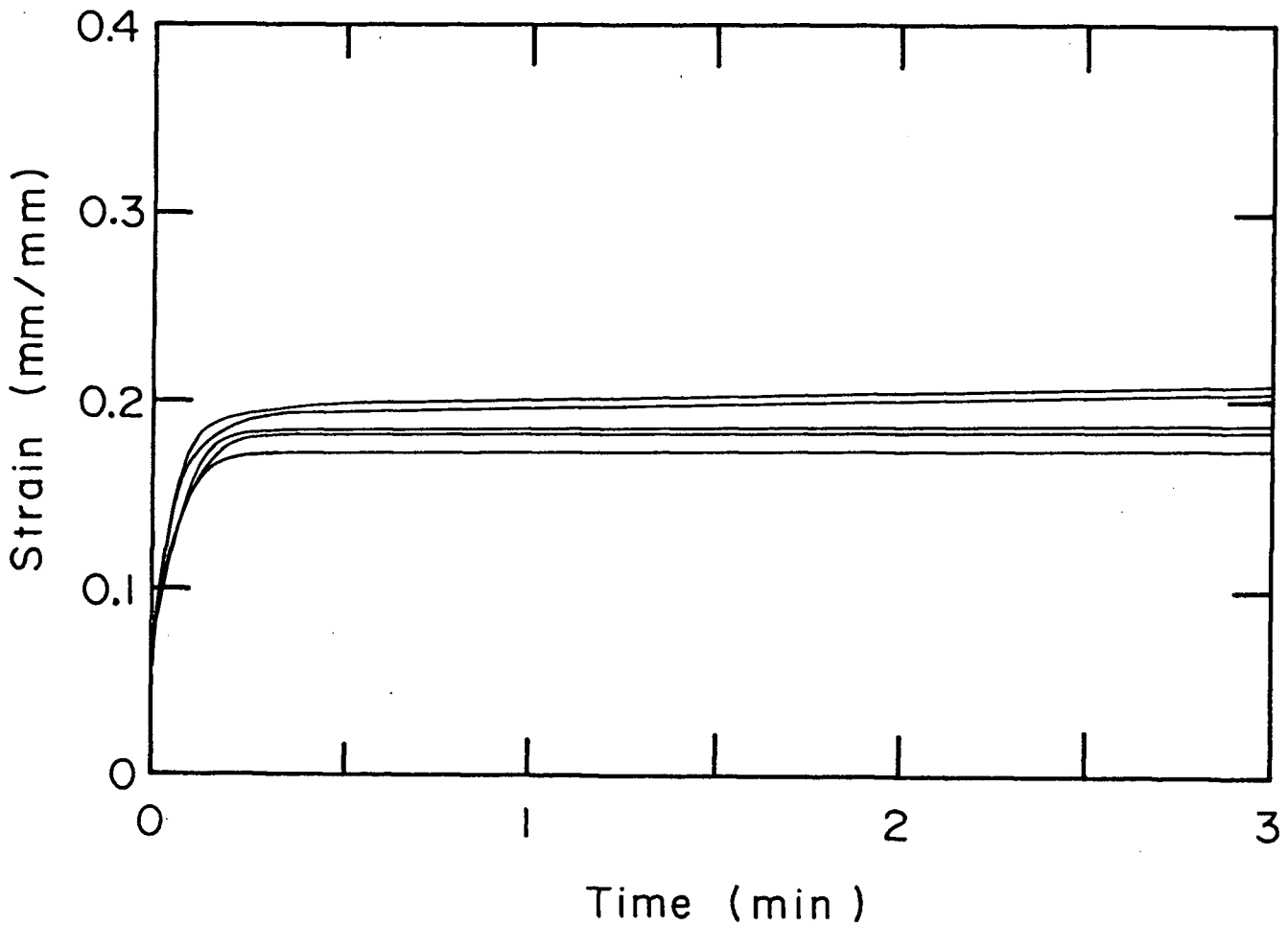

Figure 17: Observed Strain-Time Curves of Briquetting Mixture 6 (Aggregate A2 -- Binder B3)

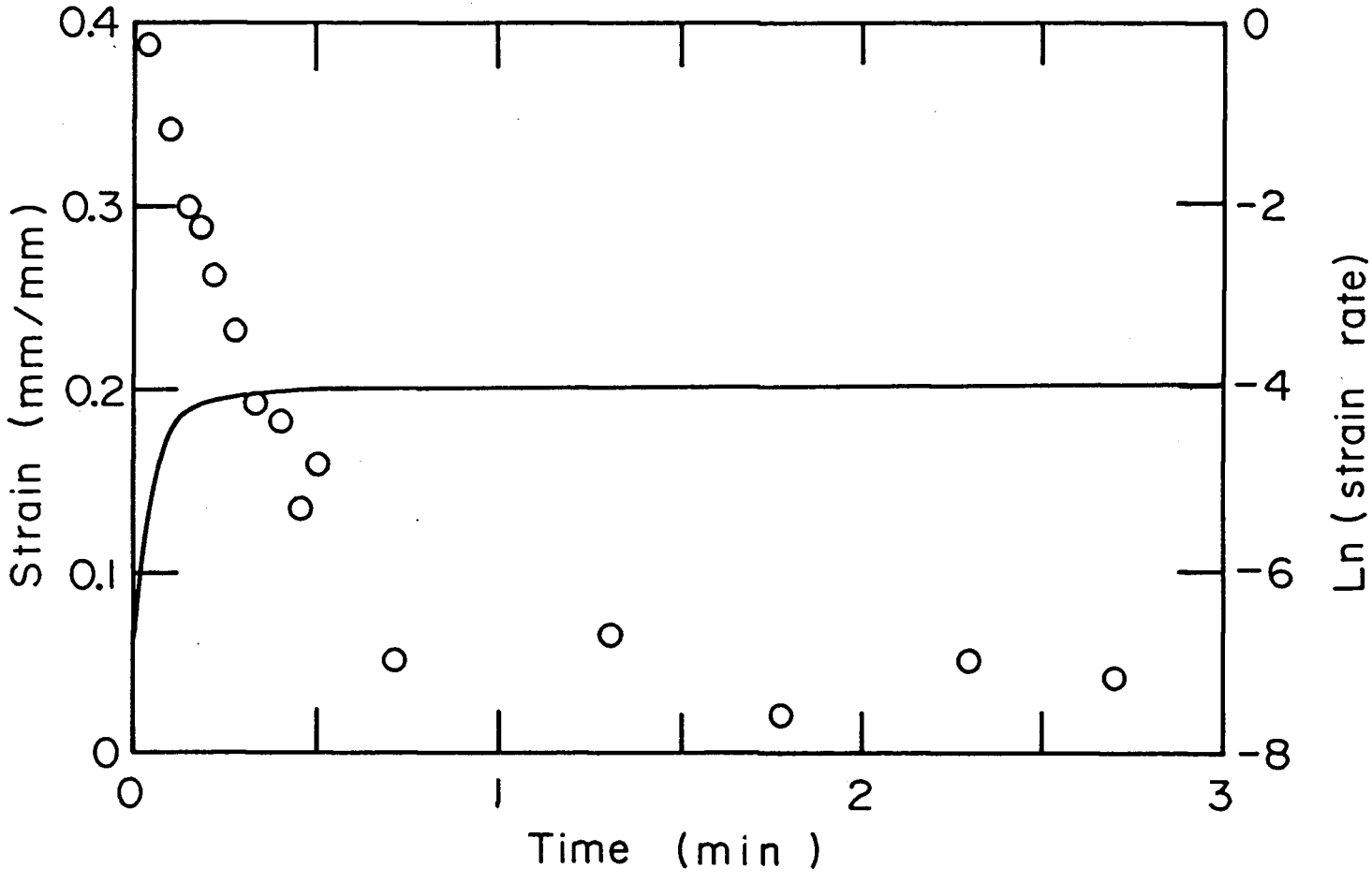

Figure 18: Relationship Between Natural Logarithm of Strain Rate and Time for Briquette 6 of Mixture 6 Superimposed on the Strain-Time Curve

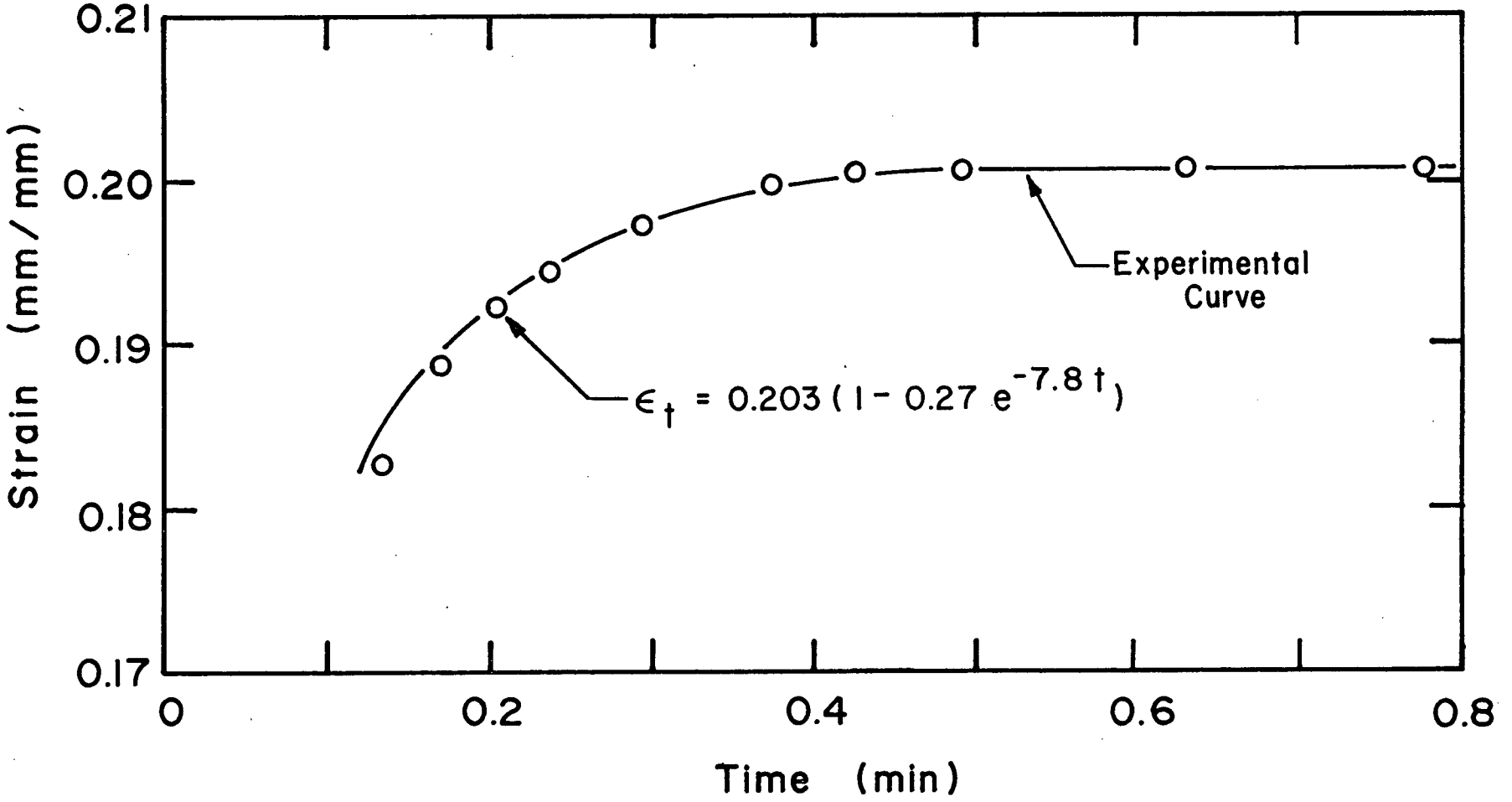

Figure 19: Predicted and Observed Strain-Time Curves for Briquette 6 of Mixture 6

for the region associated with the second compaction mechanism. The slow response of the compaction recorder prevented an accurate determination of the end of the first stage of compaction and initiation of the second stage. The discrepancy between experimental and predicted plots may be accounted for by this inaccuracy. Measured values of β, B, M_2 and η_2 are given in Tables VIIIa, b and c and summarized according to mixture type in Tables IXa and b.

3.4 Briquette Strength

Results of Ultimate Compressive Strength testing are presented in figure 20. Strength is presented as a function of briquette bulk porosity. For purposes of comparison, the observed variation of strength with bulk porosity for each mixture type was extrapolated to a common bulk porosity of 35%. The variations in strength (at 35% porosity) with aggregate charring temperature are shown in figures 21a, b and c. Error bars shown are for a 95% confidence interval on the strength value extrapolated to 35% bulk porosity. This analysis will be elaborated further in the following section.

MIX	BRIQ	k	SLOPE (min^{-1})	INTERCEPT	β (min^{-1})	B	RIGIDITY, M_2 (MPa)	VISCOSITY, η_2 (MPa min)
1	1	0.249	-8.41	-0.52	8.41	0.28	141	16.7
	2	0.277	-10.71	-0.71	10.71	0.16	217	20.3
CHAR A1	3	0.303	-9.62	-0.35	9.62	0.24	136	14.1
	4	0.279	-8.73	-0.77	8.73	0.19	189	21.6
	MEAN						171	18.2 (3.42)*
4	1	0.231	-18.2	-0.51	18.2	0.14	302	16.6
	2	0.235	-14.5	-0.69	14.5	0.15	288	19.9
CHAR A2	3	0.255	-19.3	-0.51	19.3	0.12	322	16.6
	4	0.235	-11.9	-0.79	11.9	0.16	261	22.0
	MEAN						293	18.8 (2.65)
7	1	0.229	-8.95	-0.69	8.95	0.24	178	19.9
	2	0.220	-6.45	-1.06	6.45	0.24	186	28.9
CHAR A3	3	0.262	-11.3	-0.52	11.3	0.20	191	16.9
	4	0.221	-5.79	-1.01	5.79	0.28	159	27.5
	5	0.256	-9.38	-0.64	9.38	0.22	178	19.0
	6	0.190	-10.1	-0.97	10.1	0.20	266	26.3
	7	0.283	-12.3	-0.46	12.3	0.18	194	15.8
	MEAN						193	22.0 (5.39)

TABLE VIIIa: VALUES OF EXPERIMENTAL AND MODEL PARAMETERS

FOR MIXTURES CONTAINING BINDER B1

* Standard deviation in parentheses.

MIX	BRIQ	k	SLOPE (min^{-1})	INTERCEPT	β (min^{-1})	B	RIGIDITY, M_2 (MPa)	VISCOSITY, η_2 (MPa min)
1	1	0.214	-6.91	-1.65	6.91	0.13	500	72.2
	2	0.172	-8.13	-1.51	8.13	0.16	500	61.7
CHAR A1	3	0.206	-7.60	-1.58	7.60	0.13	510	67.5
	4	0.205	-5.48	-1.98	5.48	0.12	550	102.4
	MEAN						520	76.0 (18.2)
5	1	0.186	-9.48	-0.69	9.48	0.28	261	27.5
	2	0.189	-7.81	-0.97	7.81	0.26	286	36.6
CHAR A2	3	0.177	-8.20	-1.03	8.20	0.25	317	38.7
	4	0.206	-10.12	-0.45	10.12	0.31	218	21.6
	5	0.203	-8.95	-0.59	8.95	0.31	223	24.9
	6	0.203	-7.81	-0.86	7.81	0.27	253	32.5
	MEAN						260	30.3 (6.25)
8	1	0.164	-9.06	-0.85	9.06	0.29	293	32.4
	2	0.185	-9.59	-0.79	9.59	0.26	291	30.3
CHAR A3	3	0.201	-9.62	-0.95	9.62	0.20	342	35.5
	4	0.207	-8.62	-1.06	8.62	0.19	243	39.8
	MEAN						317	34.5 (4.13)

TABLE VIIIb: VALUES OF EXPERIMENTAL AND MODEL PARAMETERS

FOR MIXTURES CONTAINING BINDER B2

MIX	BRIQ	k	SLOPE (min^{-1})	INTERCEPT	β (min^{-1})	B	RIGIDITY, M_2 (MPa)	VISCOSITY, η_2 (MPa min)
3	1	0.235	-6.80	-2.12	6.80	0.08	565	83.1
	2	0.255	-9.90	-1.59	9.90	0.08	375	49.0
CHAR A1	3	0.252	-8.65	-2.04	8.65	0.06	667	77.1
	4	0.247	-7.95	-1.90	7.95	0.08	532	67.0
	MEAN						535	69.0 (14.9)
6	1	0.217	-10.7	-0.91	10.7	0.17	265	25.3
	2	0.248	-13.5	-0.29	13.5	0.22	180	13.6
CHAR A2	3	0.198	-11.9	-0.39	11.9	0.29	176	14.8
	4	0.207	-12.8	-0.54	12.8	0.22	221	17.2
	5	0.208	-11.6	-0.28	11.6	0.31	153	13.4
	6	0.201	-12.8	-0.39	12.8	0.26	189	15.0
	MEAN						198	16.6 (4.50)
9	1	0.225	-11.6	-1.33	11.6	0.10	437	37.8
	2	0.197	-14.3	-0.63	14.3	0.19	267	18.7
CHAR A3	3	0.226	-9.83	-1.24	9.98	0.13	340	34.6
	4	0.230	-18.4	-1.09	18.4	0.08	550	29.5
	5	0.199	-13.1	-0.92	13.1	0.15	329	25.1
	MEAN						385	29.1 (7.59)

TABLE VIIIc: VALUES OF EXPERIMENTAL AND MODEL PARAMETERS

FOR MIXTURES CONTAINING BINDER B3

TABLE IX (a & b)

a. AVERAGE VALUES OF SECOND MODEL ELEMENT RIGIDITIES (M_2)

	B1	B2	B3
A1	171	520	535
A2	293	260	198
A3	193	317	385

b. AVERAGE VALUES OF SECOND MODEL ELEMENT VISCOSITIES (η_2)

	B1	B2	B3
A1	18.2	76.0	69.0
A2	18.8	30.3	16.6
A3	22.0	34.5	29.1

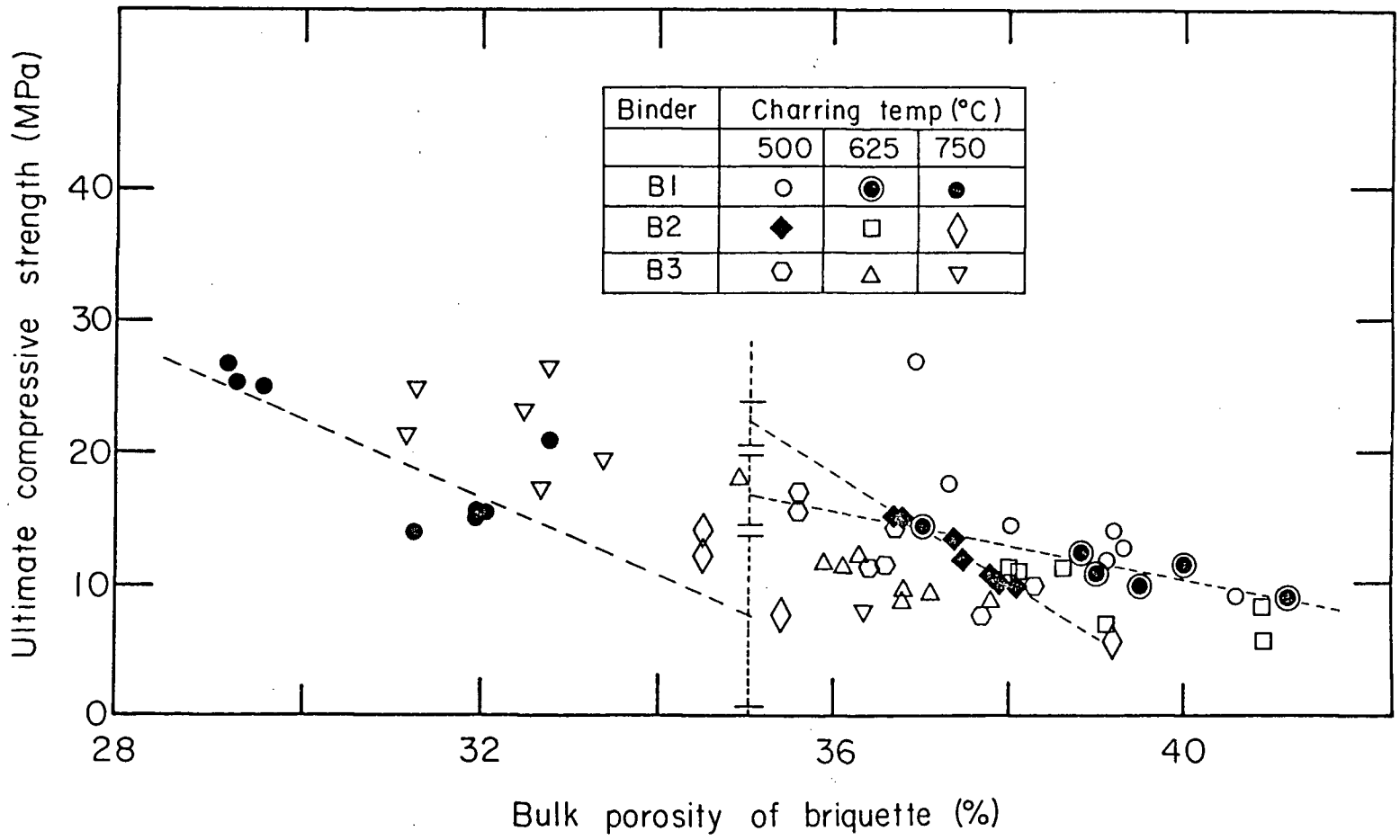

Figure 20: Relationships Between Briquette Ultimate Compressive Strength and Briquette Bulk Porosity For All Mixtures

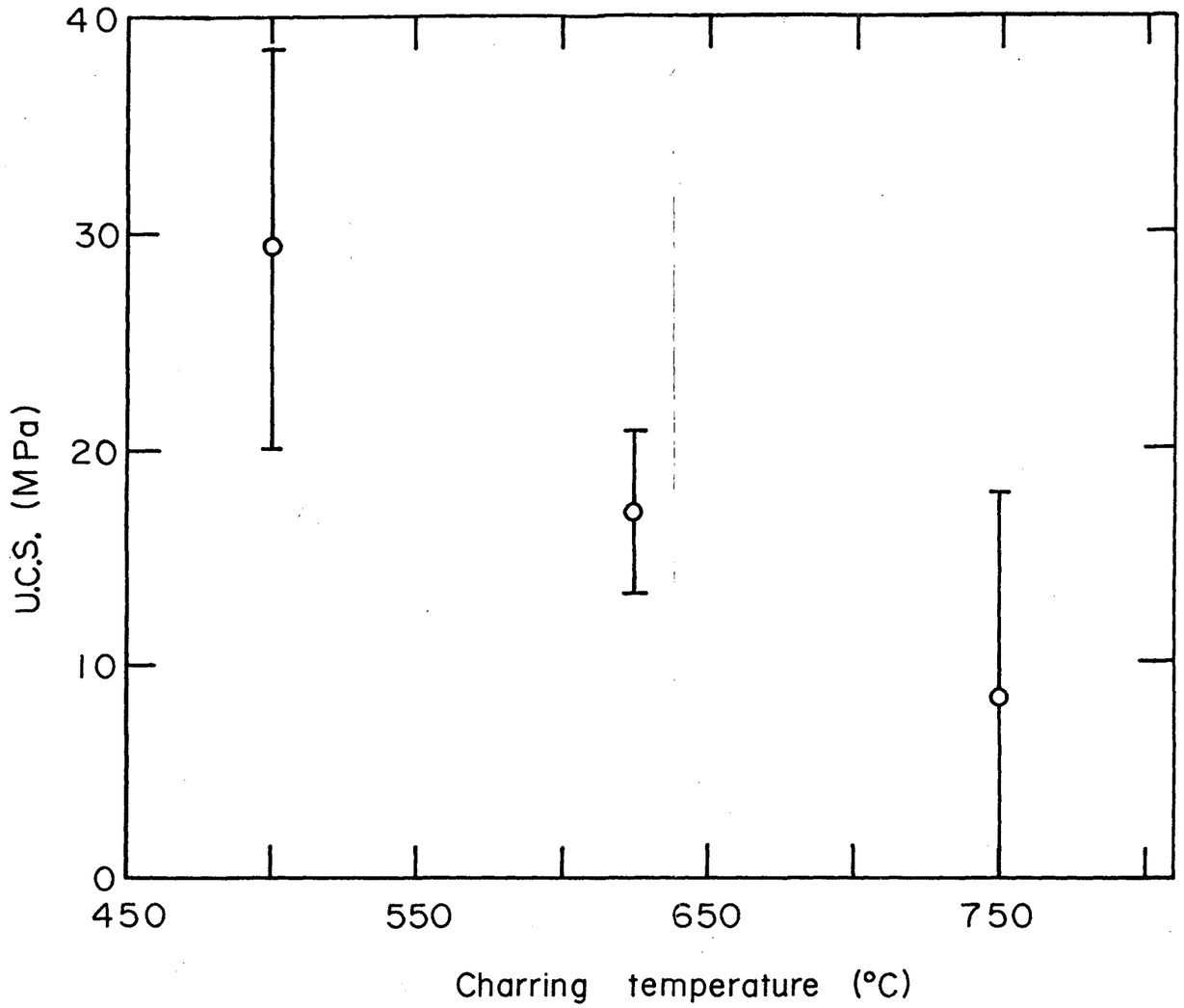

Figure 21 a: Relationship Between Briquette Ultimate Compressive Strength and Charring Temperature for Mixtures Containing Binder B1.

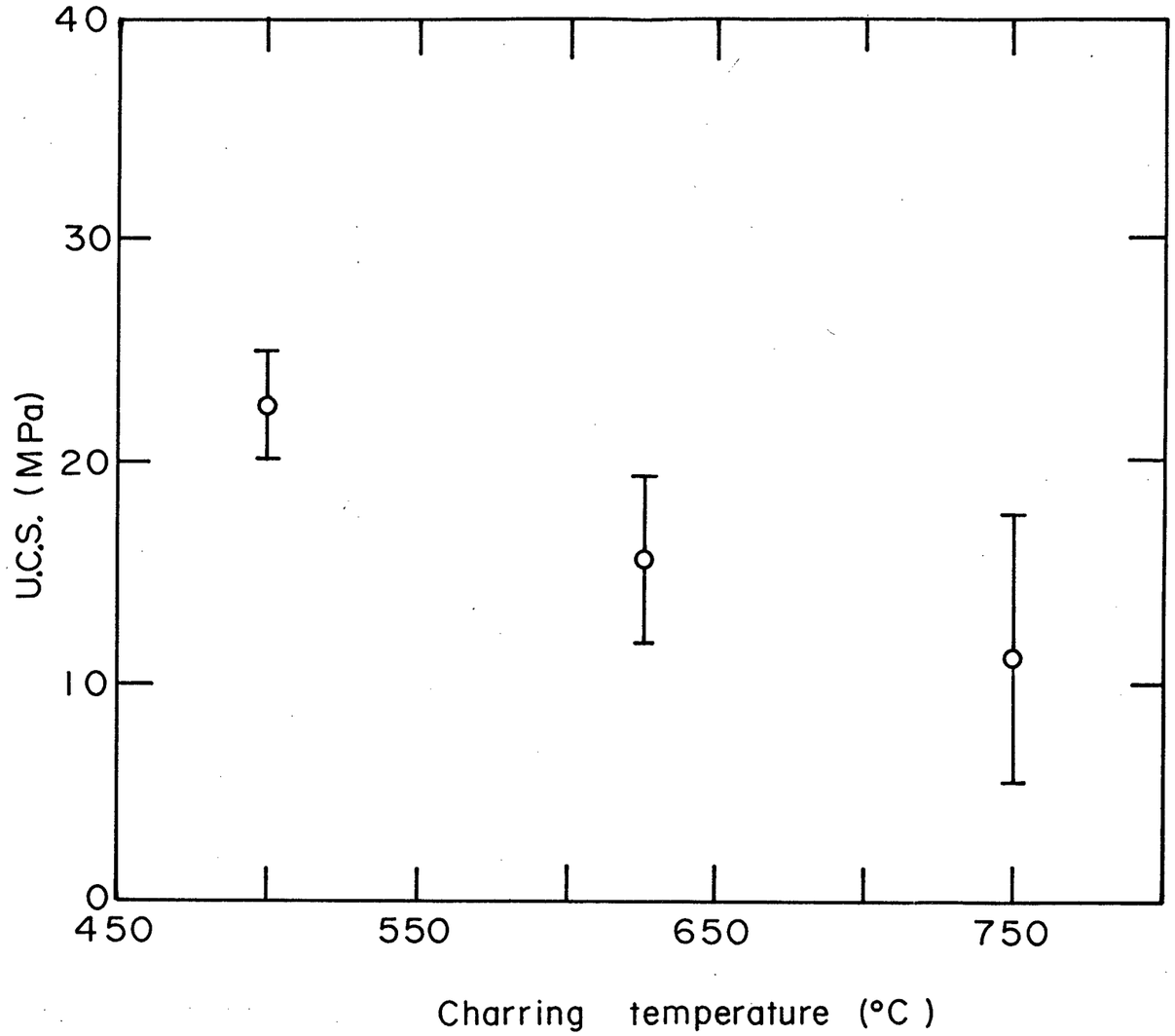

Figure 21 b: Relationship Between Briquette Ultimate Compressive Strength and Charring Temperature for Mixtures Containing Binder B2.

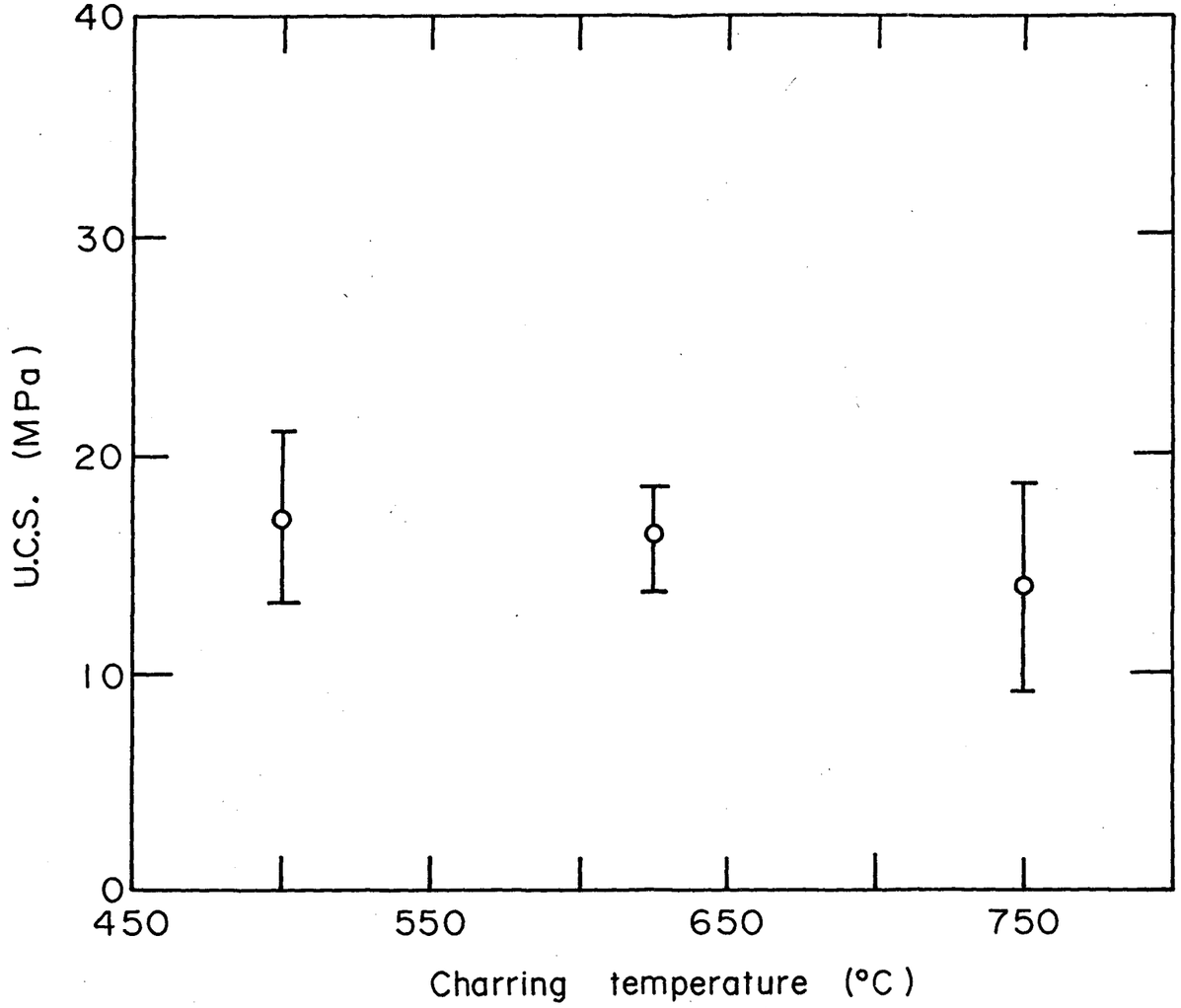

Figure 21 c: Relationship Between Briquette Ultimate Compressive Strength and Charring Temperature for Mixtures Containing Binder B3.

4 DISCUSSION

As outlined in section 1.5, the objective of this work was to investigate the formcoke system on a more fundamental level than that attempted to date. The focus of the investigation has been on the effects of material characteristics on the final briquette product. The physical characteristics of the aggregate and binder phases may affect the final composite in two ways:

1) by influencing the compaction kinetics of the briquetting process, and

2) by directly influencing the physical nature of the final product.

A range of aggregate characteristics was produced by using chars produced at three different carbonization temperatures while variations in binder properties were obtained by using three different caking coals. The compaction kinetics of various mixtures of these phases were studied using a previously established model and the final formcoke composite was characterized by its ultimate compressive strength. Interpretation of the results obtained will follow the order established above.

4.1 Applicability of Hot Compaction Model

Analysis of the compaction curves was carried out using the CCWL hot compaction model which has been described earlier (sections 1.4, 3.3 and Appendix A). It should be noted here that in the original development

of the model, no effort was made to investigate the rèproducibility of the compaction curves or the sensitivity of the calculated model parameters to small variations in these curves. One of the objectives of this work was to establish the variation of model parameter values for one char-binder system over a wide range of briquetting temperatures in an attempt to identify the ideal briquetting conditions. In the present work, the model is used to compare the model parameter values obtained under these ideal conditions for nine different char-binder systems and to identify the material characteristics responsible for the observed variations. As can be seen from Tables VIII and IX some scatter in the calculated parameter values was found. Rigidity values ranging from 171 MPa to 535 MPa were calculated. The viscosity values calculated varied from 16.6 MPa min to 76.0 MPa min with standard deviations as shown in parentheses in the table. Considering the small sample size available, these values were considered reasonable.

During the course of this study, conclusions concerning the association of particular compaction mechanisms with certain model elements were drawn. These are presented in the appropriate sections. In general, the model was found to describe the physical situation quite well and to be sensitive to small variations in the compaction curves. The observed variation in calculated values from duplicate runs was attributed to insensitivity of recording and digitizing equipment and material heterogeneity.

4.2 Effect of Material Characteristics On Compaction Kinetics

Two material properties were found to affect the final product by influencing the compaction kinetics. Binder fluidity was shown to affect

compaction viscosity during the second stage of compaction—that associated with particle flow, and aggregate porosity was shown to affect final compaction during the third stage—that associated with plastic deformation.

A major influence on the compaction kinetics of the formcoke system comes from binder fluidity. By comparing the calculated model parameters for the second stage of compaction (Tables IXa and b) with the rheological properties of the binders (Table IV), it can be seen that the observed compaction viscosity increases as the binder fluidity drops. This is shown graphically in figure 22. Binder B1 has the highest Gieseler fluidity and displays the lowest compaction viscosity values. Fluidity decreases from B1 to B3 to B2 as the corresponding compaction viscosities increase. Except for the case of mixture 6, this is true regardless of the char type used. The case of mixture 6 can be explained by loose spacer assembly allowing binder to be squeezed out during compaction as observed with this mixture. This resulted in the consistently low values of M_2 and η_2 observed for that mixture.

This comparison reinforces the association of the second model element with a particle flow mechanism. As plastic phase fluidity decreases, movement of aggregate particles within the compact becomes more difficult and the compaction viscosity of the mixture increases.

The lack of significant trends in second element rigidity and total compaction values indicates that neither of these parameters is greatly affected by mixture type. In the model, M_2 is influenced by total compaction, k, and the value of B, which is the fraction of the total model response attributable to the second element. Both of these remain approximately constant throughout the study at 0.2 and 0.1 - 0.3, respectively.

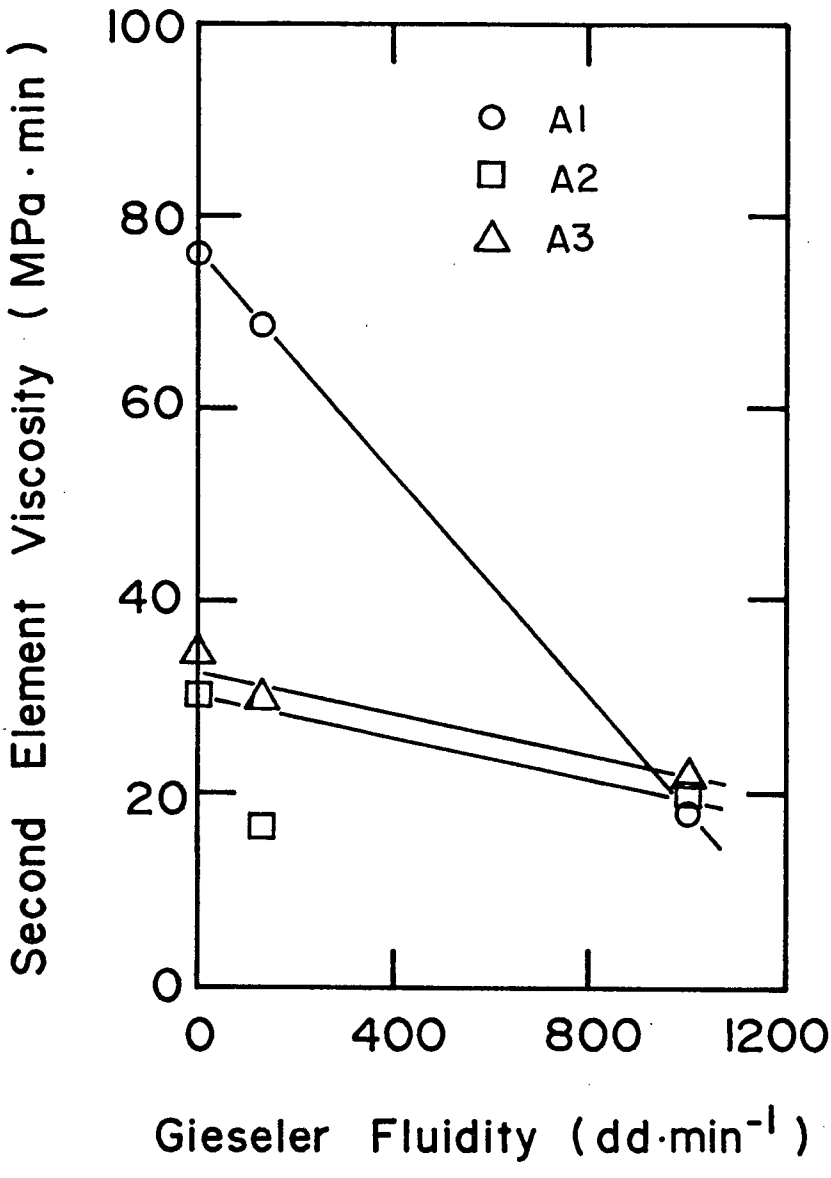

Figure 22: Relationship Between Second Model Element Viscosity and Binder Phase Fluidity

Char porosity is seen to affect the briquetting process by influencing the amount of compaction necessary to attain a given bulk density in the product. Although the value of k did not vary widely throughout the program, variations in k within a mixture type were seen to correlate with changes in briquette bulk density. When grouped according to char type, the effect of char porosity on product bulk density can be seen.

The results presented in figures 23a, b and c and summarized in Table X, indicate the relationship between total compaction and resultant briquette bulk porosity to be linear. As expected, a larger compaction results in a lower bulk porosity or, alternatively, a higher bulk density. The slopes of these curves represent the sensitivity of briquette bulk porosity to total compaction. It is seen that for a given char type, this slope is approximately constant for each binder. However, for decreasing temperature of char carbonization, the average slope is seen to increase (see Table X). In a physical sense, an equal amount of compaction will cause a greater increase in bulk density for briquettes made with higher temperature char than for the lower temperature material. This results from the need to eliminate the higher porosity present within the lower temperature char. This may be accomplished by penetration of the binder phase into the macropores (>5μm) during the particle flow stage of compaction when the binder is fluid and by collapse of the pore structure by plastic deformation in the final compaction stage due to the applied stress.

The y-intercepts of the k vs. P_b curves (figures 23a, b and c) correspond to the amount of compaction required to attain theoretical density in a briquette. This value is also seen to increase with

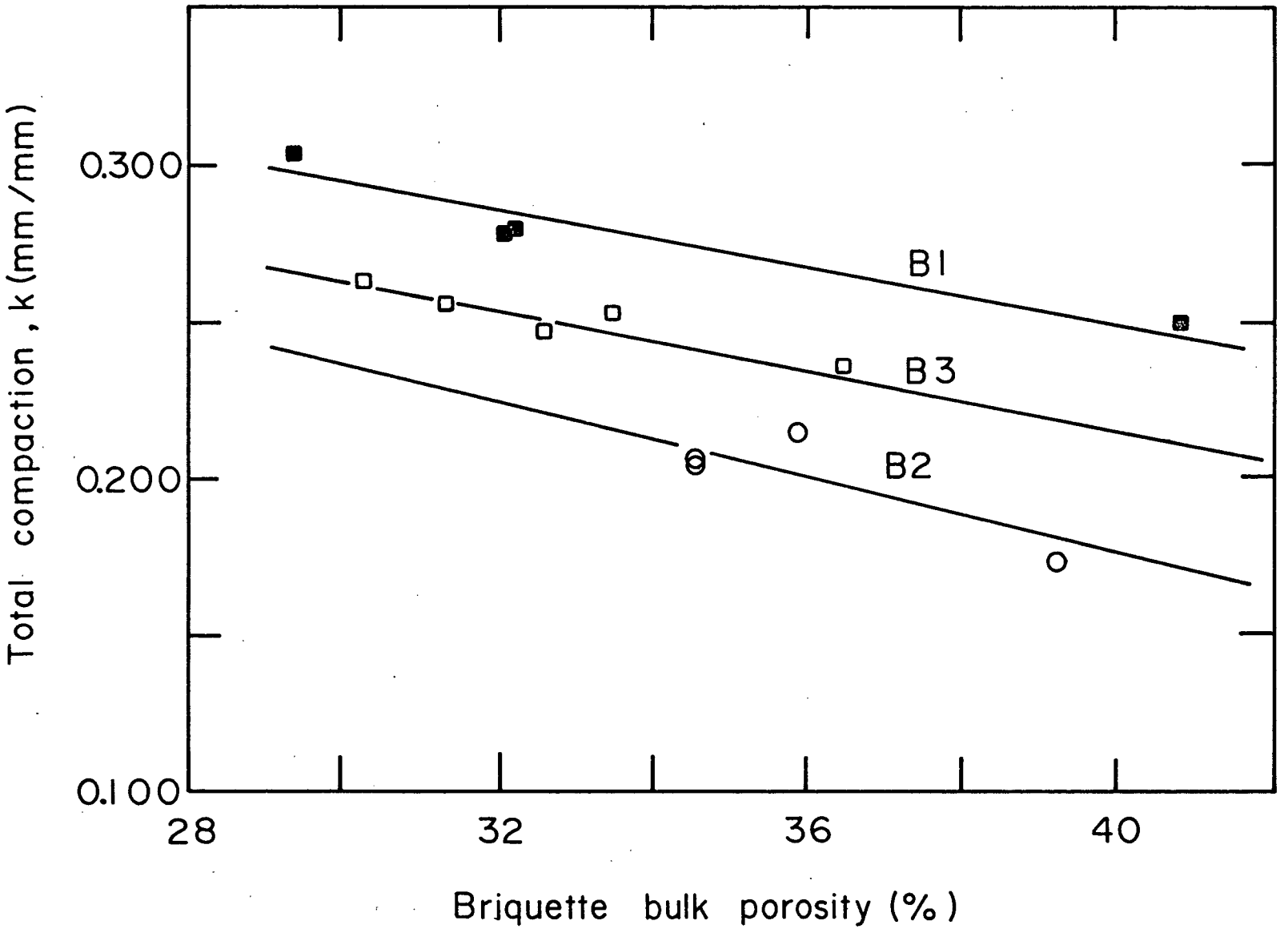

Figure 23 a: Relationship Between Total Compaction and Resultant Briquette Bulk Porosity for Mixtures Containing Char A1.

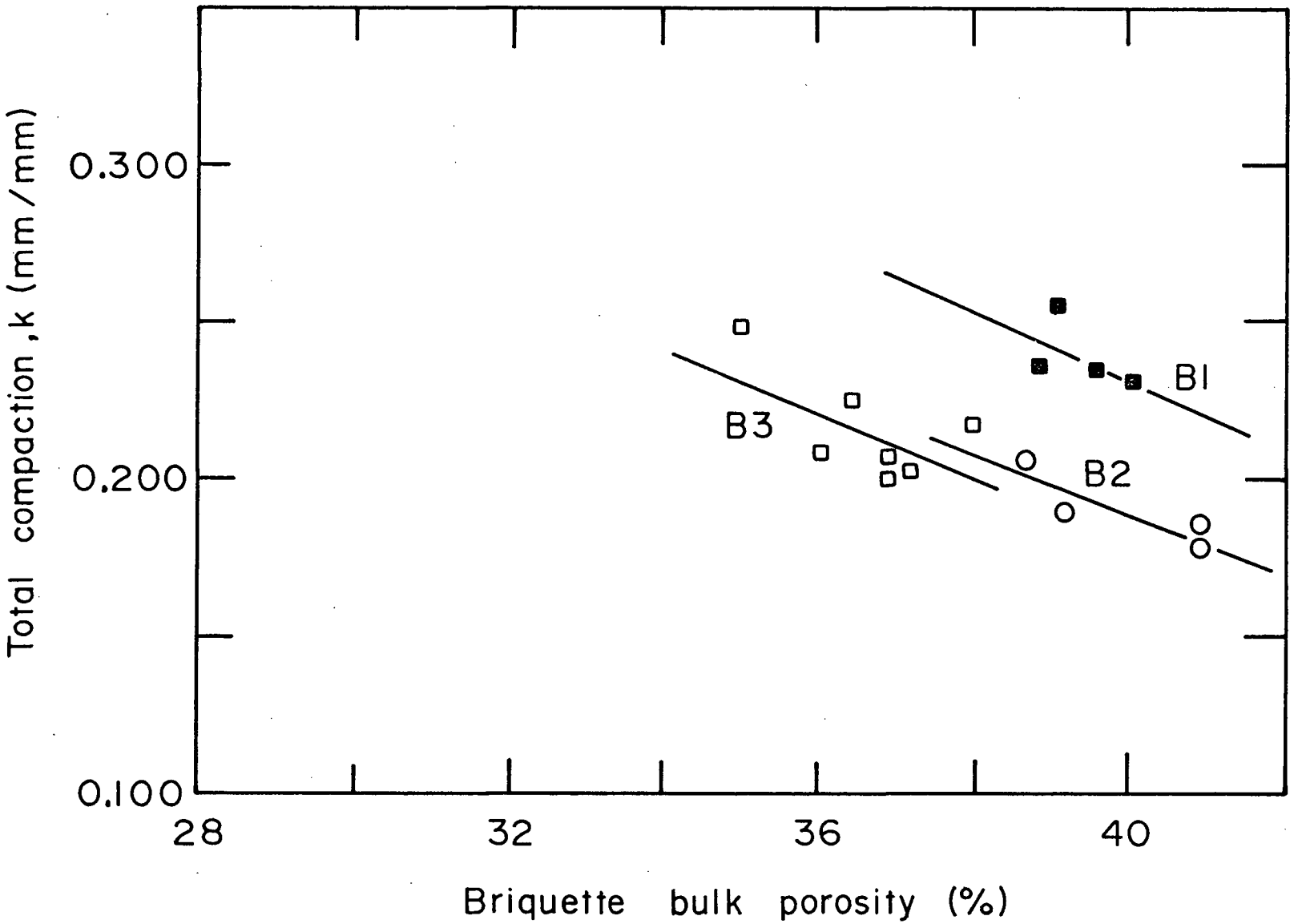

Figure 23 b: Relationship Between Total Compaction and Resultant Briquette Bulk Porosity for Mixtures Containing Char A2.

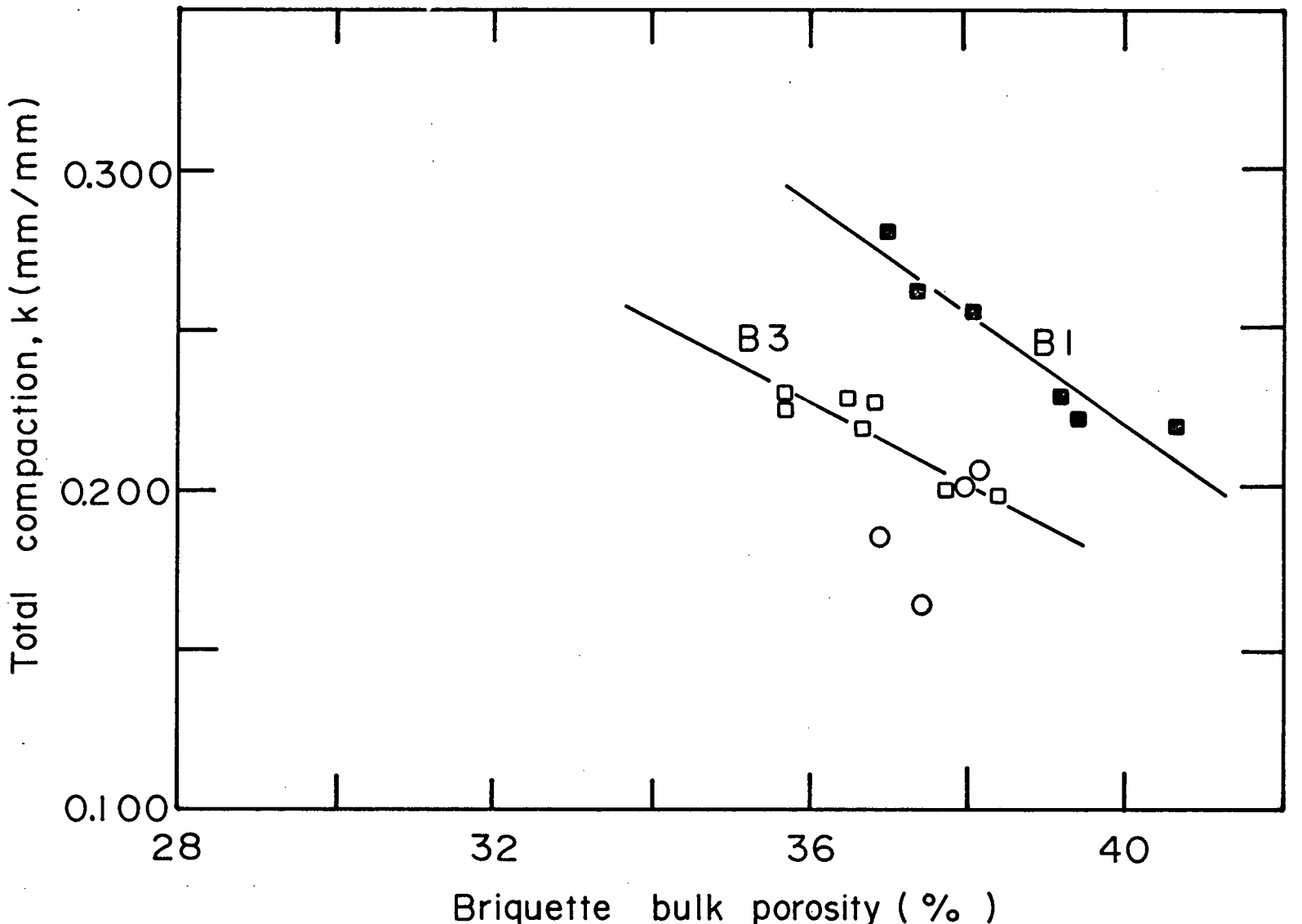

Figure 23 c: Relationship Between Total Compaction and Resultant Briquette Bulk Porosity for Mixtures Containing Char A3.

CHAR	BINDER	MIX	SLOPE a (mm/mm %$^{-1}$)	AVERAGE VALUE OF a FOR CHAR TYPE	INTERCEPT b (mm/mm)	AVERAGE VALUE OF b FOR CHAR TYPE
A1	B1	1	-4.21×10^{-3}	-5.21×10^{-3}	.418	.422
	B2	2	-7.37×10^{-3}		.465	
	B3	3	-4.04×10^{-3}		.383	
A2	B1	4	-1.06×10^{-2}	-1.00×10^{-2}	.656	.599
	B2	5	-7.85×10^{-3}		.502	
	B3	6	-1.16×10^{-2}		.640	
A3	B1	7	-1.99×10^{-2}	-1.63×10^{-2}	1.01	.846
	B2	8	-		-	
	B3	9	-1.26×10^{-2}		.682	

TABLE X VALUES OF SLOPES AND Y-INTERCEPTS OF CURVES OF TOTAL COMPACTION VS. RESULTANT BRIQUETTE BULK POROSITY

decreasing charring temperature. The intercept for the case of the highest temperature char, A1, is significant since in this char, there is virtually no accessible porosity. In this case, the response of bulk porosity to a change in compaction is associated with the binder phase alone. Increases in the compaction required to attain theoretical density above that seen for the case of aggregate A1 correspond to the contribution of the aggregate phase. Table X shows that a compaction of approximately 40% would be required to produce complete densification with A1 char and additional compactions of roughly 20% and 45% to cause the plastic deformation required for chars A2 and A3 to reach theoretical density. It may be noted that 40% volume porosity has been found to be the approximate normal packing density for a powder compact of random sized and shaped particles [54].

This analysis may be summarized in three points:

1) The aggregate phase of a formcoke does influence the compaction kinetics of the system and the final briquette product.

2) The greater macroporosity produced in char at lower carbonization temperatures requires more extensive binder penetration and plastic deformation in the briquetting operation to attain a product bulk density comparable to that obtained with higher temperature char.

3) The association of one of the elements of the CCWL hot compaction model with a plastic deformation mechanism is confirmed.

4.3 Effect of Material Characteristics On Briquette Strength

The second objective of this work was to establish how the aggregate

and binder characteristics directly affect the formcoke product: this required consideration of changes in each component while the other was held constant.

The basis of final product comparison was briquette Ultimate Compressive Strength (UCS). However, as established above, small variations in compaction can lead to significant differences in briquette bulk porosity and the bulk porosity of a specimen is known to affect its gross strength. Therefore it was first necessary to take account of variations in briquette bulk porosity.

It has been shown by Ryshkewitch [55] that the strength of a porous body can be related to its fractional porosity by an inverse exponential relationship ($UCS = Ae^{-aP_b}$) over a large range of porosity (3-60%). This empirical relationship has also been verified by a number of other workers [56]. However, it was found in this work that, over the range of porosity encountered, strength appeared to vary linearly with bulk porosity.

The linear relationship for each mixture type was extrapolated to a common bulk porosity for strength comparisons. Thirty-five percent was chosen as being both a median figure for the experimental data available and a reasonable commercial value. The statistical reliabilities of these extrapolations were established using the 95% confidence limits for the predicted strength values [57]. From these results, the separate contributions of char and binder can be isolated by considering first a constant binder and varying char and then a constant char with varying binder.

4.3.1 Char Characteristics

To eliminate binder property effects, briquetting mixtures of a

single binder and different chars can be considered. In these cases, variations in UCS are associated with variations in char properties.

Examination of briquette fractures showed separation to occur primarily along the char-binder interface with some instances of binder fracture (figures 24a and b). Even in briquettes made with 500°C char, where hardness and density studies indicated lowest char strength, failure through the aggregate phase was not observed. From this it is concluded that in the systems studied, briquette strength is not dependent on the mechanical strength of the aggregate phase.

Both the porosity and RVM content of the char were seen to decrease with charring temperature (Table VI and figure 15, respectively), paralleling the decrease in briquette UCS.

The total volume of space contained in pores of larger than a given diameter has been presented in Table VI. These data indicate that pore volume decreases with increasing carbonization temperature, especially for pores of 1 - 5 μm diameter and larger. Lahaye and Aubert [44] concluded that 5 μm diameter pores are the lower limit of penetration of tar in non-outgassed coke. However it is felt that pores of diameter less than 1 μm are not penetrated under any circumstances. Further to this, volumes measured for diameters below 0.1 μm may only be reflections of char compressibility, as suggested by Toda and Toyoda [22]. In the present case, the roughly equal increases in apparent volume from 0.1 to 0.01 μm (experimental lower limit) indicate a similar contribution from this material compressibility for each of the char types used.

These results indicate that the greater pore volume and mean pore size found in the lower temperature char contribute to a higher gross

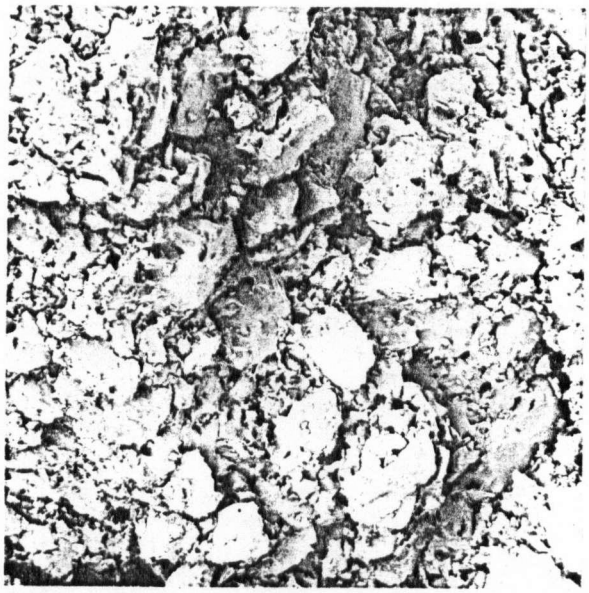

Figure 24a.: Photomicrograph Showing Aggregate-Binder Interfacial Failure (60X)

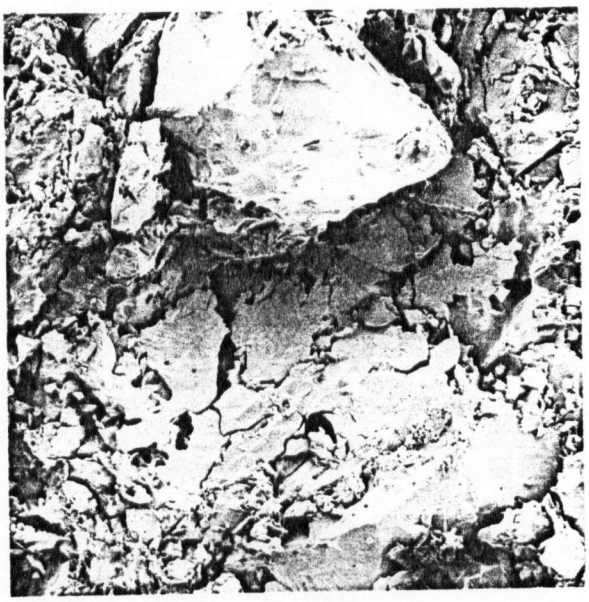

Figure 24b.: Photomicrograph Showing Binder Phase Fracture (130X)

composite strength. This is confirmed by the interfacial strength measurements performed on the binder-graphite rod specimens (section 2.3.1 - Table VIII) where introduction of surface roughness resulted in increased shear strength. Other authors have found similar results. For example, in their work on Soderberg anodes, Dell and Peterson [43] concluded that a pore structure accessible to the binder is essential for a good bond and Vetyukov et al. [42] have indicated that surface roughness is more important than the type of carbon material used.

All the above studies were concerned with graphitic or calcined petroleum coke aggregates. It has been indicated that materials of this type may show weaker aggregate-binder bond strengths than carbonaceous materials produced at lower temperatures. As carbonization temperature is increased, the solid product of pyrolysis takes on an increasingly denser, less reactive and more ordered structure. Sukhorukov et al. [39], in studying a range of materials from crude to calcined petroleum coke to graphite, showed that the more ordered, higher temperature materials showed weaker adhesion bonds. Chaklader et al. [33] found that briquette strength was lower where a higher rank coal-char material was used. The measured decrease in RVM content with rising carbonization temperature may be considered as a concurrent phenomenon with this ordering process. It is therefore possible that a part of the measured decrease in briquette strength with increasing charring temperature (figures 21a, b and c) may have been due to a decrease in char-binder interfacial strength.

4.3.2 Binder Characteristics

To eliminate char-property effects, briquetting mixtures of a single char and different binders can be considered. In these cases,

variations in UCS are associated with variations in binder properties.

For aggregate A3 (500°C char), briquette strength decreases for binders in the order B1 - B2 - B3. For the higher temperature aggregates, A2 (625°C) and A1 (750°C), there is little or no significant variation in briquette strength from one binder to another. The lower temperature char case (mixtures 7, 8 and 9) is considered first.

As noted earlier, failure occurred primarily at the char-binder interface. With the char-type held constant, this indicates two possible explanations for the measured variation in composite strength: the bond strength across the char-binder interface varies with the binder used; and/or the extent of penetration into the available pore structure varies with binder due to differences in fluidity. Although the former cannot be measured directly, a correlation is seen between binder fluidity and briquette strength. By comparing Table IV and figures 21a, b and c, it is seen that the decrease in fluidity from binder B1 to B3 parallels the decrease in briquette strength. With lower fluidity, B3 was less able to penetrate the available pore structure of the char, resulting in less binder-char interlocking and interfacial area and a lower gross composite strength. The exception of binder B2 to this pattern is explained by the fact that a higher briquetting pressure was used with those mixtures containing B2. At the nominal briquetting pressure of 10 MPa, it was not possible to produce a coherent briquette using this binder.

This conclusion is consistent with the results found with the higher temperature char mixtures. With virtually no large pore structure available for binder penetration, briquette strength is seen to become relatively insensitive to binder fluidity. In fact, the average briquette

strength appears to be approximately the same for all binders with the higher temperature chars. The strength of briquettes made with aggregate A1 (750°C) can be interpreted as reflecting the strength of the char-binder interfacial bond, which does not appear to be significantly different for the binders investigated. Hence it appears that, for a given char, it is primarily binder phase distribution that influences composite strength.

In this regard, the results of the wetting studies carried out indicate that there is no difficulty in attaining equilibrium wetting conditions of the system. The benzene-soluble extracts of each binder were seen to wet the amorphous carbon substrate almost immediately upon melting and the SRC pitch was seen to attain a consistently low equilibrium contact angle on each of the chars studied. It can therefore be said that, thermodynamically, the system favours penetration of the aggregate by the binder phase and that it is the kinetics of the spreading and penetration of the binder phase which control the aggregate-binder distribution.

This leads to a further indication of the relative importance of the two char-characteristic effects on strength discussed earlier. Given that the primary effect of varying the binder is to change the extent of binder penetration into the available pore structure, the amount by which the slope (Δstrength/Δcharring temperature) of figure 21a (binder B1) exceeds that of figure 21c (binder B3) can be associated with the difference in interfacial strength from binder to binder. From this it appears that briquette strength in this study is more sensitive to the availability of char pore structure than to variation in char-binder interfacial strength

from char to char. However, the contribution of the latter effect cannot be entirely ruled out because of the limited range of binders investigated and the fact that all the char types were produced from a single coal.

It should be further pointed out that two effects may be responsible for the way in which an increase in char porosity can lead to an increase in briquette strength. The increased porosity may simply provide greater contact area of the char-binder interface or it may cause fracture to occur through the binder phase. Binder failure has been observed (figure 24b) and this would indicate some contribution of binder strength to briquette strength. Although it has not been possible to clearly determine the extent of these two contributions, the comparative insensitivity of briquette strength to the binder involved implies this contribution was small in the present investigation.

It is suggested that future studies be carried out to investigate the strength properties of formcoke at blast furnace temperatures. An associated problem is the manner in which the green briquette strength investigated in this work is affected by the post-briquetting high temperature carbonization step. It should be recognized that larger sample sizes will be required to improve the statistical reliability of studies of this type and that a wider range of aggregates and binders should be considered. It may also be useful to investigate the third stage of compaction in detail.

5. CONCLUSIONS

1. The hot compaction behaviour of the char-binder systems studied has been shown to be influenced by the porosity of the aggregate-char phase and the fluidity of the binder-coal phase. Char porosity affects the amount of total compaction necessary to attain a given briquette bulk density, greater porosity requiring more compaction. This porosity is eliminated by penetration of the binder phase and by plastic deformation due to the applied stress. Binder fluidity influences compaction viscosity during the second stage of compaction (that associated with particle flow), higher binder fluidity leading to lower compaction viscosity. This is due to the relative ease with which the binder phase can penetrate and surround the aggregate particles.

2. The bulk density of the formcoke product is affected by the total compaction attained during the briquetting process. For the materials used in this study, it is found that compactions from 15 to 25% produce briquettes from 60 to 70% bulk density and that the sensitivity of bulk density to compaction appears to be independent of the binder phase. It is predicted that compaction of 40% would be necessary to attain 100% bulk density for the char material without significant porosity. This value increases with introduction of porosity in the char phase.

3. Briquette failure was found to occur primarily at the char-binder interface with occasional binder phase fracture. This indicates that the

strength of the briquette systems studied is independent of the strength of the char phase. Briquette strength is affected by char porosity and by the bond strength across the char-binder interface, the former effect predominating in the systems studied. Higher char porosity leads to higher strength by increasing aggregate-binder interfacial area and by promoting physical interlocking of the two phases. The effect of interfacial bond strength is inferred from the results of other authors, which indicate that use of char material carbonized at higher temperatures leads to lower interfacial strength. Higher binder fluidity increases composite strength by allowing more extensive penetration of the char pore structure by the binder phase.

4. The CCWL hot compaction model for char-binder coal systems was found to be applicable to the systems investigated. A solution of the mechanical analog of this model was developed and shown to be compatible with the original solution. Analysis of the experimental compaction curves using this model reinforces the assumption of non-interaction of compaction mechanisms and the association of the second and third compaction stages with particle flow and plastic deformation, respectively. Good agreement between duplicate runs was demonstrated, differences being attributed to inconsistency in the briquetting apparatus, slow response of the recording equipment and the heterogeneity of the materials used.

6. BIBLIOGRAPHY

1. Smith, E.J., Hoss, K.P. "Present and Future Position of Coal in Steel Technology," Ironmaking and Steelmaking, No. 1, 10-19, 1976.

2. Coal in British Columbia - A Technical Appraisal. British Columbia Task Force Technical Committee February, 1976.

3. Potter, N.M. "Presidential Address, 1970: Formed Coke," Journal of the Institute of Fuel, 43, No. 359, 497-510, 1970.

4. C. Simeons. Coal - Its Role in Tomorrows Technology, Permagon Press, 1978.

5. Anonymous. "Handicapping the Formcoke Sweepstakes," 33 Magazine, February, 33-38, 1975.

6. Jasienko, S. "The Nature of Coking Coals," Fuel, 57, No. 3, 131, 1978.

7. Cordier, J.A., Rochas, R. "HBNPC Formcoke Tests in Unisor Blast Furnaces," Agglomeration '77, 2, Chpt. 59, AIME-Sastry.

8. Hermann, W., Schmit, R. "The Ancit Process," Agglomeration '77, 2, Chpt. 58, AIME-Sastry.

9. Sugasawa, K. et al. "Japanese Blast Furnace Trials With Formed Coke," Stahl und Essen, 93, No. 1, 24-31 1973 (H.B Translation No. 8967).

10. Snowden, P.F. "The Auscoke Project - Recent Developments," BHP Technical Bulletin, 20, No. 1. 1976.

11. Foch, P. "Processes For Manufacturing Formed Coke - General Survey and Present State of the Art," Ironmaking Proceedings, 30, 238-258, 1971.

12. Ahland, E., Hehmann, J., Peters, W. "Suitability of Coal For Production of Formed Coke," Ironmaking Proceedings, 31, 285-300, 1972.

13. Potter, N.M. "Further Thoughts on Formed Coke," Journal of the Institute of Fuel, 45, 313-319, 1972.

14. Voice, E.W., Ridgion, J.M. "Changes in Ironmaking Technology In Relation To the Availability of Coking Coal," Ironmaking and Steelmaking, No. 1, 2, 1974.

15. Darmann, O., Henkel, S., Haverkamp, K.D. "The Application of Hot Briquettes and Formed Coke In the Blast Furnace," Ironmaking Proceedings, 30, 261-262, 1971.

16. Rhys-Jones, D.C. Char Briquettes - An Outline of the Theory and Practice of Manufacture, National Coal Board, U.K., 1969.

17. Berkowitz, N. "Fundamental Aspects of Coal Briquetting," Proceedings of A Coal Briquetting Conference, 3-23, 1949.

18. Chemistry of Coal Utilization, Supplementary Volume, H.H. Lowry (ed.), J. Wiley and Sons, 1963.

19. Smith, F.W., Reynolds, D.A. "The Effect of Temperature, Charge Density. and Blending On the Carbonization of Coal," U.S.B.M. Report of Investigations 5110, 5, 1955.

20. Dainton, A.D. "Rheological Properties of Semicoke At High Temperatures," Fuel, 41, 279-284, 1962.

21. Gryaznov, N.S., Nechaev, Yu, A., Zolotuckhin, A.I. "Determination of the Modulus of Elasticity of Coke During the Carbonization Process," U.D.C. 662. 749, 1972.

22. Toda, Y., Toyoda, S. "Application of Mercury Porosimetry to Coal," Fuel, 51, 199-201, 1972.

23. Chaklader, A.C.D., Warren, I.H., Chow, C. "Characterization of Formed Cokes and Factors Affecting Form-Coking," Second Annual Report, E.M.R. Research Agreement No. 2239-2-68-77, Dept. Energy, Mines and Resources, Ottawa. 1977.

24. Evans, D.G., Hermann J.A. "Porosity of Brown Coal Char," Fuel, 49, 108-112, 1970.

25. White, J.L., Zimmer, J.E. "Microstructure and Thermal Expansion of Graphite," Second German Carbon Conference, 197, 1976.

26. Toda, Y., Hatami, M. Toyoda, S., Yoshida, Y., Honda, H. "Fine Structure of Carbonized Coals," Carbon, 8, 565-571, 1970.

27. Marsh, H., Rand, B. "Microporosity in Carbonaceous Materials," Third Conference on Industrial Carbons and Graphite, London, SCI, 172-182, 1971.

28. Gregg, S.J., Olds, F.M., Tyson, R.F.S. "Microporostiy In Carbons," Third Conference on Industrial Carbons and Graphite, London, SCI, 184-188, 1971.

29. McCartney, J.T. "Scanning Electron Microscopy of Metallurgical Cokes and Residues From Rapid Pyrolysis of Coals," Fuel, 50, 457-460, 1971.

30. Patrick, J.W., Sims, J.J., Stacey, A.E. "Quantitative Characterization of the Texture of Coke," Journal of Microscopy, 109, Pt. 1, 137-143, 1977.

31. Toda, Y. "Changes In Macropore Structure of Coals With Heat Treatment," Fuel, 52, 36-40, 1973.

32. Spitzer, Z., Biba, V., Kadlec, O. "The Complete Pore Structure Analysis of Fine Porous Solids," Carbon, 14, 151-156, 1976.

33 Chaklader, A.C.D., Warren, I.H , Chow, C. "Characterization of Formed Cokes and Factors Affecting Form-Coking," Third Annual Report, EMR Research Agreement No. 2239-2-68-77, Dept. Energy, Mines and Resources, Ottawa, 1978.

34. Loison, R., Peytavy, A., Boyer, A.F., Grillot, R. "The Plastic Properties of Coal," Chemistry of Coal Utilization, Supplementary Volume, Chpt. 4, 184, J. Wiley and Sons, 1963.

35. Howard, H.C. "Pyrolytic Reactions of Coal," Chemistry of Coal Utilization, Supplementary Volume, Chpt. 9, 392, J. Wiley and Sons, 1963.

36. Wenzel, R.N. "Resistance of Solid Surfaces to Wetting By Water," Industrial and Engineering Chemistry, 28, No. 8, 988-994, 1936.

37. Good, R.J. "A Thermodynamic Derivation of Wenzel's Modification of Young's Equation for Contact Angles; Together With a Theory of Hysteresis," J. Am. Chem. Soc. 74, 5041-2, 1952.

38. Adam, N.K. "Principles of Penetration of Liquids Into Solids," Discussions of the Faraday Society, 3, 5-11, 1948.

39. Sukhorukov, I.F., Babenko, E.M., Gavrina, M.V. "Surface Phenomena At the Carbonaceous Material - Coal Tar Pitch Boundary," Tsvetnye Mettaly, 38, 70-73, 1965.

40. Agrawal, D.P., Berkowitz N. "On the Wetting of Carbon Surfaces By Carbonaceous Binders," Proceedings of the 9th Biennial Briquetting Conference, 104-114, 1965.

41. Dmitrieva, G.V., Rhys, M.A., Smirnova A.S., Shuraeva, E.A. "Wettability and Impregnability of Carbon Materials By Coal Tar Pitch," International Chemical Engineering, 7, No. 2, 252-255, 1967.

42. Vetyukov, M.M., Ofitserov, V.F.. Chalik, S.M., Sverdlin, V.A., Nikulin, V.N. "Wetting of Carbon Electron Materials By Coal-Tar Pitches," Tsvetnye Mettally, 47, 23-26, 1974.

43. Dell, M.B., Peterson, R.W. "Wettability of Petroleum Cokes By Pitch," Industrial and Engineering Chemistry Prod. Res. and Dev., 9, No. 2, 190-194, 1970.

44. Lahaye, J., Auber, J.-P. "Interaction Between a Coke and a Tar--1. Influence of the Surface Chemical Functions of Coke. 2. Limit of Tar Penetration in Coke Porosity," Fuel, 56, 185-191, 1977.

45. Greenhalgh, E., Moyse, M.E., "Contact Angle of Pitch On Carbon Surfaces," Third Conference on Industrial Carbons and Graphite, 539-549, 1971.

46. Fitzgerald, D. "Viscoelastic Properties of Coal During Carbonization," Fuel, 36, 389-394, 1957.

47. Habberjam, G.M. "Compaction Phenomena In Char Briquetting," British Journal of Applied Physics, 15, 1233-1242, 1964.

48. Jayasinghe, S.S., Pilpel, N. "The Cohesive Properties of Coal When Heated," Journal of the Institute of Fuel, 51-55, February, 1970.

49. Bradford, D.J., Doyle, A.J., Fahy, B.A., Greenhalgh, E. "Distribution of Pitch Binder In Binder/Coke Mixtures," Third Conference On Industrial Carbons and Graphite, London, SCI, 528-538, 1971.

50. Collett, G.W., Rand, B. "Rheological Investigation of Coal-Tar Pitch During Its Transformation To Mesophase," Fuel, 57, 162-170, 1978.

51. Chow, C., Chaklader, A.C.D., Warren, I.H., Leeder, W.R. "Hot Compaction Behaviour of Char/Binder Coal Systems," Fuel, 57, 387-393, 1978.

52. Bradbeer, R.S., Chaklader, A.C.D., "Reactive Hot Pressing of Colloidal Boehemite," Material Science Research, 6, 395, 1973.

53. Krokosky, E. "Behaviour of Time-Dependent Composite Materials," Modern Composite Materials, Broutman and Krock (ed.), Chpt. 4, 122, Addison-Wesley, 1967.

54. a. McGeary, R.K. Journal of the American Ceramic Society, 44, 513, 1961.

b. Smith, W.O., Foote, F.D. Phys. Rev., 34, 1272, 1929.

55. Ryshkewitch, E. "Compression Strength of Porous Sintered Alumina and Zirconia," Journal of the American Ceramic Society, 36, 65, 1953.

56. Knudsen, F.P. Journal of the American Ceramic Society, 45, 94, 1962.

57. Walpole, R.E., Myers, R.H. Probability and Statistics for Engineers and Scientists, 292, Macmillan, 1972.

7. APPENDICES

APPENDIX A. Derivation of CCWL Model For Hot Compaction of Char/Binder Systems

The system considered is one whose response to an input stress is time varying. The stress input is considered to be characterized by a step function, $u_t(t)$, such that

$$\sigma = \sigma_o \, u_t(t)$$

where: $u_t(t) = \begin{cases} 0 \text{ for } t \; 0 \\ 1 \text{ for } t \; 0^+ \end{cases}$

The response of the system to this stress input is described by the relationship:

$$\varepsilon = k \, (1 - Ae^{-\alpha t} - Be^{-\beta t} - Ce^{-\gamma t}) \qquad (1)$$

or, introducing the transfer function, χ,

$$\varepsilon = \chi \, \sigma$$

Therefore, the problem is to determine the transfer function for the system concerned.

The response of a linear system to a unit pulse input, $u_o(t)$ is the derivative of the system response to a unit step function, $u_t(t)$. The derivative of equation (1) is

$$\dot{\varepsilon} = kA\alpha e^{-\alpha t} + kB\beta e^{-\beta t} + kC\gamma e^{-\gamma t}$$

and a Laplace transformation $\mathcal{L}(\dot{\varepsilon})$, can be applied

$$x = \frac{E}{\Psi} = \mathcal{L}(\dot{\varepsilon}) = \frac{a}{s+\alpha} + \frac{b}{s+\beta} + \frac{c}{s+\gamma}$$

where: $a = kA\alpha$ $\quad$ x = transform operator
$b = kB\beta$
$c = kC\gamma$
ψ = stress in transform space = 1
s = independent variable in the Laplace space, $[F(t)] \rightarrow f(s)$.

By considering the boundary condition: $A + B + C = 1$,

$$x = \frac{a(s+\beta)(s+\gamma) + b(s+\alpha)(s+\gamma) + c(s+\beta)(s+\alpha)}{(s+\alpha)(s+\beta)(s+\gamma)}$$

$$= \frac{s^2[a+b+c] + s[a(\beta+\gamma) + b(\gamma+\alpha) + c(\beta+\alpha)] + k\alpha\beta\gamma}{s^3 + s^2[\alpha+\beta+\gamma] + s[\alpha\beta+\beta\gamma+\gamma\alpha] + \alpha\beta\gamma} \qquad (2)$$

It can be seen from the definitions of a, b and c that:

$$k\alpha\beta\gamma = a\beta\gamma + b\gamma\alpha + c\beta\alpha$$

And by introducing the following terms:

$M = \alpha + \beta + \gamma$
$P = a + b + c$
$Q = a(\beta+\gamma) + b(\gamma+\alpha) + c(\beta+\alpha)$
$R = k\alpha\beta\gamma$
$N = (\alpha\beta + \beta\gamma + \gamma\alpha)$
$T = \alpha\beta\gamma$

equation (2) can be rewritten:

$$x = E = \frac{s^2P + sQ + R}{s^3 + s^2M + sN + T}$$

The differential equation which describes the stress-strain response of the system is given by the inverse of the Laplace transform, ie.:

$$\dddot{\varepsilon} + M\ddot{\varepsilon} + N\dot{\varepsilon} + T\varepsilon = P\ddot{\sigma} + Q\dot{\sigma} + R\sigma \qquad (3)$$

An electrical analog may be obtained by replacing ε and σ by q and v respectively ($q = \int i dt$):

$$\dddot{i} + M\ddot{i} + N\dot{i} + T\int i dt = P\ddot{v} + Q\dot{v} + Rv$$

with the corresponding time derivative:

$$\ddddot{i} + M\dddot{i} + N\ddot{i} + Ti = P\dddot{v} + Q\ddot{v} + R\dot{v} .$$

In the Laplace transform space,

$$\frac{I}{V} = \frac{s^3P + s^2Q + sR}{s^3 + s^2M + sN + T} \qquad (4)$$

Of the various circuits possessing the correct transfer function, the simplest is symmetric coupling:

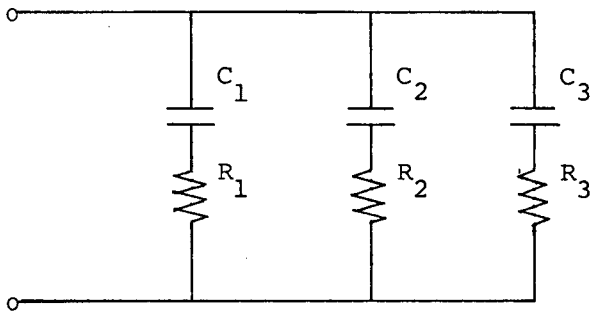

whose mechanical equivalent, with $C \leftrightarrow \frac{1}{M}$ and $R \leftrightarrow \eta$, is:

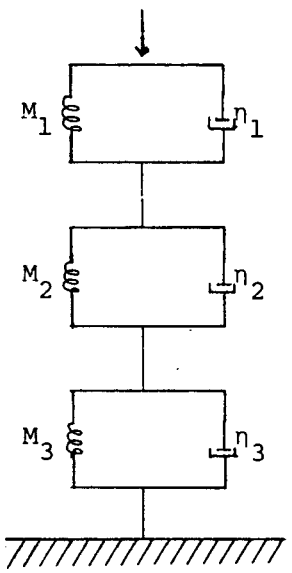

Substituting the mechanical equivalents into the solution of equation (4) shows the constants of equation (3) to be given by:

$$M = \frac{M_3}{\eta_1} + \frac{M_2}{\eta_2} + \frac{M_1}{\eta_3}$$

$$N = \left(\frac{M_1 M_2 M_3}{\eta_1 \eta_2 \eta_3}\right)\left(\frac{\eta_1}{M_1} + \frac{\eta_2}{M_2} + \frac{\eta_3}{M_3}\right)$$

$$T = \frac{M_1 M_2 M_3}{\eta_1 \eta_2 \eta_3}$$

$$P = \frac{1}{\eta_1} + \frac{1}{\eta_2} + \frac{1}{\eta_3}$$

$$Q = \frac{M_1}{\eta_1}\left(\frac{1}{\eta_2} + \frac{1}{\eta_3}\right) + \frac{M_2}{\eta_2}\left(\frac{1}{\eta_1} + \frac{1}{\eta_3}\right) + \frac{M_3}{\eta_3}\left(\frac{1}{\eta_1} + \frac{1}{\eta_2}\right)$$

$$R = \frac{M_1 M_2 + M_2 M_3 + M_3 M_1}{\eta_1 \eta_2 \eta_3}$$

Since M, N, T, P Q and R are determined from experiment, the values of M_1, M_2, M_3, η_1, η_2, η_3 can be found by solving these six equations simultaneously.

APPENDIX B. NORMALIZED COMPACTION CURVES

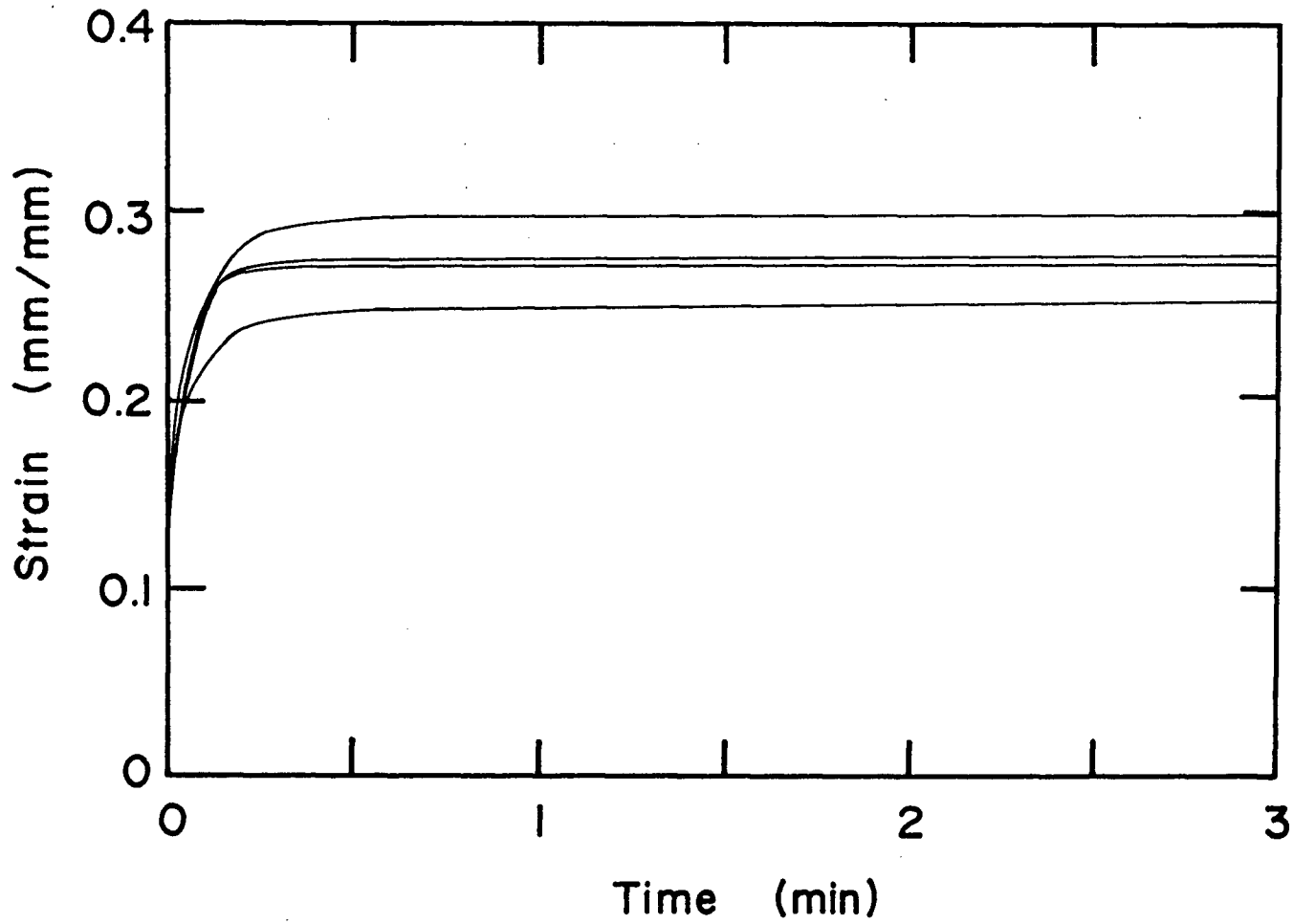

Figure B-1: Compaction Curves of Mixture 1 (Binder B1 - Aggregate Carbonized at 750°C)

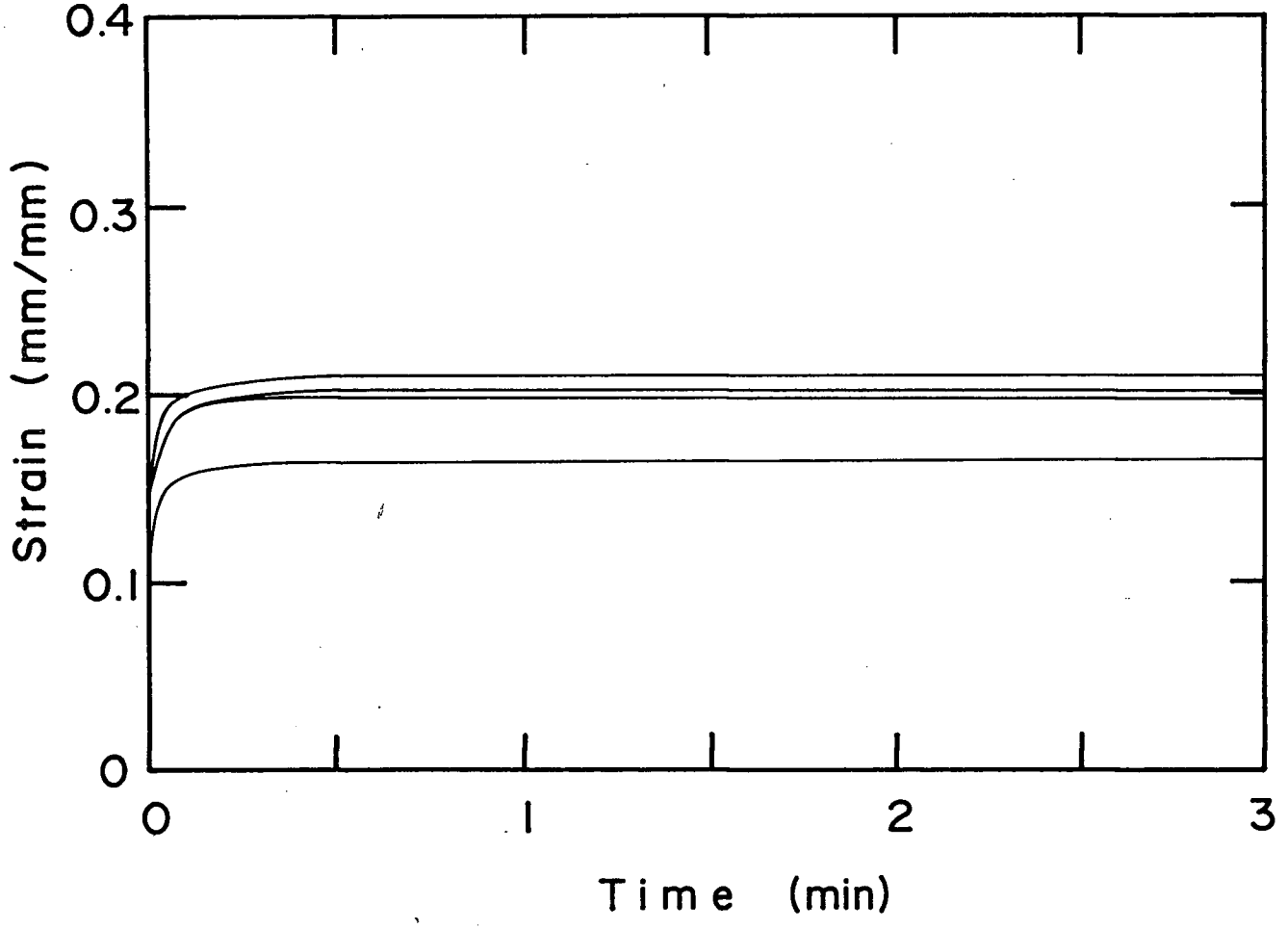

Figure B-2: Compaction Curves of Mixture 2 (Binder B1 - Aggregate Carbonized at 625°C)

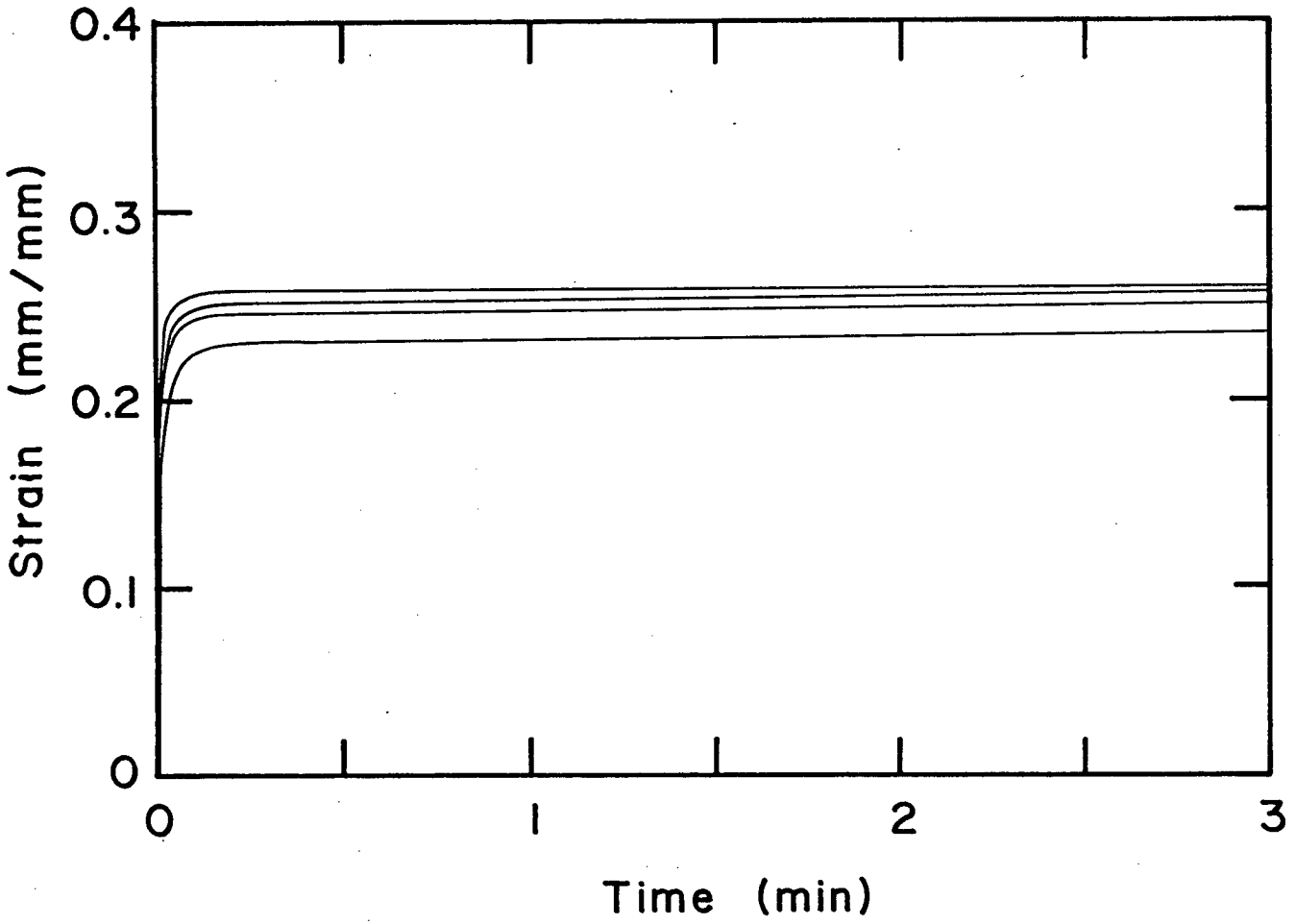

Figure B-3 Compaction Curves of Mixture 3 (Binder B1 - Aggregate Carbonized at 500°C)

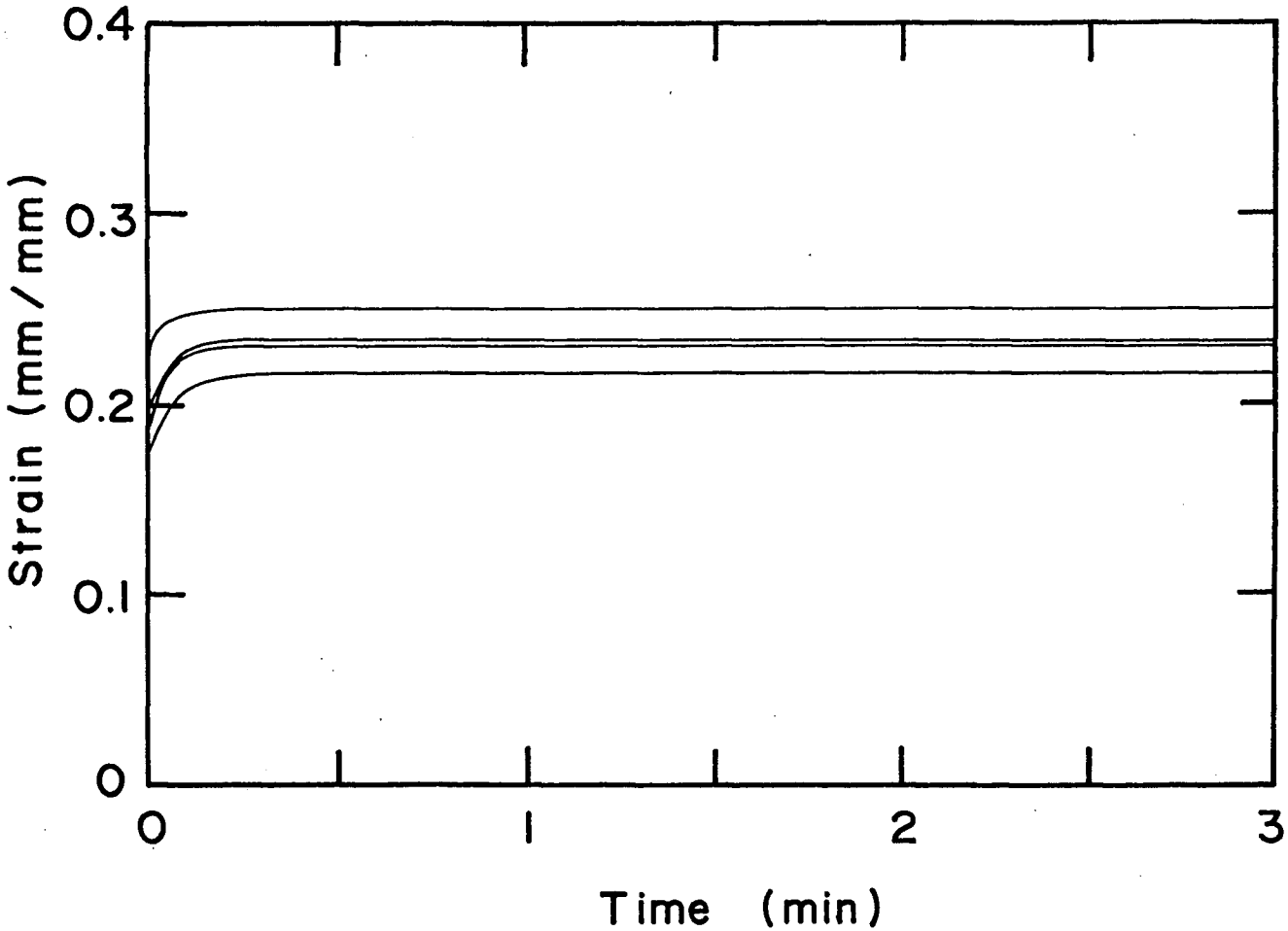

Figure B-4: Compaction Curves of Mixture 4 (Binder B2 - Aggregate Carbonized at 750°C)

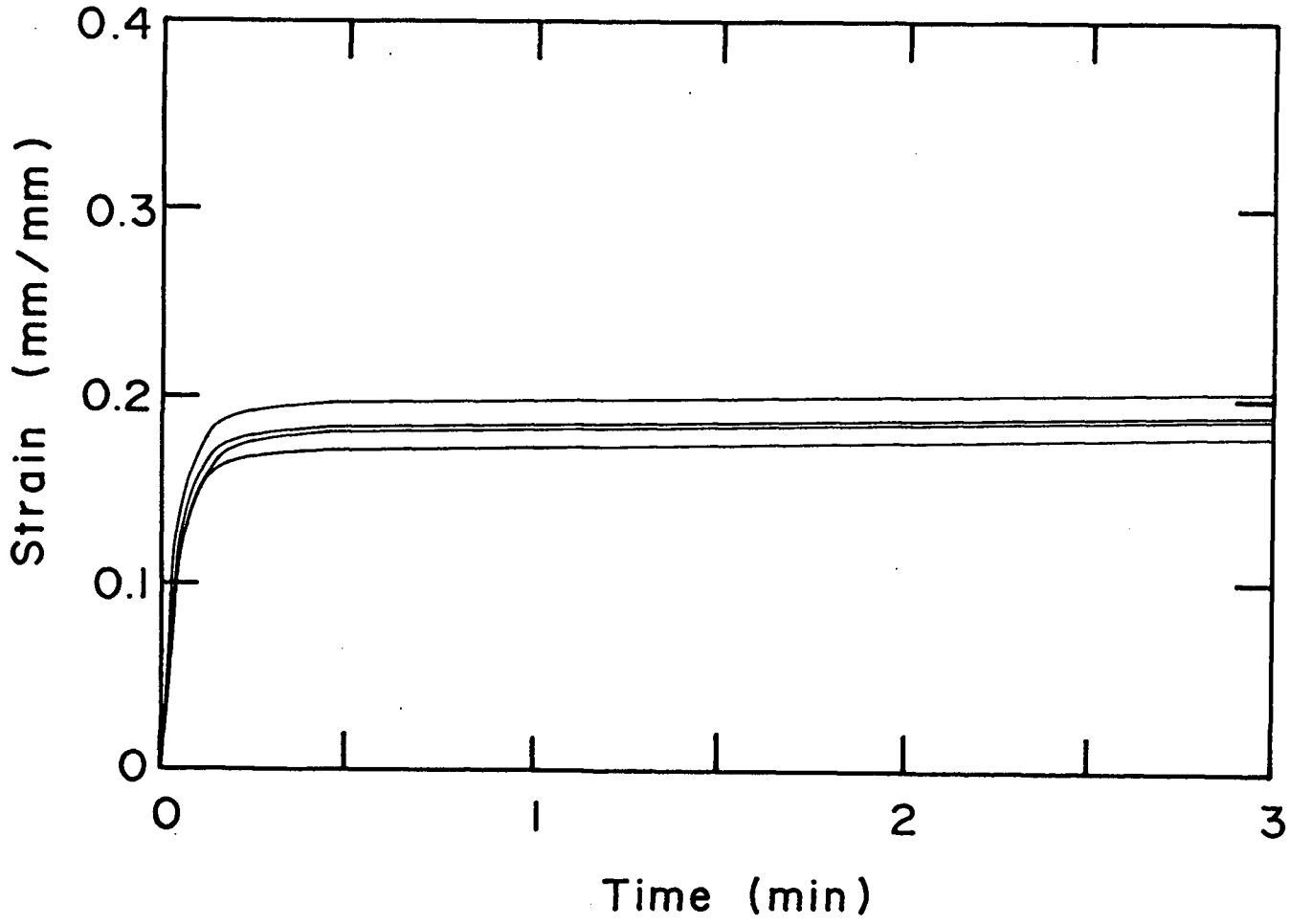

Figure B-5: Compaction Curves of Mixture 5 (Binder B2 - Aggregate carbonized at 625°C char)

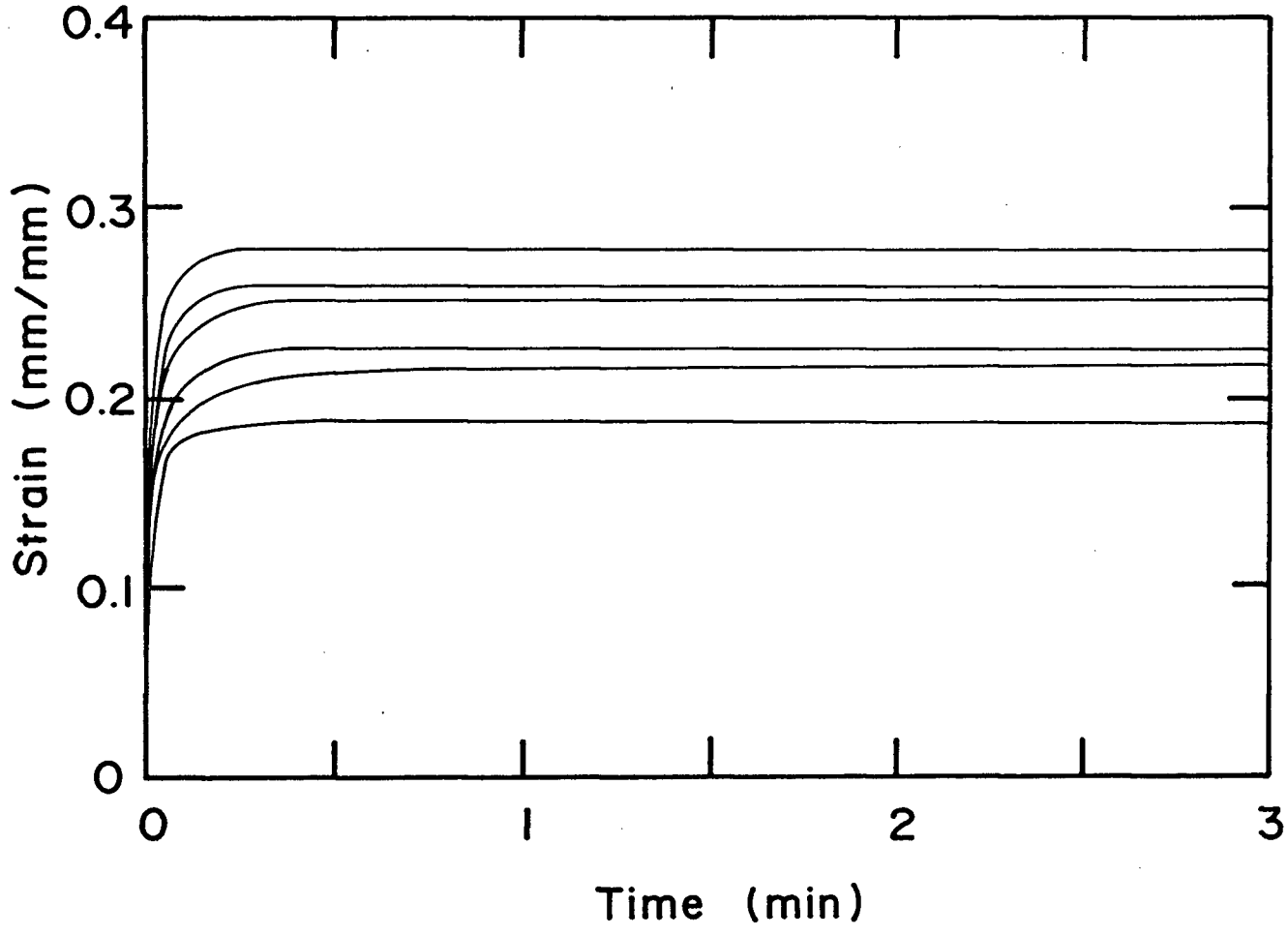

Figure B-6: Compaction Curves of Mixture 7 (Binder B3 - Aggregate Carbonized at 750°C)

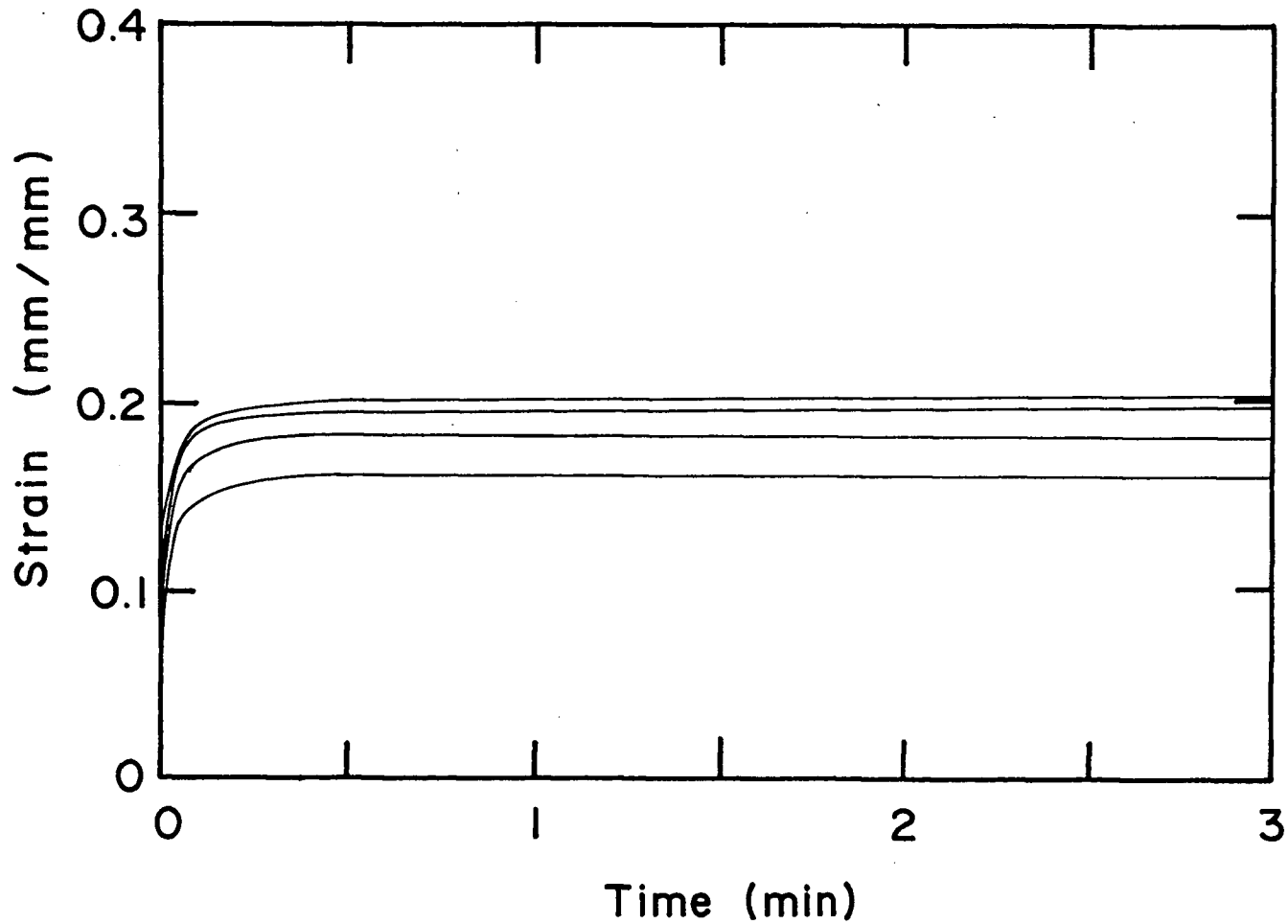

Figure B-7: Compaction Curves of Mixture B (Binder B3 - Aggregate Carbonized at 625°C)

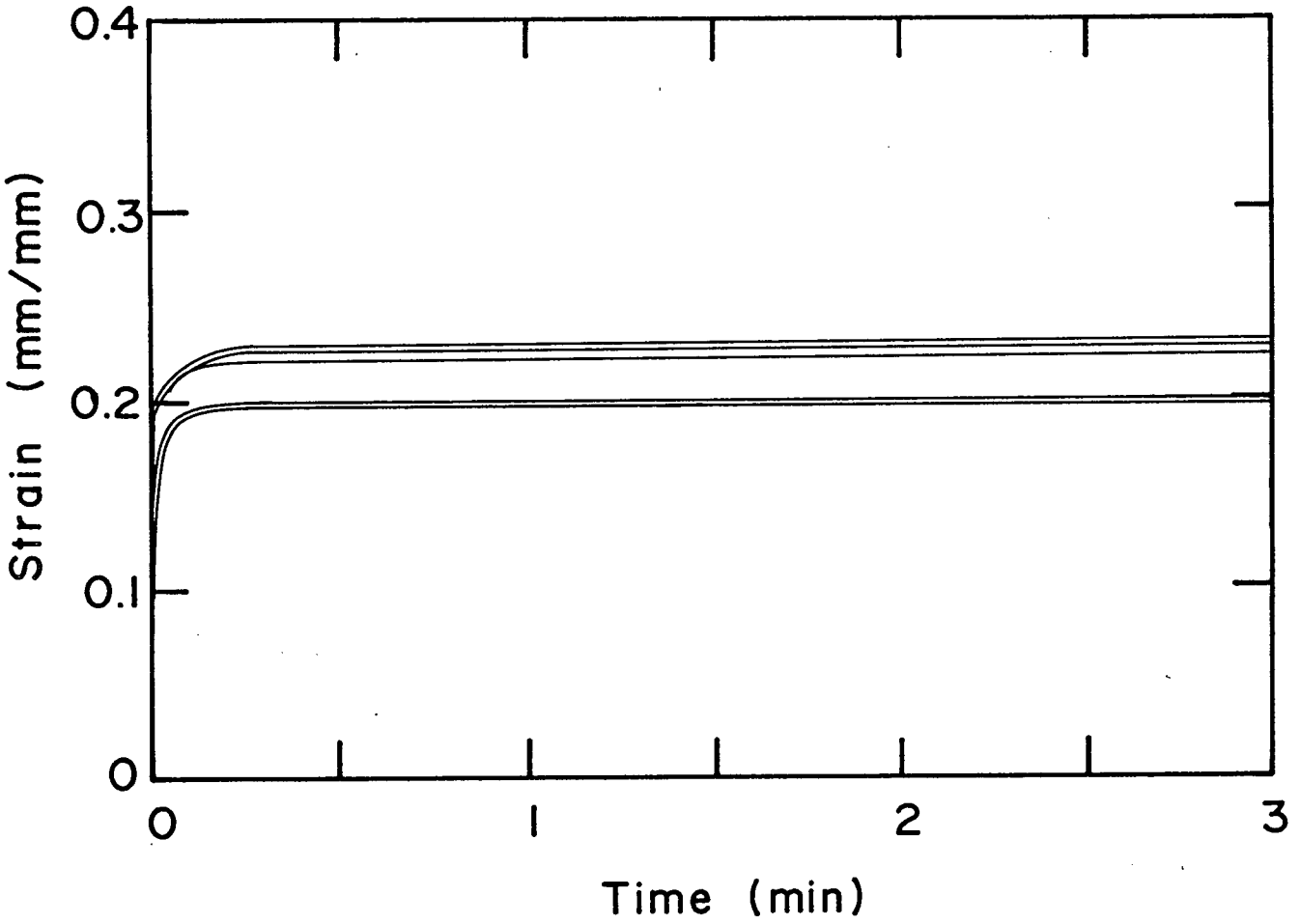

Figure B-8: Compaction Curves of Mixture 9 (Binder B3 - Aggregate Carbonized at 500°C)

APPENDIX C. GLOSSARY OF TERMS

Aggregate - that portion of a briquetting mixture which acts effectively as an inert filler — made by low temperature carbonization of a non-caking coal.

Anthracite - highest rank coal; less than 14% volatile matter; NCB group 100; International Classification code 100.

Binder - that portion of a briquetting mixture which takes on fluid properties under compacting conditions and forms the matrix of the final product.

Bituminous - coals which demonstrate agglomerating properties; ranging from low (14-22%) to medium (22-30%) to high (above 30%) volatile.

By-Product Oven - the standard conventional coking oven; typical modern dimensions: 6 m high x 15 m long x 0.5 m wide; heating is from external flues, preventing dilution of gases produced.

Caking Coal - a coal in which an accumulation of the plastic phase is observed during pyrolysis.

Char - the solid product of low temperature (450°C-700°C) carbonization of coal.

Coal Extract - that fraction of a coal which is soluble in an organic solvent, typically chloroform, pyridene or benzene.

Coke - the solid product of high temperature carbonization of a coking coal conforming to a set of industrial chemical and physical standards.

Coking Coal - a caking coal which falls within a range of acceptable plastic and chemical properties or one which does when blended with other coals.

Formcoke - the product of any of a number of alternative processes for producing blast furnace coke from traditionally unacceptable coals; usually in the form of briquettes.

Gieseler Plastometer - an apparatus in which a constant torque is applied to a stirrer rod imbedded in the coal sample. Rotation of the stirrer is possible only when the coal is in its plastic state. The amount of rotation is measured with increasing temperature and used to indicate sample fluidity parameters.

Kelvin Element - viscoelastic model element consisting of a spring and dashpot connected in parallel.

Mesophase (Metaplast) - intermediate fluid phase of coal formed as a result of depolymerization of the coal macromolecule.

Proximate Analysis - an analysis which breaks coal composition into four parts: moisture, volatile matter, fixed carbon, and ash; covered by ASTM D 271 68.

Rank - the order of a coal on any of a number of classfication systems; classfications are based on volatile matter content, caking properties and calorific value. Generally, rank increases with fixed carbon and decreasing volatile matter.

Ruhr Dilatometer - a device which follows the length of a coal sample under specific heating conditions; the sample may be brought quickly to temperature and the contraction/dilatation followed with time or it may be heated slowly, both procedures yielding a number of rheological parameters.

Sub-bituminous - coals which do not demonstrate agglomerating properties, but with volatile matter contents greater than 33%; classification is by calorific value:
A - 10500-11500 BTU lb^{-1} (24.4-26.8 $MJkg^{-1}$)
B - 9500-10500 BTU lb^{-1} (22.1-24.4 $MJkg^{-1}$)
C - 8300-9500 BTU lb^{-1} (19.3-22.1 $MJkg^{-1}$)

Tumbler Index - value arrived at by rotating a closely sized coal sample in a drum a specified number of revolutions and sizing the degraded product to give percentage passing or standing on a given screen.

Volatile Matter Content - the weight fraction of a moisture-free coal which is lost as gaseous products of pyrolysis; these typically include combustible (hydrogen, carbon monoxide, methane and other hydrocarbons) and incombustible (carbon dioxide and water vapour) gases and tar vapours.